A Liquid Gallium-Air Battery Study

By

Tyler Trettel Howard

A Master's thesis submitted to the faculty of the

Worcester Polytechnic Institute

In partial fulfillment of the requirements for the

Degree of Masters of Science in Chemical Engineering

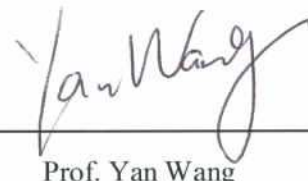Date: December 22, 2016

Approved:

_____
Prof. Ravindra Datta, Advisor

_____
Prof. Nikolaos K. Kazantzis

(Committee Member)

_____
Prof. N. Aaron Deskins

(Committee Member)

_____
Prof. Yan Wang

(Committee Member)

_____
Prof. Susan C. Roberts

(Department Head)

Abstract

Increasing energy demands world-wide must be met with more effective systems to produce, store, and distribute energy. Ideally, these systems should avoid fossil fuels and incorporate renewable technologies. To accommodate for the intermittent nature of renewable energies, a rechargeable gallium-air flow battery system for electrical grid applications is suggested. Using liquid gallium-air flow batteries could meet the rigorous world-wide demands for storage capacity, discharge duration, and durability necessary for the electrical grid. Toward this goal, a batch gallium-air battery was build and investigated. The performance of the system has been incrementally improved to a 30 hour discharge duration. Some insights into the mechanism of the gallium-air reaction was also obtained. However, recharging experiments were mostly unsuccessful. Despite the failures caused by carbonation and the separator drying, the Ga-Air system remains promising.

Acknowledgements

Contents

Table of Figures

Table of Tables

1. Introduction

Energy is a fundamental need of every advancing society. Industrialized societies continuously create higher energy demands to match advancing technologies and ever higher standards of living; and societies that are just starting to enter the global market have also begun to ramp up on their own energy needs. In fewer than 25 years, the global energy demand is expected to rise by at least 37% (IAE, 2014). This is an exceptional opportunity for global innovation, but it has historically come at a cost. As most nations begin to develop, they often choose easily accessible energy sources such as fossil fuels (Friedman, 2008). To avoid global climate change consequences, it is essential that a strong movement toward renewable energies occurs. If an energy technology could be developed at offers the ease of fossil fuels, but without their environmental consequences, it would become an highly lucrative and globally beneficial technology.

As renewable energies such as wind and solar currently stand, they are incredibly effective technologies that are continuously growing in affordability and in efficiency. Unfortunately, the majority of these energy sources fail to meet the requirements of the electrical grid, failing to deliver adequate energy during peak consumption hours and wasting energy during non-peak hours (Huggins, 2010). A rechargeable battery system to assist current electrical grid infrastructures to balance supply and demand is an immediately attractive solution that will continue to remain effective as smart grids are developed. The focus of this investigation is to provide some insights to a potential new battery technology that could help develop such an energy storage and supply system: the liquid gallium-air battery.

The proposed design for this battery incorporates an open-air system with a separator to facilitate the reaction between the gallium and air. This design is quite attractive since it only

requires air as an oxidant and uses a metallic anode. Additionally, the liquid anode is promising for future flow battery applications. The batch gallium-air system tests consisted of a vertically stacked anode current collector, gallium anode, electrolyte-soaked separator, gas diffusion layer, and cathode current collector. This schematic is shown in detail in Figure 3-1 (page 30).

Chapter 2, the literature review, describes currently existing commercial batteries and currently researched batteries. It provides a more in-depth rationale as to why the Ga-Air system was chosen for this investigation over the other promising battery candidates. Additionally, it establishes the strong theoretical potential of the Ga-Air system.

Chapter 3, methodology, describes the design of the batch test cell and the different testing methods employed over the course of this investigation. Since the Ga-Air system is a newly established system, there is very little background research on it. The methodology aims to describe the tests necessary to garner a more complete understanding of the Ga-Air system's performance.

Chapter 4, results and discussion, shows the data gathered through the tests of this investigation. The data are analyzed in the section and possible interpretations are offered. Various results are considered such as open circuit voltage, discharge duration under different conditions, rechargeability, and cyclic voltammetry. The causes of Ga-Air system failure are also analyzed in depth.

Some noteworthy results that incrementally improved the discharge performance were the causes of cell failure. In particular, separator drying and potassium hydroxide carbonation encouraged an investigation of anion exchange membrane separators. While the best zirconia cloth separators reached a discharge duration of 30 hours, anion exchange membranes could still reach 16 hours and were more promising for recharging.

Chapter 5, the conclusions and recommendations, mark the major takeaways from this investigation. It goes over the most reliable baseline performance of the investigation, areas where error occurred, and how this error could be avoided in future investigations.

In conclusion, it was determined that a batch gallium-air battery system could sustain a continuous discharge voltage of approximately 1 V for up to 30 hours at 1.41 mA/cm^2 and 55°C. Other separators and conditions varied this performance; however, virtually all tests were susceptible to separator drying and potassium hydroxide carbonation causes of failure. Despite these failures, different separators were tested for possible insights. This lead to the conclusion that the AEM separator is worthy of continued investigation because of its resilience to the typical causes of cell failure. Moreover, a flow battery set-up would be promising to significantly increase the total performance of the system.

2 Literature Review

2.1 Energy Storage

The demand for easily accessible energy from fossil resources has continued to increase substantially as society has continued to progress. This growth is naturally linked to global population growth but is more importantly tied to the continual motion for societies to urbanize, industrialize, and become more prosperous (Friedman, 2008). For this reason, energy will only continue to become more important, and as more energy is consumed, the effects of these energies will become more pronounced. While renewable energies have generally little environmental impact, energy extracted from fossil fuels is a particular concern. In fact, the current energy consumption of the United States is largely derived from fossil fuels, making up 85% of the total United States' electrical energy consumption. Of this 85%, more than a quarter of the energy is acquired through coal burning (Weber et al. 2011), which is one of the most carbon-dense fossil fuels, resulting in high amounts of CO_2 production. In contrast, only 6.6% of the United States' energy consumption was from renewable sources, with the remaining percentage supplied through nuclear (Ibrahim, 2008).

While the current fossil fuel consumption of the United States is quite concerning, rapid industrialization and energy consumption on the global level is also becoming a major concern. As other nations begin to industrialize, many of them have turned to fossil fuels to accelerate growth. For example, China in 2008 began to increase its fossil fuel consumption substantially to accelerate development, which followed suit with the industrialization period in the United States and Britain. As other developing nations also follow this example, there could be a continued worldwide increase in use of fossil fuels, which could have calamitous effects on the global climate (Friedman, 2008).

One reason use of fossil fuels for electricity generation is so dominant over renewable technologies is their flexibility to be used as electrical energy is needed. Throughout the day, for example, the demand for energy increases and decreases periodically, as shown in Figure 2-1 (Huggins, 2010). The reason for this periodic energy demand is caused by higher energy demands for heating or cooling depending on the time of day. Energy demands also typically increase in the evenings because of the standard 9-5 workday.
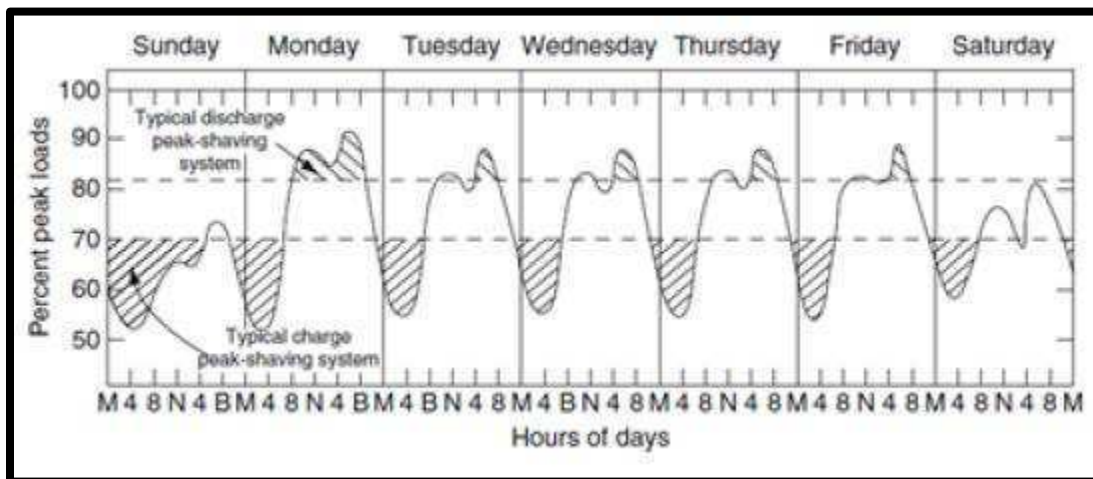
Figure 2-1: The variation in energy demand throughout an entire week (Huggins, 2010).

While renewable energies if integrated into the grid also periodically vary in energy production throughout the day, the energy profiles of consumption and production often do not match. This results in significant losses during non-peak hours and, more importantly, insufficient energy produced during peak consumption hours. Fossil fuels power plants are able to address the variable energy demands throughout the day because additional power plants can be activated during peak consumption hours. However, renewable energies often do not have this convenience, since "turning on" more solar panels at night would do virtually nothing to address the peak energy demands.

One suggested solution to increase the viability of integrating renewable energies into the grid for non-peak hours is to use an electrical energy storage (EES) system to store unused

17

energy generated during non-peak hours. These energy storage systems are not limited

exclusively to batteries, and can actually be broken down into two subcategories of storage:

indirect and direct. Figure 2-2 shows a breakdown of energy storage and its constituents.
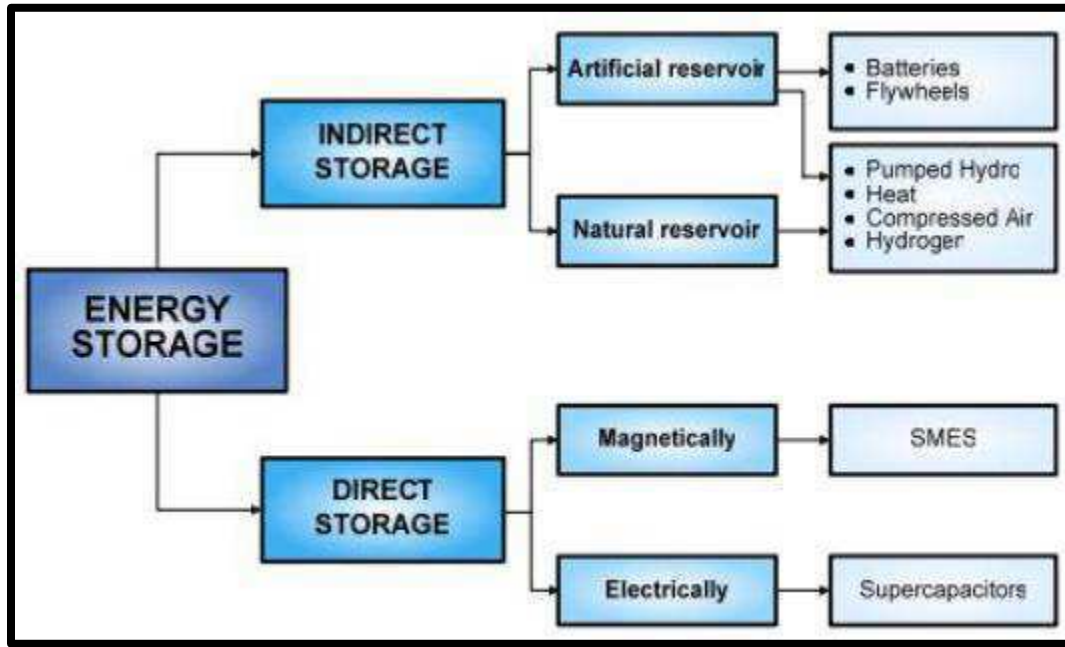
Figure 2-2: Energy storage is separated into direct and indirect storage. These are further broken down into artificial and natural reservoirs and magnetic and electrical storage. (San Martin, et al, 2011).

The primary focus of this investigation will be the indirect storage methods, such as an

artificial reservoir. In fact, artificial storage reservoirs in the form of batteries is the primary topic

of interest. Current battery technologies are quite effective for portable applications, continually

accommodating for the smaller sizes of devices, typically based on lithium-ion batteries.

However, batteries could also offer a meaningful improvement to the current electric grid

system. Rechargeable batteries can accommodate for difference scales, storing both the

electricity of large scale renewable energy farms and also excess energy produced by homes that

could have solar panels, for instance. In any case, if a grid solution using batteries is considered,

a considerable number of rechargeable batteries will be required (Ibrahim, 2008), because of the

huge amount of storage needed, reaching upwards of 22,000 MW (Huggins, 2010).

Should a rechargeable battery system be used for a large-scale grid energy storage solution, it is important that the batteries are able to produce the electrical energy as needed to address peak hours. This solution is highly preferable to a smart grid solution because it does not require a significant overhaul of the existing energy distribution infrastructure. While a smart grid is certainly one of the best long-term solutions to energy consumption issues that we currently face and will most likely face in the future (Friedman, 2008), a more immediate and less expensive solution should certainly be considered if it allows for a smoother transition into a renewable energy based grid. Using battery storage linked with renewable energies will be effective to store unused energy during the non-peak hours and will also be effective to expend that stored energy to meet the demand during peak hours. An example of the curve smoothing is shown in Figure 2-3 (Huggins, 2010).
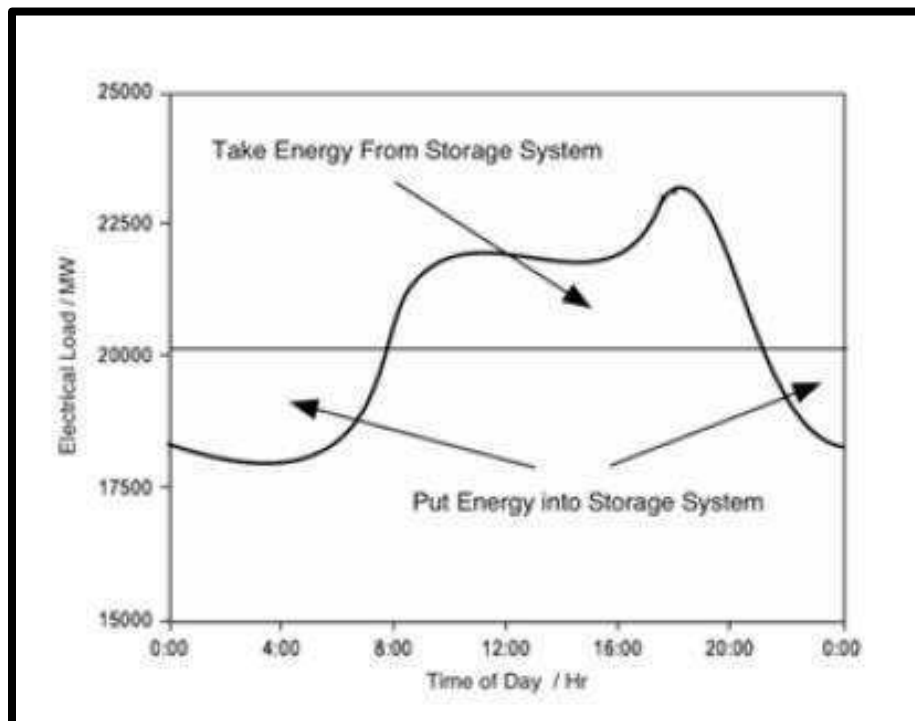
Figure 2-3: An example situation in which an energy storage system is integrated with the grid (Huggins, 2010).

While designing a rechargeable battery system that meets the demands of the grid appears simple initially, there are six important properties of the batteries that must be considered before a system can be properly developed (Hu, et al. 2016):

1. **Capacity:** The maximum storable energy of the battery

2. **Available Energy:** The maximum amount of energy that the battery can output; represented by a percentage of capacity

3. **Discharge Duration:** The maximum duration the battery change discharge when under peak load

4. **Efficiency:** The ratio of energy released against total stored energy

5. **Durability:** The maximum number of discharge/charge cycles the battery can undergo without experiencing losses to the capacity

6. **Autonomy:** The maximum duration the battery can draw power until all usable energy is consumed

7. **Cost:** The minimum investment necessary to create the system

All of these factors are fundamental in a rechargeable battery storage system intended for grid applications; however, the most important factors for the battery design must first consider capacity, then discharge duration, then durability. Capacity is essential for the performance of the battery system, because it dictates the level of the flat line in Figure 2-3. If the overall capacity of the system is too low, there is no scenario in which the storage system can help mitigate peak hour demands. Discharge duration is the next consideration, since the grid operates on a daily regimen. For this reason, the total discharge duration of the battery system must be no less than half a day since it can spend the other half of the day charging. In an ideal scenario, the batteries should be able to last much longer. Durability is the final important consideration, since a

rechargeable system must be consistently rechargeable. In order to avoid frequent replacement, the battery system must be robust to numerous discharge/charge cycles. It is important that this system is durable because if frequent replacements are required, costs and material replacements can be prohibitive. To avoid this, the battery system must be durable.

There are a wide variety of current batteries that exist that could serve as a candidate for a rechargeable battery grid. Additionally, there are also some batteries that are currently being researched that may be even more promising than currently existing technologies. Figure 2-4 shows many different energy storage technologies' power rating against their discharge duration (Dunn et al., 2011).
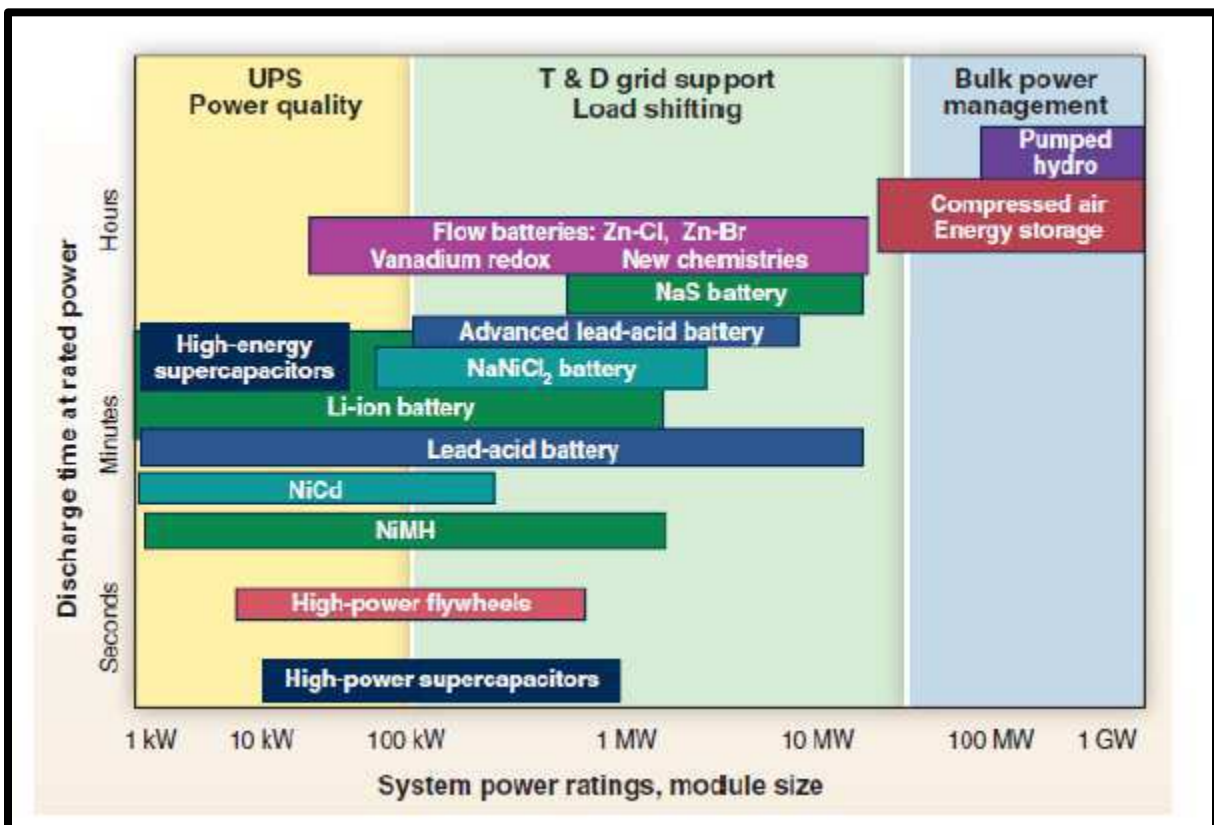
Figure 2-4: The many energy storage technologies compared for both system power and discharge duration (Dunn, et al., 2011).

The middle section (T & D grid support and Load shifting) section in Figure 2-4 predominately includes battery technologies. This includes a wide variety of batteries. Some of

the most promising batteries for this application are flow batteries, NaS batteries, advanced and basic lead-acid batteries, and NaNiCl$_2$ batteries since they span at least half of the middle section in Figure 2-4. For this investigation, batteries that are similar in design to flow batteries will be the primary focus of the literature review.

2.2 Battery Chemistry

2.2.1 Primary Batteries

Batteries consist of two basic parts: the anode and the cathode. In a primary cell, the anode is the negative electrode and the cathode is the positive electrode, which are separated by an electrolyte layer. When the circuit around a battery is completed an electrochemical redox reaction can occur between the anode and cathode while the electrons move through the wire and can be harnessed to do work. As long as the reaction is favorable, the battery will continue to operate until the reaction between the anode and the cathode reaches equilibrium. For a primary battery, this corresponds to the "death" of the battery, and it must be discarded and replaced. In other words primary batteries are non-rechargeable.

Initial battery designs started as a primary battery, with one of the oldest examples being the galvanic cell, or voltaic pile, constructed in the 1800s by Alessandro Volta (Kipnis, N., 2003). This initial design consisted of two different metals submerged in an aqueous electrolyte solution where the anode and cathode chambers were separated by a porous separate that allows the diffusion of anions, e.g. SO_4^{2-}, while largely precluding the cations. When these metals were connected by a wire, electricity was able to flow. An example of a simple galvanic cell is shown in Figure 2-5:
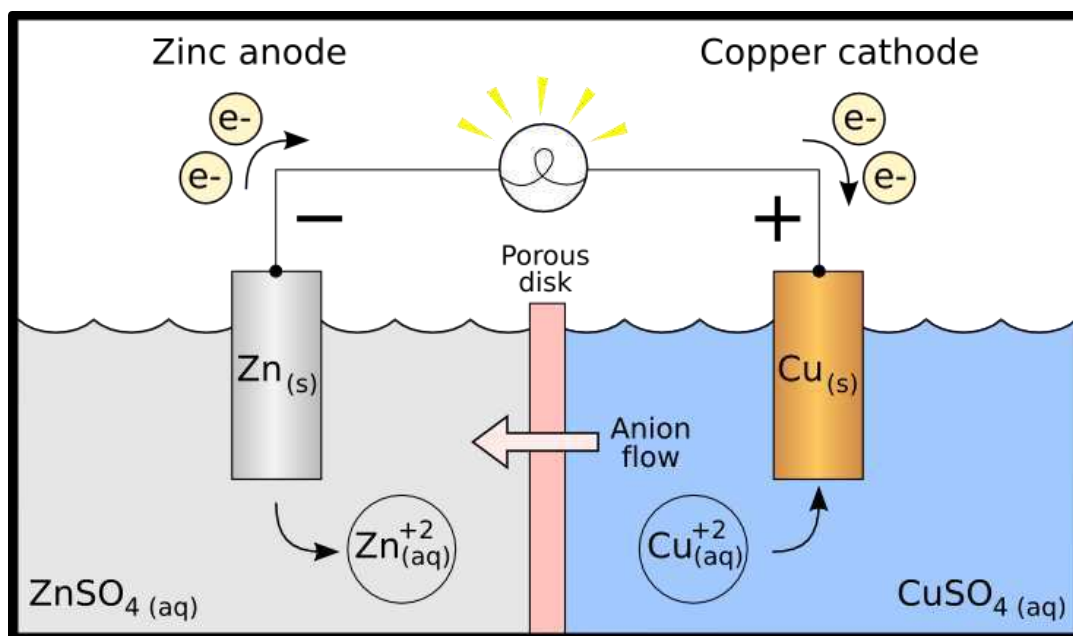
Figure 2-5: A galvanic cell depicting a reaction between Zn and Cu in a Sulfate solution (Ohiostandard).

This is a classic example of a primary battery consisting of two different metals engaged in a redox reaction. When this reaction has reached an equilibrium, the galvanic cell is entirely spent, and the zinc plate and aqueous solutions must be replaced before the cell could be re-used. Because the copper plate is predominately present as a surface for the copper deposition from the $CuSO_4$ solution, it is not necessary to replace it. Ultimately, primary batteries were a basic technology that were effective in establishing a means to harvest electricity from chemical reactions. However, because they are not electrically rechargeable, they are essentially unsuitable for electricity storage.

2.2.2 Secondary Batteries

A secondary battery is quite similar to a primary battery; however, it is suitable for electrical storage because the system is rechargeable. Unlike a primary battery, which always has a specific negative anode and a positive cathode, the charges of a secondary battery's electrodes can reverse during the charging process (Kiehne, 2003) with the electrons flowing in the

opposite direction with the help of an eternal power source. This ultimately causes the reduction

of one electrode and oxidation of the other, allowing for the electrodes to be reversed and the

battery to be reused. Lithium ion batteries are very notable for their recharging capabilities;

Figure 2-6 depicts the charged and discharged states of a lithium ion battery.
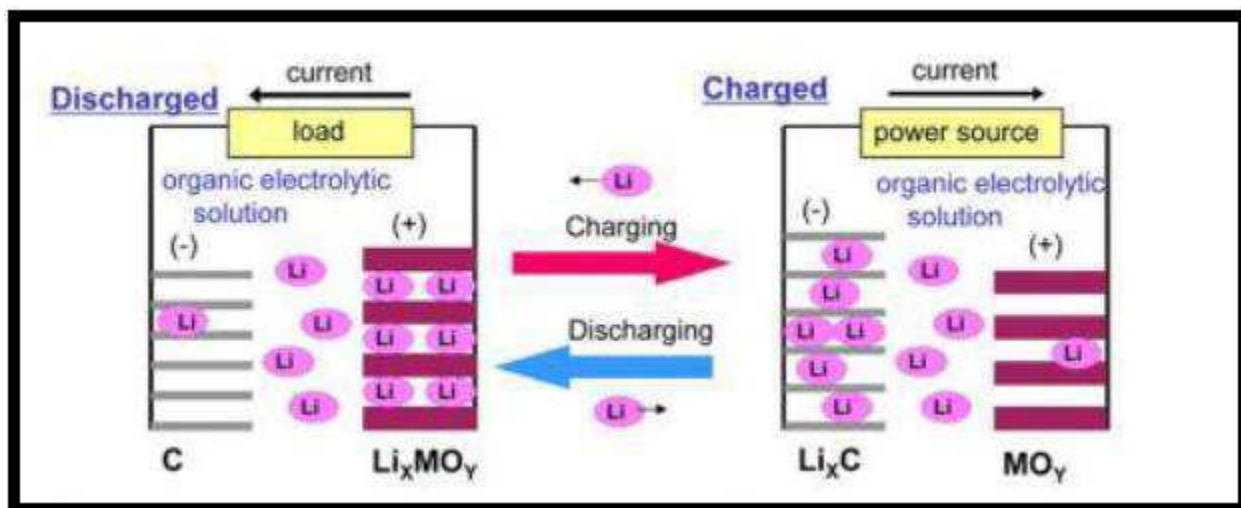
Figure 2-6: The charged and discharged state of a lithium ion battery (Horiba, 2014).

While it is technically possible for almost all batteries to be rechargeable, it often is not

thermodynamically or mechanically feasible to construct a secondary battery from all possible

electrochemical redox reactions. Oftentimes, there are many factors at play when a redox

reaction is considered for a battery, dependent on the thermodynamics and reaction kinetics

(Cheng et al., 2011). Moreover, in practice, it is difficult to construct a battery that provides close

to the theoretical performance of the redox reaction since certain limiting factors exist for the

anode and cathode kinetics as well as mass transfer limitation in the separator and electrodes.

These potential losses are frequently additive during battery performance and are simply referred

to as overpotential. These overpotential losses determine the cell efficiency for energy storage.

If effective materials and chemistry are found for designing secondary battery, it is

typically rigorously examined for rechargeability. While the process of recharging conceptually

causes the system to "refresh," there are often irreversible losses each time the battery is discharged and recharged including morphological changes such as dendrite foundation. An effective secondary battery is able to minimize these losses and achieve numerous discharge/charge cycles over its lifetime. All reversible batteries thus do have a finite lifetime.

2.3 Current Battery Designs

2.3.1 Flow Batteries

Many recent developments have begun to make flow batteries more attractive for large-scale energy storage. Unlike most batteries where all materials are contained within the anode and the cathode chambers, flow batteries consist of an electrolyte for each electrode that is constantly refreshed from separate tanks of aqueous solutions. The anode, this cathode, and the separator are still static in this cell, but the flowing electrolytes ensure a long discharge duration for the battery and high resilience to multiple cycles. The basic design of a flow battery is shown in Figure 2-7 (Webber, et al., 2011).
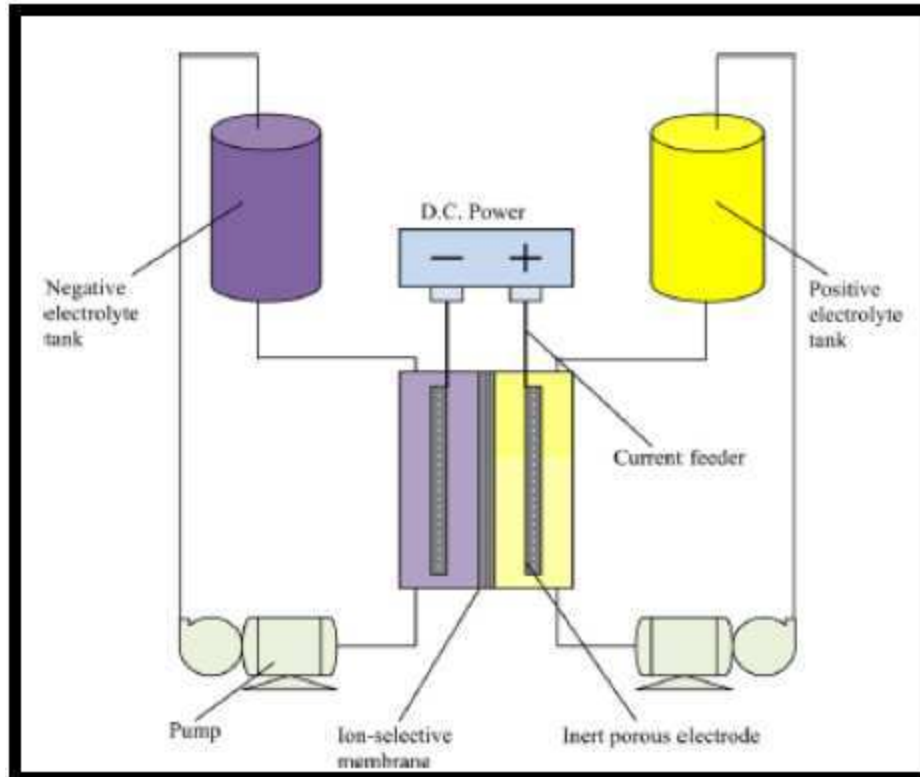
Figure 2-7: Schematic of a generic flow battery system (Skyllas-Kazacos et al., 2011).

While only a single cell is shown in Figure 2-7, flow batteries are designed to be scalable, consisting of multiple cells that all share the same electrolytes. This allows for flow batteries to sum to high voltages very efficiently (Wang, 2010; Weber, et al., 2011). Moreover, the flowing electrolyte is refreshable, which is incredibly effective for recharging, ensuring that flow batteries have high performance and durability. Additionally, they can reach up to 85% efficiency (Skyllas-Kazocos et al, 2011). The key feature of flow batteries that is attractive is that power (number of cells) requirements are decoupled from capacity (tank size) requirements. On the other hand, in conventional batteries these are coupled. More storage simple means more batteries, whereas in flow batteries, this is accommodated by increasing the size of storage tanks.

The construction of the cell consists of an anode and a cathode submerged in their respective electrolyte solutions. These solutions are separated by an ionic exchange membrane

and separator, which allows for the passage of specific ions to allow the battery to function, without allowing the electrolytes to mix. During discharge reaction, it is actually the anodic electrolyte that is oxidized, while the electrons are passed through the anode to the cathode. This, in turn, reduces the cathodic electrolyte. Because the anode and cathode are virtually unaffected, fresh anodic and cathodic electrolyte can flow into the system to continue to react. For recharging, the same process occurs, except the cathodic electrolyte is oxidized and the anodic electrolyte is reduced. This design is highly robust because the actual redox reaction is occurring between flowing solutions. This is advantageous because the electrolytes are immune to dendrite formation, which is often a major factor in causing conventional batteries to fail extended discharge/charge cycles (Weber, et al., 2011).

One specific flow battery design was developed by Skyllas-Kazacos et al. (2011), using a zinc-bromide redox reaction. A schematic of the design is shown in Figure 2-8.
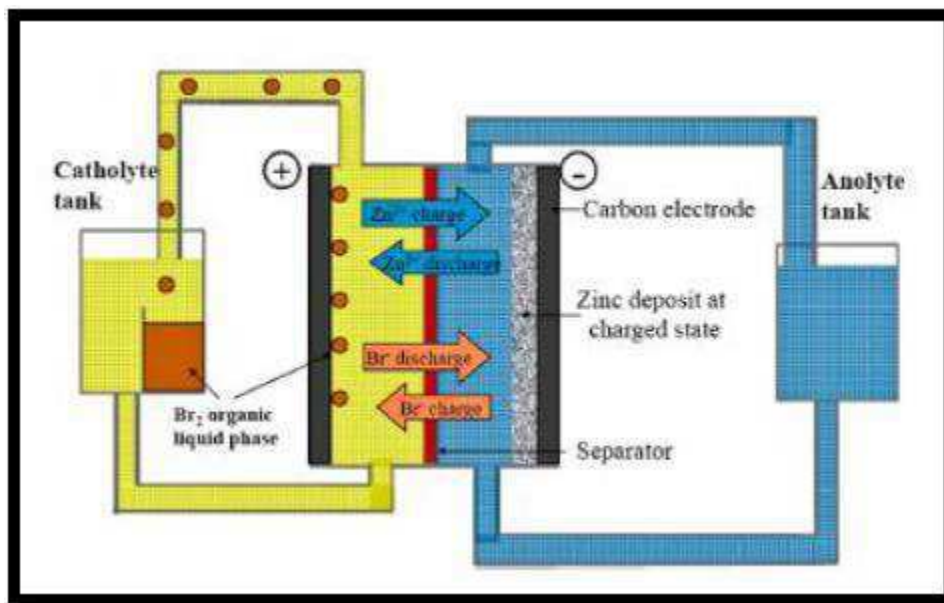
Figure 2-8: Schematic of a zinc-bromide flow battery system (Skyllas-Kazacos, et al., 2011).

This battery consists of a bromine cathode solution and a solid zinc anode. While this is a functional version of a flow battery, it is often limited in performance, particularly because of the

variable thickness of the zinc anode. Moreover, this battery currently faces issues with low energy density, but this can ultimately be addressed by many of these batteries in series (Skyllas-Kazacos, et al., 2011).

Despite the great promise of flow batteries, they are expensive, requiring roughly $2500 per kilowatt. Additionally, there is still a lot of information that is largely unknown concerning the overall performance of these batteries; however, this is primarily because the technology is still very new. These issues may be addressed as the technology is studied more, as flow batteries are still a very new type of battery that has only recently been acquiring attention. As this technology receives more attention, future research is going to have to be used to solve a significant issue facing flow batteries: active material crossover through the membrane. Since the electrolyte solutions are the primary active components in a flow battery, it is vital that they remain separated throughout the entire operation. If the two solutions are allowed to mix, the battery system will fail and a significant amount of fuel will become contaminated (Weber, et al., 2011).

One area of research is currently addressing the issue of active material crossover using a vanadium sulfate for the anode and cathode of the battery. Vanadium has a large number of oxidized states (+2, +3, +4, and +5), which it can vary among in the presence of sulfate ions. The anode of this system contains V^{2+} (charged) or V^{3+} (discharged) while the cathode contains V^{5+} (charged) or V^{4+} (discharged). While the usage of vanadium in a flow battery eliminates any safety concerns surrounding active material crossover, it does not prevent it from happening entirely, which will still result in the failure of the cell (Schwenzer, et al., 2011). While the vanadium flow battery system shows promise, the initial investment and inconsistent cause of failure are being investigated further.

2.3.2 Metal-Air Batteries

Metal-air batteries have a common component, the oxygen electrode, with zinc-air batteries being the primary example. Since the basis of metal-air reactions fundamentally consists of electrons moving from the metal to the oxide, the design for metal-air batteries typically consists of a metal anode, oxygen/oxide cathode, and an anion exchange membrane (AEM). However, due to the generally more stable nature of metal oxides, most metal-air batteries are not rechargeable since it is generally inefficient to attempt to undo the oxidation process within a battery. Of course, because of this stability, the performance and energy density density of these types of batteries is also higher than those of the standard alkaline batteries or lead-acid batteries.

The zinc-air battery has been a stepping stone for the design of liquid metal-air batteries since it is a commercially available primary metal-air battery with similar chemistry. Of course, zinc-air batteries face the limitation that they are not rechargeable, which has started to be addressed in some research (Deiss, et al, 2002). Nevertheless, commercially available zinc-air batteries have offered some useful insights to the design of metal-air batteries. Like most batteries, the ion (oxide ion) is carried through an electrolyte layer, which consists of an AEM in the zinc-air battery. However, the zinc-air battery ensures an effective reaction between zinc and oxygen by creating an electrolyte-zinc slurry to increase the surface area of the zinc. An example of this system is shown in Figure 2-9 (Deiss, et al, 2002).
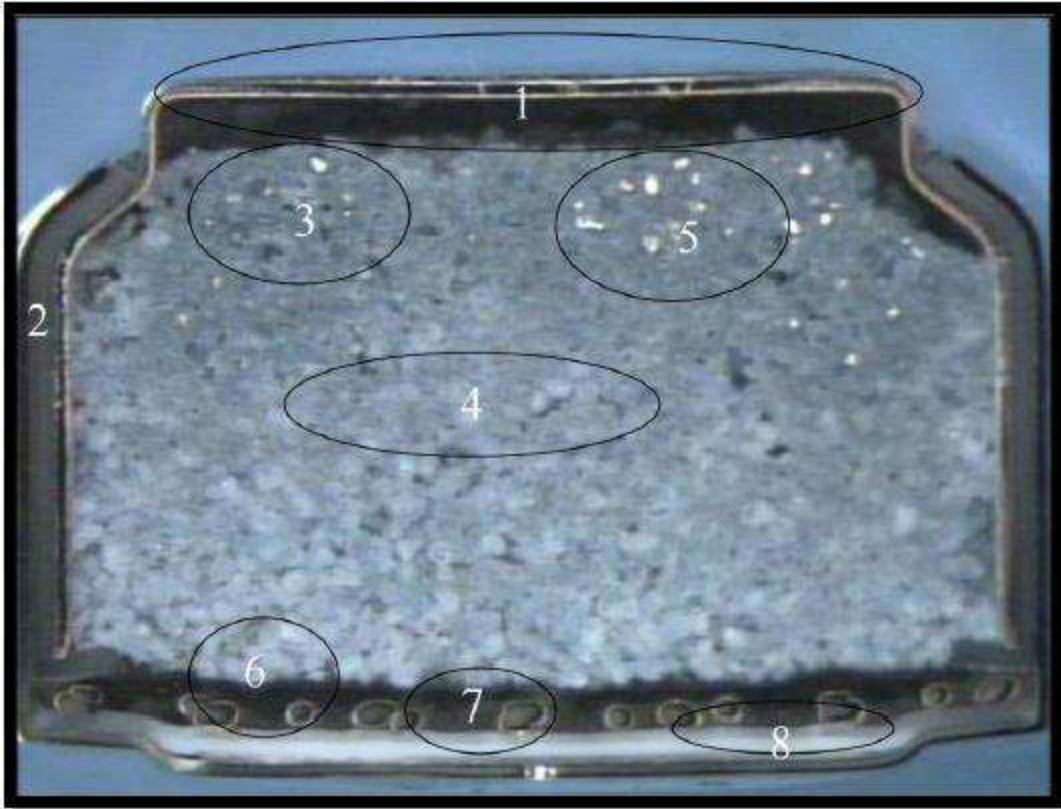
Figure 2-9: Commercial primary Zn-Air battery (size D13) cutout(Deiss, et al, 2002).

The D13 Zn-Air battery shown in Figure 2-9 shows the 3-dimensional reaction metal-electrolyte interface. Areas circled in Figure 2-9 are as follows:

1. Headspace in cell

2. Electrical insulation to prevent short circuiting

3. Type II discharged zinc particles (without dendrite formation)

4. Type I discharged zinc particles (with dendrite formation)

5. Non-discharged zinc particles

6. Mesh screen for cathode assembly

7. PTFE layer for cathode assembly

8. MnO_2 catalyzed gas diffusion layer

Some of the attempts at improving the rechargeability of the Zn-Air system have been made by setting up the system in a manner similar to a fuel cell. Deiss et al. (2002) created this experiment using purer conditions in an effort to address the dendrite formation in standard Zn-Air system recharging. The schematic of their design is shown in Figure 2-10.
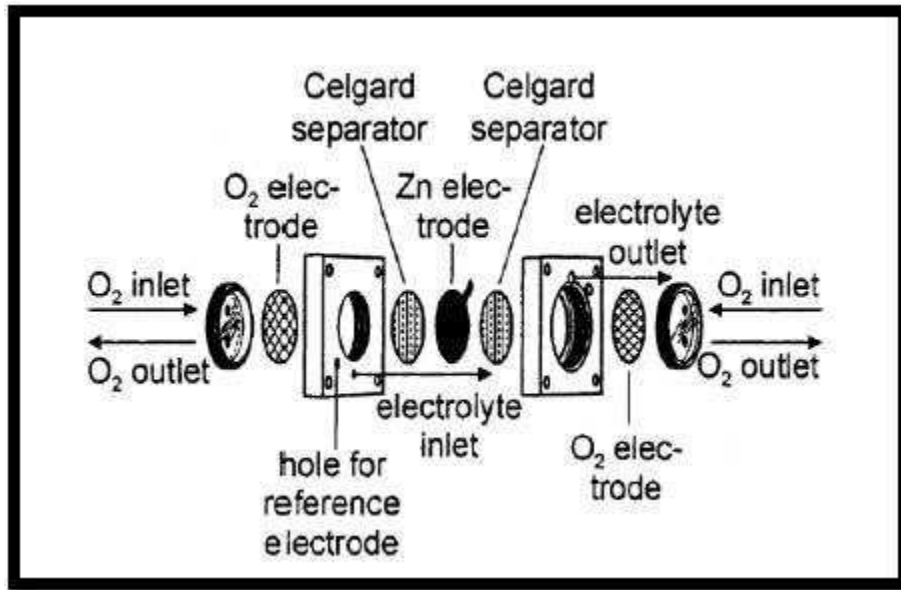
Figure 2-10: Zn-Air system with two air cathodes (Deiss, et al., 2002).

There have been other developments with metal-air batteries, most notably being lithium-air, which has had limited success. Like many other metal-air batteries, lithium-air batteries exhibit high energy density and high reactivity; however, it is also known to suffer from the same disadvantages, such as poor rechargeability and degradation. This degradation is natural among most metal-air batteries and typically consists of the formation of dendrites. However, some research shows that lithium-air may have potential when using a solid electrolyte interphase (SEI) on the anode, which serves as a stabilizer and a suppressant for dendrite formation (Lee et al., 2011). Nevertheless, this development has proven to be a useful tool in improving liquid metal-air battery design.

Commercially available metal-air batteries, primarily zinc-air batteries, also serve as an excellent standard to determine the effectiveness of new battery designs. Since these batteries are fairly well developed, they can be used as a reference for possible stepping stones in liquid metal-air battery designs. For example, electrolyte-zinc slurries are common in zinc-air batteries, which could be a useful technique for liquid metal components. Nevertheless, primary metal-air batteries, especially Zn-Air batteries are fairly well established technologies that currently face major issues with recharging. For this reason, they will be used as a baseline in this investigation.

2.3.3 Liquid Metal Batteries

Liquid metal batteries are a conceptual advance in battery technology development. While it is still in fairly early developmental phases, Sadoway et al. have made significant steps in advancing this technology for pontential application in energy storage (Sadoway, 2003). Because the entire battery consists completely of liquid components, the technology is faced with certain limitations, but also offers some meaningful advantages. In the typical, the liquid metal battery consists of three immiscible phases, a liquid metal layer case, an electrolyte layer, and another liquid metal layer, while in a charged state; or a liquid metal layer, electrolyte layer, and liquid metal alloy layer while discharged. Since it is essential that the two liquid metal layers remain out of contact, this unfortunately limits liquid metal batteries to more stationary applications. Moreover, because the reaction powering the battery consists of a metal-metal alloy reaction, current densities and voltages are generally fairly low for liquid metal batteries.
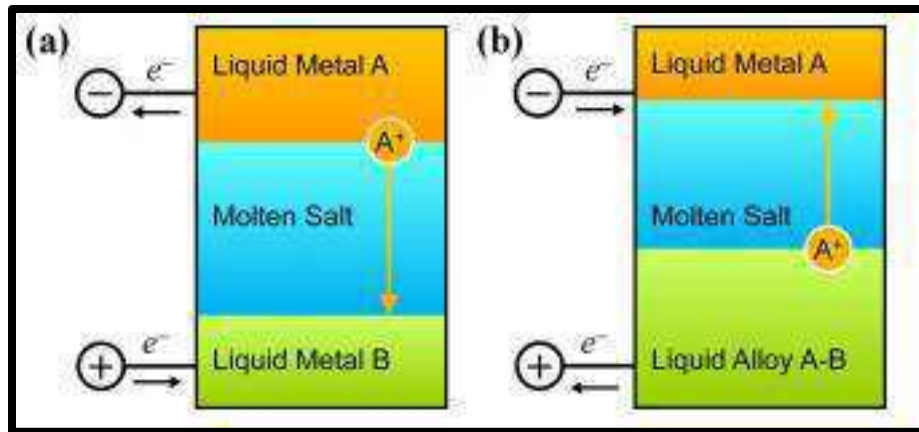
Figure 2-11: Liquid metal battery in two different states: a) discharging and b) charging (Kim, et al., 2012).

Nevertheless, liquid metal batteries have a distinct advantage in the form of their rechargeability and inherent sustainability. Also, because the ions are so easily passed through the molten salt electrolyte layer with its high conductivity, it is fairly trivial to recharge a liquid metal battery. And because liquid metal batteries generate fairly low potentials, it also takes a fairly low amount of energy to recharge them.

Electrode materials that specifically work well for liquid metal batteries typically have three desirable properties: low melting points, moderate to good electrical conductivity, and low cost. Since these batteries use molten salts as electrolytes, low melting point specifically means any metals with a melting point below 1000ºC, which includes most metals that satisfy the other desirable properties. Anodes and cathodes of liquid metal batteries are separated by the deposition potentials of the metals. Generally, the anodes should have a deposition less than -2.0 V and the cathodes should have a deposition potential greater than -1.0 V. As with all batteries, the greater the difference in deposition potential, the better the battery performs. Reasonable anode and cathode candidates for liquid metal air batteries are highlighted in Figure 2-12 in orange and green, respectively (LaMonica, 2013).

Figure 2-12: Different candidates for anodes (orange) and cathodes (green) (LaMonica, 2013).

One notable example of a successful implementation of a liquid-metal battery is a three layer battery, using a magnesium anode and an antimony cathode (LaMonica, 2013). In fact, this system has already seen quite a bit of success being scaled up to a 500 kW system that is able to store up to 1 MWh of energy. Moreover, the system is incredibly durable, able to withstand thousands of discharge/charge cycles over its lifetime. Of course, there is no dendrite formation or any other irreversible morphological changes. Figure 2-13 shows the relationship between the discharge capacity of the battery against the number of full depth of discharge cycles (Ambri, 2016). Because of the current design's durability and capacity, it is already a promising candidate for a rechargeable battery system to assist a electrical grid.
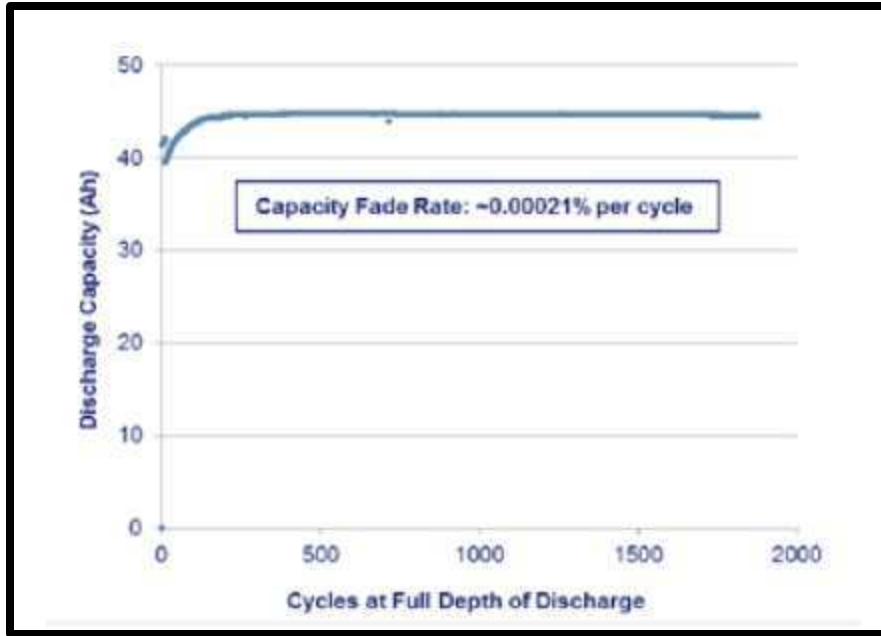
Figure 2-13: Discharge capacity against number of discharge/charge cycles of a three layer liquid-metal battery (Ambri, 2016).

Despite the possible advantages of liquid metal batteries, they do face certain downsides: high operating temperatures, low specific energy densities, low cell voltages, corrosive metals, and potentially high discharge rates. Since it is quite common for these batteries to have energy densities lower than 300 W*h*kg^{-1} and voltages lower than 1.0 V, any system using liquid metal batteries would require significantly more cells than other batteries. In fact, a typical liquid metal battery would have to be 100 times more massive than a standard lead-acid battery to have the same energy output (IAE 2014). Moreover, issues of corrosion are fairly correlated to the high temperatures required for the cells. At higher temperatures, materials' corrosive properties can have a meaningful impact on performance. This issue can be partly combated using metal alloys instead of pure metal components. Nevertheless, the battery proposed from Ambri holds great promise and is certainly worth pursing in future investigations. However, the high operating temperatures and corrosive conditions makes this system challenging.

2.3.4 Liquid Metal-Air Batteries

Liquid metal- air batteries bridge the individual shortcomings of metal-air batteries, liquid metal batteries, and flow batteries. In particular, the liquid metal design combats dendrite formation and low life cycles limiting metal-air batteries, while the metal-air reaction offers higher energy densities than both liquid metal batteries and flow batteries. Despite these advantages, liquid metal-air batteries have not yet been investigated in detail. Nevertheless, this novel technology is very promising due to its high energy density, its resistance to dendrite formation, and its longevity in spite of numerous charge/discharge cycles (Otaegui et al., 2014).

Many different materials were considered to further investigate liquid metal-air batteries. These candidates were eliminated to some of the more accessible battery systems and metals with low melting points. A comparison of the theoretical energy densities of the commercially available Zn-Air system and a proposed Ga-Air system are shown in Table 2-1. The products of the Ga-Air system is also considered in this calculation, where gallium hydroxide ($Ga(OH)_3$) and gallium oxide (Ga_2O_3) are the two products.

Table 2-1: Energy Densities of Zn-Air and Ga-Air Systems

Electrochemical System	Gravimetric Energy Density (Wh/kg)	Volumetric Energy Density (Wh/L)
Zn-air	1,361	9,723
Ga-air (gallium hydroxide)	1,895	11,549
Ga-air (gallium oxide)	1,989	12,121

Due to its stability and overall high general voltage, the gallium-air system looks to be quite promising when compared to other designs. Most of those designs can only attain voltages typically 80% as high with comparable current densities. Additionally, gallium is reasonably

abundant in the Earth's crust, at 19 ppm (Gagnon, 2007). While this may seem like a low relative

abundance, it is nearly identical to lithium, which is 20 ppm (Gagnon, 2007), a metal that is

frequently used for batteries. Gallium is not mined directly, like lithium, and is instead found as a

byproduct to bauxite mining (Kramer, 2006). While the abundance of these materials are similar,

the prices are dissimilar, however. As of 2013, gallium was priced around $280 per kilogram

(USGS, 2013), whereas lithium was priced at $95 per kilogram as of 1998 (Ober, 1998).

Moreover, the liquid design offers a distinct advantage over traditional alkaline metal-air

batteries because of ease of charging and simplicity of replacing the anode material by flowing a

liquid metal (as opposed to replacing a chunk of reacted solid metal oxide/hydroxide).

Ultimately, this makes liquid gallium-air batteries a very novel concept.

However, gallium in an electrochemical system is not very well researched, although its

physical properties are quite attractive for the scope of this investigation. Some of gallium's most

notable physical properties are its low melting point of 29.77°C, minimal safety concerns, and

minimal corrosion at low temperatures (Howard, et al., 2015). Chemically, it has quite a few

desirable properties as well. Firstly, its low activation energy barrier enables it to react easily

with oxygen at lower temperatures in the presence of alkaline solutions. Secondly, it is possible

that its oxidized layer may improve the transport of oxygen to internal locations in the gallium by

using the stable intermediate $Ga(OH)_4^-$ (Chung, 2013). The conditions at which this phenomenon

may occur are most easily visualized using gallium's Pourbaix Diagram in Figure 2-14

(Schweitzer, 2009).
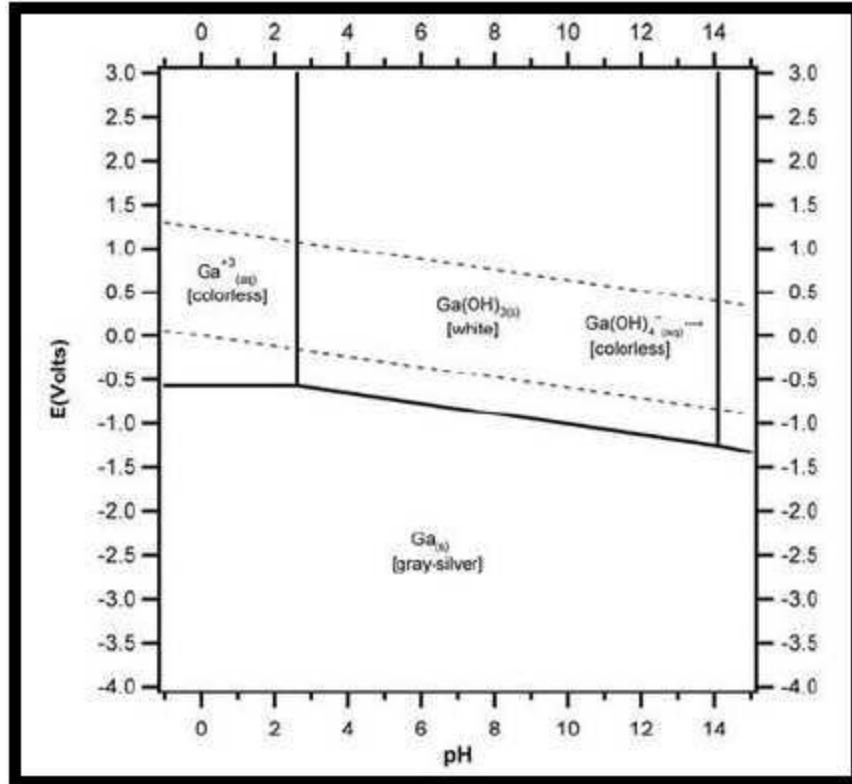
Figure 2-14: Gallium's Pourbaix diagram; the thermodynamically stable region lies between the dotted lines (Schweitzer, 2009).

The thermodynamically favorable region in gallium's Pourbaix diagram mostly lies above 0 V for the entire range of operating pH's. This means that the reaction between gallium and oxygen is quite favorable at any pH. Since sparse amounts of research has been performed on this reaction, the Ga-Air system will be the primary focus for this investigation.

3 Methodology

3.1 Design of the Battery

Modifications were made to the Li-Air Swagelok cell used in an investigation by Beattie et al. (2009), to use the same cell for the Ga-Air system. Figure 3-1 shows an exploded view of the cell construction.
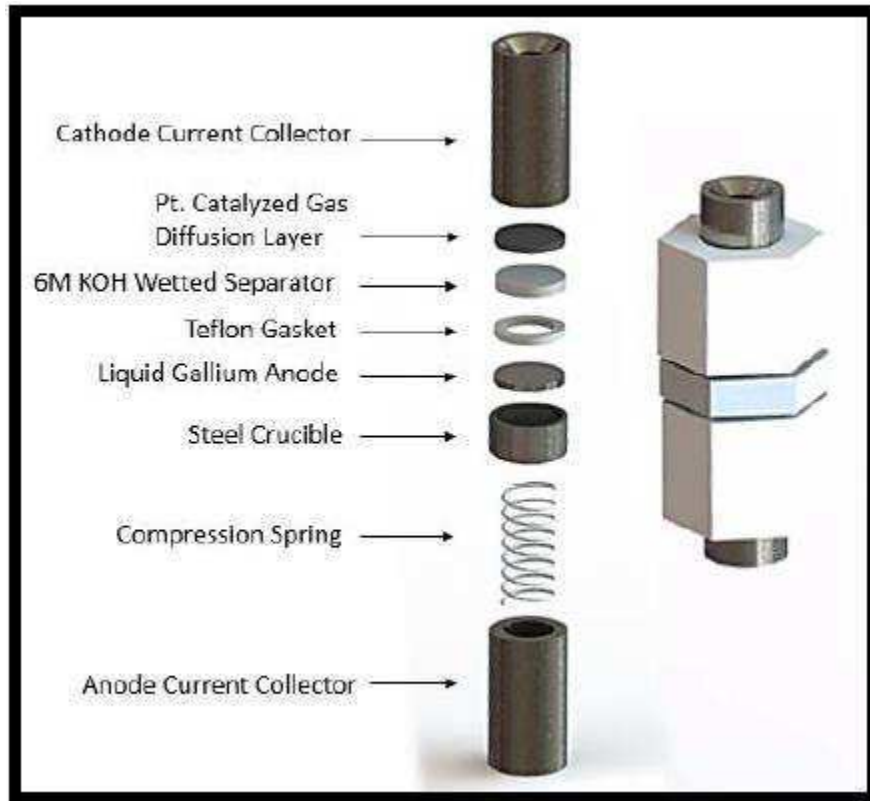
Figure 3-1: Exploded and constructed view of the Swagelok cell used for the Ga-Air system. The cell is stacked vertically, consisting primarily of an anode current collector, gallium anode, electrolyte-soaked separator, gas diffusion layer, and cathode current collector. This cell is normally oriented with the cathode facing down.

3.2 Materials

All materials used to construct the Ga-Air system were chosen to be both non-toxic and environmentally friendly, with the exception of potassium hydroxide (KOH), which is the electrolyte for the passage of hydroxyl ions from the cathode to the anode.

3.2.1 Mechanical Parts

Some mechanical parts of the Swagelok cell had to be made to specification. The current

collectors consisted of three primary component types:

- Two stainless steel node current collectors, manufactured by Target Machine (Figure 3-2)

- Stainless steel crucible machined by WPI Unit Operations Lab.

- McCaster Carr 302 Stainless Steel Precision Compression Spring (0.750 in long, 0.36 in

   O.D., 0.026 in thick wire).
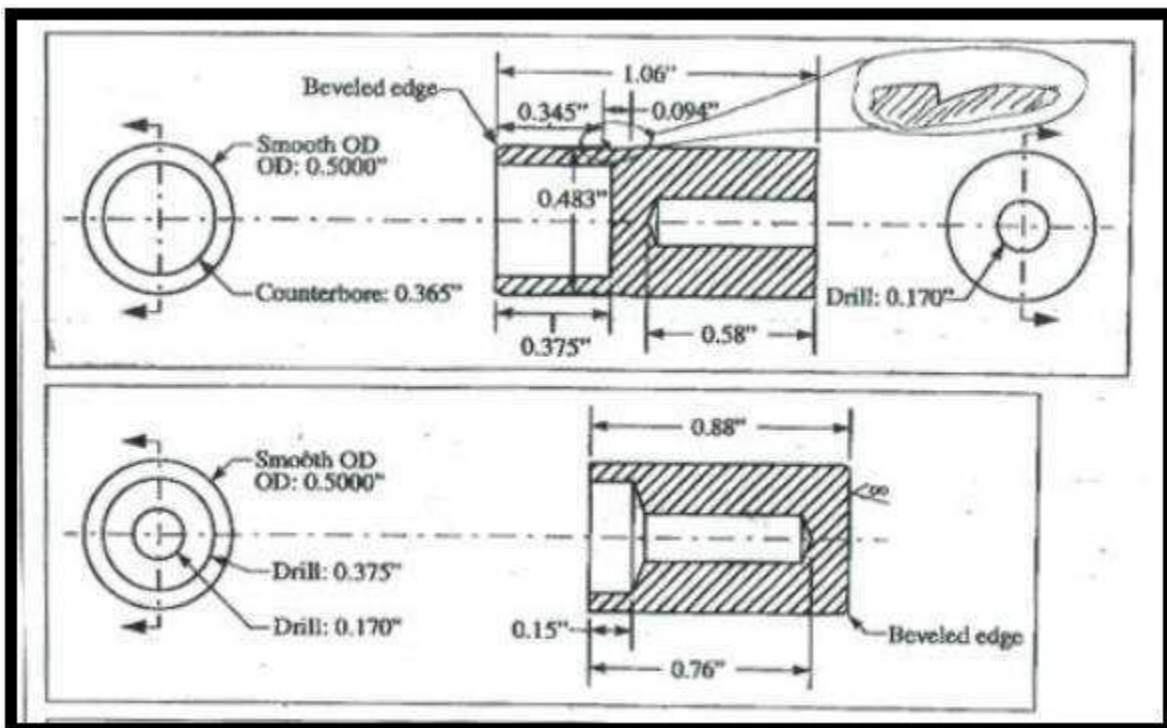
Figure 3-2: The two stainless steel current collectors: anode (top) and cathode (bottom) (Part Number PC-08, 0.5" OD).

These components were held together in a PTFE or stainless steel Swagelok Tube Fitting

with Ferrules, Union, 1/2 in. Tube OD encasing.

3.2.2 Liquid Metal Anode

The anode used for all of this investigation was pure gallium metal, which was melted

down prior to testing. It was the material of choice because of its highly desirable physical and

chemical properties. Physically, it has a low melting point (29.77°C), self-healing, and non-toxic. Chemically, it is reactive with oxygen and has an approachable thermodynamic reversibility.

3.2.3 Electrolyte and Separator

A potassium hydroxide solution soaked separator was used for all tests throughout the investigation. For the majority of tests, this separator was soaked with 33.6 wt.% potassium hydroxide solution (6M KOH). This concentration was chosen because it has a high ionic conductivity and can potentially produce gallium tetrahydoxyl gallate ions ($Ga(OH)_4^-$), which will help pass oxygen ions to unreacted parts of gallium metal. To prevent leakage, the separator was placed on top of the anode stainless steel crucible with a Teflon spacer to avoid battery short circuit. Tests primarily used yttria-stabilized zirconia cloth as the electrolyte separator material. Zircar woven cloth type ZYK-15 (yttria-stabilized zirconia) was used for the Ga-air cell. In some additional applications, glass fiber cloth was used as a separator instead, using EMD Millipore Glass Fiber Filters without Binders with a pore size of 1μm. To avoid carbonation of the potassium hydroxide electrolyte for some tests anion exchange membranes (AEM) from Membrane International, model AMI-7001S, were also tested as a separator material. The AEM consists of a long chain polymer to counteract the time of carbonation (Vega et al., 2010). SEPARION (Litarion S240P30) was also attempted as a separator as it is also an organic compound of PET non-woven which should have resistance to carbonation.

3.2.4 Air Cathode

Two different air cathodes were used during the course of the investigation. Prior research for metal-air batteries has utilized MnO_2 catalysts (Otageui, 2014), which were a basis for a cathode used in this investigation. The first and less common cathode material was a proprietary MnO_2-Carbon blend with a nickel mesh. The second and most common cathode used

was a Pt-catalyzed gas diffusion layer (GDL), which allowed for a more effective reduction and evolution of oxygen from air. The GDL was constructed from graphitized carbon. This GDL was then lightly coated in a fine platinum catalyst layer. This was obtained from FuelCell.com part number EC-TP1-030T-Pak.

3.3 Ga-Air Cell Set Up and Testing

The Ga-Air system was assembled in the following two locations:

- A benchtop located in WPI's Fuel Cell Laboratory

- A fume hood located at Bayreuth University's Battery Laboratory, in Bayreuth, Germany

The cell was assembled by first constructing the inner components—the crucible, the spring, and the anode/cathode. After these components were assembled, they were placed inside a Swagelok fitting. More detailed procedures can be found in Appendices A-D.

The cell was assembled from the anode to the cathode. 1.2 to 1.6 grams of gallium was melted and put into the crucible. After that, a Teflon gasket was layered on top of the crucible to ensure sealing and to prevent the gallium from leaking. The Teflon gasket was manufactured using two hole punches: one with the same outer diameter of the crucible and the other with a smaller diameter to allow contact between the gallium and the electrolyte. Next, the KOH soaked separator was placed on top of the gasket, and finally the GDL was placed on the separator with the catalyzed side down and in contact with the electrolyte. The cathode current collector node was then screwed on to the PTFE union to guarantee proper contact between layers. The separators that were used were zirconia cloth, an anion exchange membrane (AEM), glass fiber sheets, or SEPARION (Litarion S240P30). An additional set up was included for pure oxygen feed tests.

Oven tests were reserved exclusively for tests over 80°C; otherwise, a heating lamp was generally used as it provided more uniform heating over the range of 30°C to 80°C. Preliminary temperature tests were used to determine the most consistent heating methods for the Ga-Air system (Figure 3-3). The heating lamp generally heated consistently, but had a maximum limit of 70°C. Oven heating could exceed this maximum temperature, exceeding 100°C, but had a variance of ±10°C. Water bath heating was also attempted, which could consistently heat up to 60°C, but it increased the difficulty of cell maintenance.
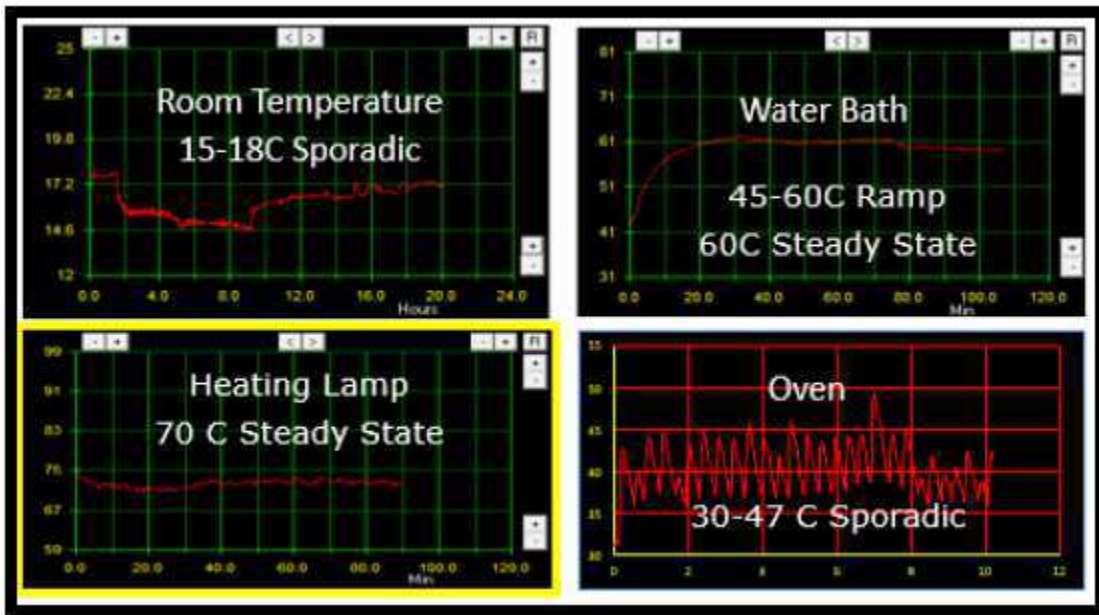
Figure 3-3: Evaluations of various available heating instruments

When the cell was constructed, it was placed, cathode side down, under the heat lamp for 5 to 10 minutes. This time period was to ensure that the gallium was entirely liquid prior to testing. The cell remained in the position shown in Figure 3-4 for the entirety of the test. The active electrical areas of the cell was restricted exclusively to the anode and cathode current collectors. All other parts of the cell were insulated.
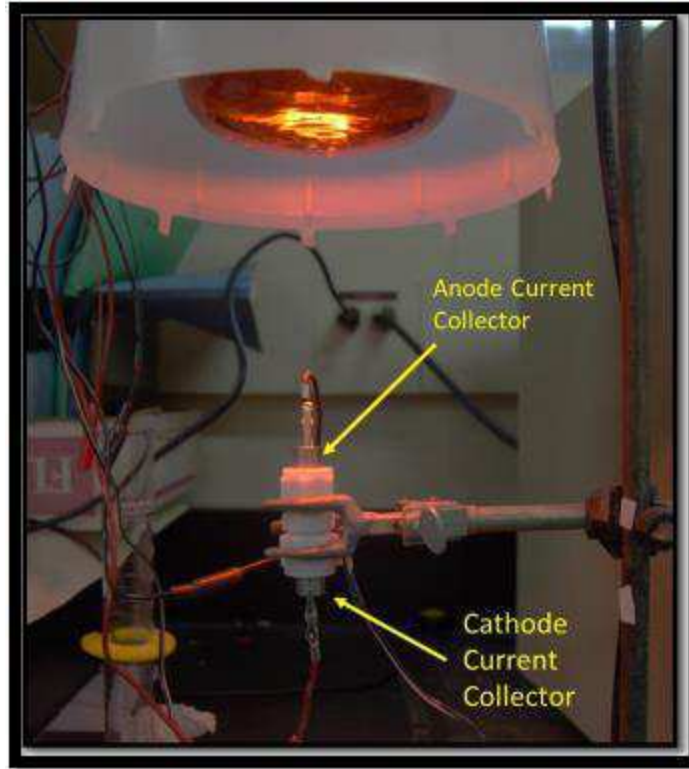
Figure 3-4: The ring stand setup under a heat lamp

For oven tests, the cell was either placed in the same orientation in a ring stand inside the oven or in a pre-made rack as shown in Figure 3-5.
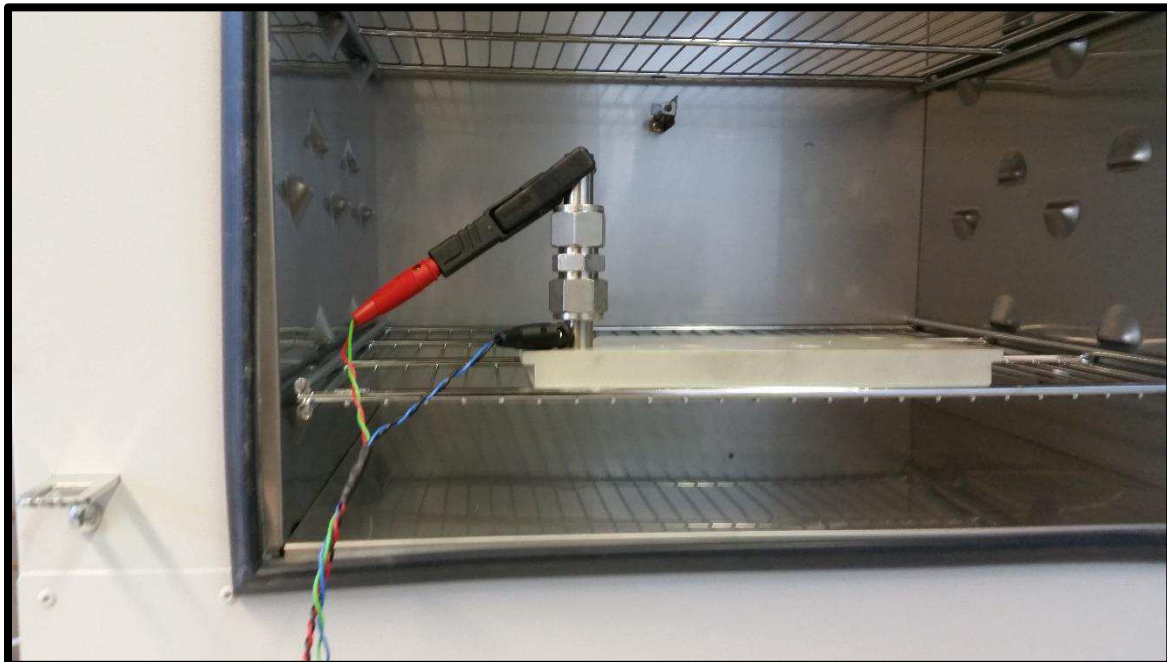
Figure 3-5: The pre-made rack for the heating in the oven

3.3.1 Zirconia Cloth, Glass Fiber Sheet, and SEPARION Electrolyte Fabrication

Zirconia cloth type ZYK-15 manufactured by Zircar Zirconia, Inc., glass fiber sheet from

EMD Millipore Glass Fiber Filters without Binders, or SEPARION (Litarion S240P30) was cut

to a defined specification and wetted with 33.6 wt.% KOH. The separator was first cut using a

metal punch with a diameter of 11.8mm. Then the cut zirconia paper was soaked for 20 minutes

in 33.6 wt.% KOH solution. The solution was covered throughout the 20 minute soaking period

to prevent premature carbonation of the KOH. The step-by-step procedure is described in

Appendix B: Electrolyte Procedure.

3.3.2 Anion Exchange Membrane Procedure

To determine the potential effect of carbonation of the KOH electrolyte, tests using an

anion exchange membrane (AEM), manufactured by Membrane International model AMI-

7001S, were also conducted. The AEM, like the zirconia paper, was cut to the same size using a

punch and was soaked in a 33.6 wt.% KOH solution. The AEM, based on required preparation

technique, was soaked for over 24 hours in the alkaline electrolyte prior to assembly and testing.

After the initial soaking, both sides of the AEM was rinsed using deionized water and then

wetted with a few drops of 33.6 wt.% KOH solution. Then the separator was applied to the cell

in the same manner as the zirconia cloth. A more detailed step by step procedure is available in

Appendix B: Electrolyte Procedure.

3.3.3 Pure Oxygen Testing

Pure oxygen tests were set up by connecting an oxygen tank to tubing that led to the air

cathode of the assembled cell. A needle valve was included in order to more precisely adjust the

flow. Further Teflon tubing was connected with an inner diameter of 1/8". This small diameter

allowed for the tubing to fit into the open part of the cathode node of the Swagelok cell to directly flow oxygen into the cathode. This set up provided enough room for the leads to be attached to the cell so measurements could be taken.

3.4 Battery Analyzer Testing Procedure (BAWIN500 Program)

All testing was performed on a modified version of Battery Metric's MC2020 model. This model was specifically customized such that it could precisely discharge and charge the batteries at low currents (0.1mA, 1mA, 10mA). The software used with this was Battery Metric's BAWIN500 program. More details for these procedures and screenshots can be found in Appendix E.

3.4.1 Polarization Testing

Polarization curves were obtained by loading a saved customizable program. This program was designed to perform a galvanostaircase polarization, where current is increased in a step-wise manner for a brief period of time. The battery was discharged over a range of currents from 0 to 15 mA. Each step discharged the cell for 20s with data points logged every 10 seconds. The steps increased in 0.1 mA increments until 7 mA was reached and then the current was increased in 0.5 mA increments until it reached 15 mA. In this case, the cut off voltage was set to 0.001V to allow for the full range of currents to be tested.

3.4.2 Discharge Testing

Similar to the polarization testing, a program was set up to run discharge tests. The discharge tests allowed for a 2 minute initial pause period in order to get an average OCV and then the program would drain a constant 0.5 mA current from the cell until the cell voltage reached a 0.3 V cutoff. This test was often completed after performing a polarization test in order to achieve each type of test for a specified set of conditions.

4 Results and Discussion

4.1 Theoretical Calculations

Before thoroughly exploring the actual performance of the Ga-air reaction, it is important to establish a baseline expectation in the areas of polarization and discharge performance. Starting with polarization, White (2005) developed a polarization model for Zn-air batteries based on the Butler-Volmer equation (Equation 4.1). In this equation, additional considerations for diffusion limitations are also considered; while this equation was developed with the Zn-air battery in mind, it is applicable for other metal-air systems, including Ga-air systems.

$$V = V_0 - \frac{RT}{\alpha_A F} \sinh^{-1}\left[\frac{1}{2}\left\{\frac{\frac{i_A}{i_{A,0}}}{1-\frac{i_A}{i_{A,L}}}\right\}\right] - \frac{RT}{\alpha_C F} \sinh^{-1}\left[\frac{1}{2}\left\{\frac{\frac{i_C}{i_{C,0}}}{1-\frac{i_C}{i_{C,L}}}\right\}\right] - i\left(\frac{L_{KOH}}{\sigma_{KOH}}\right) - iR_i \qquad (4.1)$$

This equation actually considers the overpotential loss from both electrodes and both electrode ionic and electronic conductivity loss. The values used for the variables in the equation are shown in Table 4-1. V is the modeled voltage, V_0 is the theoretical open circuit voltage, R is the ideal gas constant, T is the system temperature, α_A and α_C are the anodic and cathodic charge transfer quotients, F is the Faraday constant, i_A and i_C are the anodic and cathodic current overpotentials, L_{KOH} is the contact surface area, σ_{KOH} is the conductivity, and R_i is the interfacial cell resistance. Using these variables, it is possible to model polarization curves for a variety of electrochemical systems for a given chemistry. For the purposes of this investigation, two polarization plots were generated for the two possible products of the Ga-air system: Ga_2O_3 and $Ga(OH)_3$.

Table 4-1: Parameters for the Ga-air system polarization models

UNIVERSAL CONSTANTS			
Parameter	Value or Expression	Unit	Reference
F	96.485	C/mol	(Dean and Lange, 1999)
R	8.314	J/mol K	(Dean and Lange, 1999)
OPEN CIRCUIT VOLTAGE			
V_{0,Ga_2O_3}	1.717	V	Calculated, Eq 4-3
$V_{0,Ga(OH)_3}$	1.643	V	Calculated, Eq 4-3
AIR CATHODE OVERPOTENTIAL PARAMETERS			
α_C	$\alpha_O = 0.5$		(Song and Zhang, 2008)[1] (Song & Zhang, 2008)[1]
$i_{C,0}$	$I^0_{O_2} = I^0_{O_2} e^{-Ea/RT}$ $I^0_{O_2} = (9.89 * 10^{-6} Acm^{-2}) e^{-Ea/RT}$ $I^0_{O_2} = (9.89 * 10^{-6} Acm^{-2}) e^{-57.3/RT}$	A/cm^2	(Song and Zhang, 2008)[1] (Qiol et al., 2013)[2] (Song & Zhang, 2008)[1]
$i_{C,L}$	6.56×10^{-11}	A/cm^2	Fitted (White, 2005)
LIQUID GALLIUM ANODE OVERPOTENTIAL PARAMETERS			
α_A	0.5 (Zirconia Cloth) 0.5 (Anion Exchange Membrane)		Fitted from Tafel Plot
$i_{A Ga_2O_3,0}$	3.87×10^{-4} (Zirconia Cloth) 9.922×10^{-5} (Anion Exchange Membrane)	A/cm^2	Fitted from Tafel Plot
$i_{A Ga(OH)_3,0}$	7.25×10^{-5} (Zirconia Cloth) 2.119×10^{-5} (Anion Exchange Membrane)	A/cm^2	Fitted from Tafel Plot
$i_{A,L}$	$i_{AL} = \left(\frac{v_{A,e^-}}{-v_{A,OH^-}} \right) F \gamma_{MA} P_{OH^-,A} c_{OH^-,B}$	A/cm^2	Fitted (White, 2005)
ELECTROLYTE OVERPOTENTIAL PARAMETERS			
σ_{KOH}	$\sigma_{KOH} = K_1(100*w) + K_2(T) + K_3(T^2)$ $+ K_4(T*100*w)$ $+ K_5(T^2(100*w)^{K_6})$ $+ K_7\left(\frac{T}{100*w}\right) + K_8(\frac{100*w}{t})$	S/cm	(Gilliam et al., 2007)[3]
L_{KOH}	0.22	cm^2	Measured
iR_I	0	V	Assumed

[1]For oxygen reduction reaction on a Pt catalyst
[2]Exchange current density for oxygen reduction reaction on a Pt catalyst with 33.6wt% KOH
[3]KOH ionic conductivity as a function of weight percent (100*w) and temperature (T). Empirically fit correlation constants (K_n) found in Figure 4-1

correlation constant	value	units
K_1	0.279 844 803	S/cm
K_2	−0.009 241 294 82	S/(cm K)
K_3	−0.000 149 660 371	S/(cm K^2)
K_4	−0.000 905 209 551	S/(cm K)
K_5	0.000 114 933 252	S/(cm K^2)
K_6	0.176 5	
K_7	0.069 664 851 8	S/(cm K)
K_8	−28.981 565 8	S K/cm

Figure 4-1: Correlation constants relating the conductivity of KOH by weight percent and temperature (Kiehne, 2003).

These parameters were found through a combination of previously collected literature and experimental results. The cathodic polarization parameters were found from literature review of the oxygen reduction reaction on a platinum catalyst in the presence of aqueous alkaline electrolyte. Additionally, polarization loss parameters were also found in literature review, with the exception of the interfacial resistance (iR_I), which was assumed to be 0. While this assumption only holds for a well assembled cell, it was maintained for this model because it only serves as an offset for the polarization curve, leaving the overall shape unaffected.

Because literature relating to the gallium oxidation reaction is quite sparse, experimental data was generated to estimate the anodic polarization parameters. These kinetic parameters can be measured from experimental Tafel plots. Since two potential products are postulated for the Ga-air system, there are two possible thermodynamic potentials. These plots were created according to the following equation:

$$\eta = A * \ln\left(\frac{i}{i_0}\right) \qquad (4.2)$$

Where η is the overpotential, A is the Tafel Slope (kT/eα) (defined above), and i and i_0 are the current density and exchange current density, respectively. This equation generated Figure 4-2 with the standard cell configuration with zirconia cloth and 33.6wt% KOH at 65°C and Figure 4-3 with the standard cell configuration with anion exchange membrane and 33.6wt% KOH at 65°C..
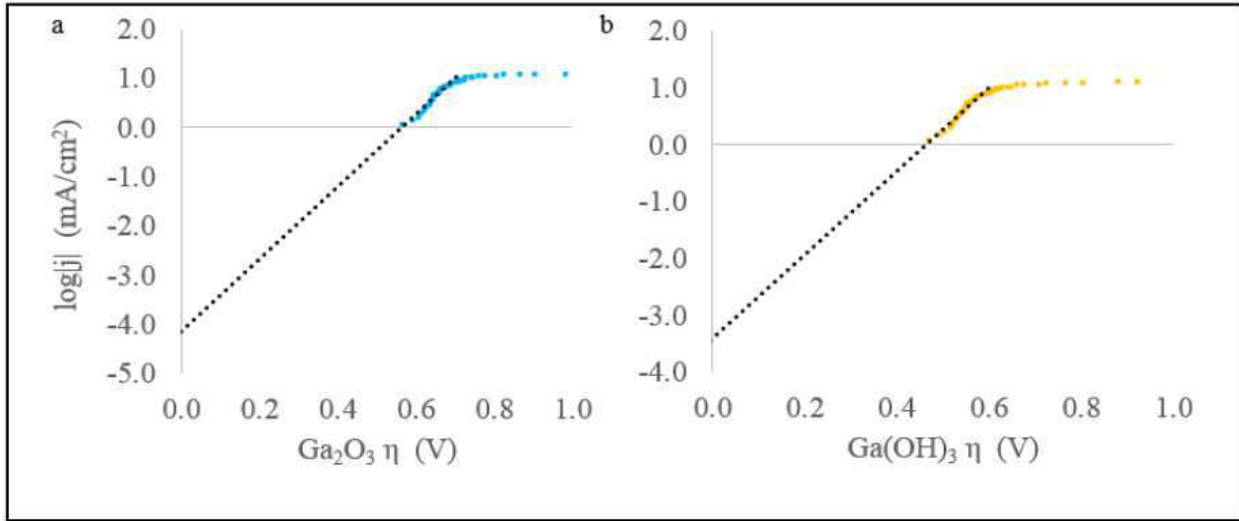
Figure 4-2: Experimental Tafel plots for the Ga-air system with zirconia cloth and 33.6wt% KOH at 65°C for (a) Ga₂O₃ and (b) Ga(OH)₃
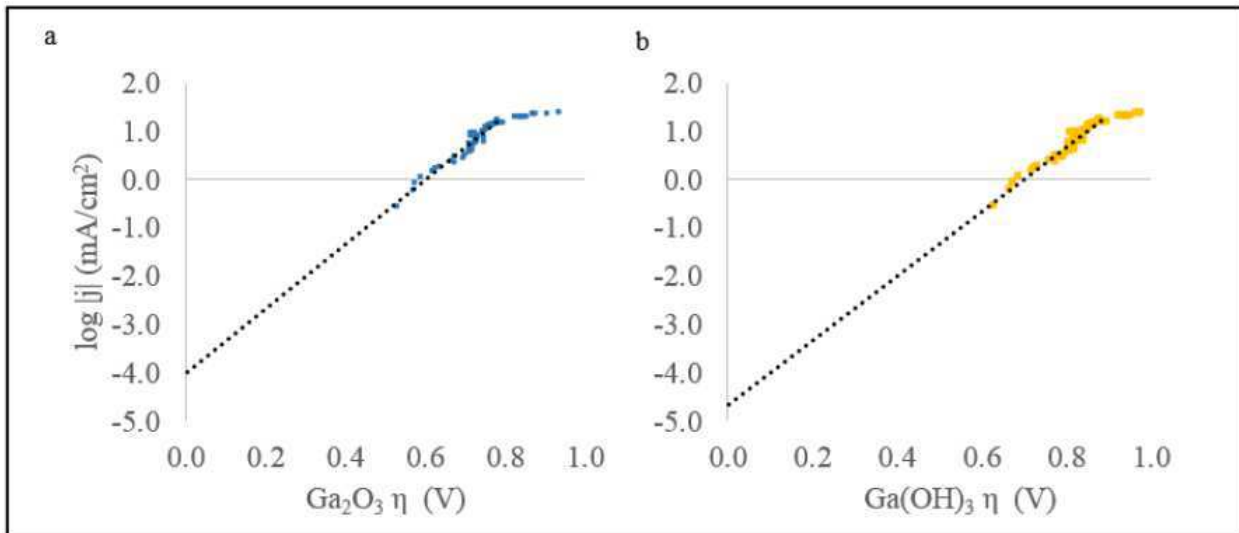
Figure 4-3: Experimental Tafel plots for the Ga-air system with an anion exchange membrane and 33.6wt% KOH at 65°C for (a) Ga₂O₃ and (b) Ga(OH)₃

For all of the Tafel plots, there was a fairly linear region near low overpotentials, resulting in an R^2 of 0.97 for the zirconia cloth and 0.95 for the anion exchange membrane. The linear region of these plots can be extrapolated to an overpotential of zero, resulting in the exchange current density, i_0. The slope of this line can be used to find the anodic charge transfer coefficient, α_A. These values are tabulated in Table 4-2. Thus transfer coefficients are all approximately 0.5.

Table 4-2: Kinetic modeling parameters for Ga$_2$O$_3$ and Ga(OH)$_3$ resulting from Figure 4-2 and Figure 4-3

Electrolyte Configuration	Anodic Oxidative Species	Tafel Slope (V dec^{-1})	Charge Transfer Coefficient	Exchange Current Density (mA/cm^2)	Fitted Limiting Anode Current Density (mA/cm^2)
Zirconia Cloth	Ga$_2$O$_3$	7.352	0.51	3.87×10^{-4}	8.5
	Ga(OH)$_3$	7.352	0.51	7.25×10^{-5}	8.5
Anion Exchange Membrane	Ga$_2$O$_3$	6.705	0.55	9.922×10^{-5}	17
	Ga(OH)$_3$	6.705	0.55	2.119×10^{-5}	17

With this set of parameters, the modified Butler-Volmer equation (Eq 4.1) can be used to model the Ga-air system for both zirconia cloth and anion exchange membrane as shown in Figure 4-4.
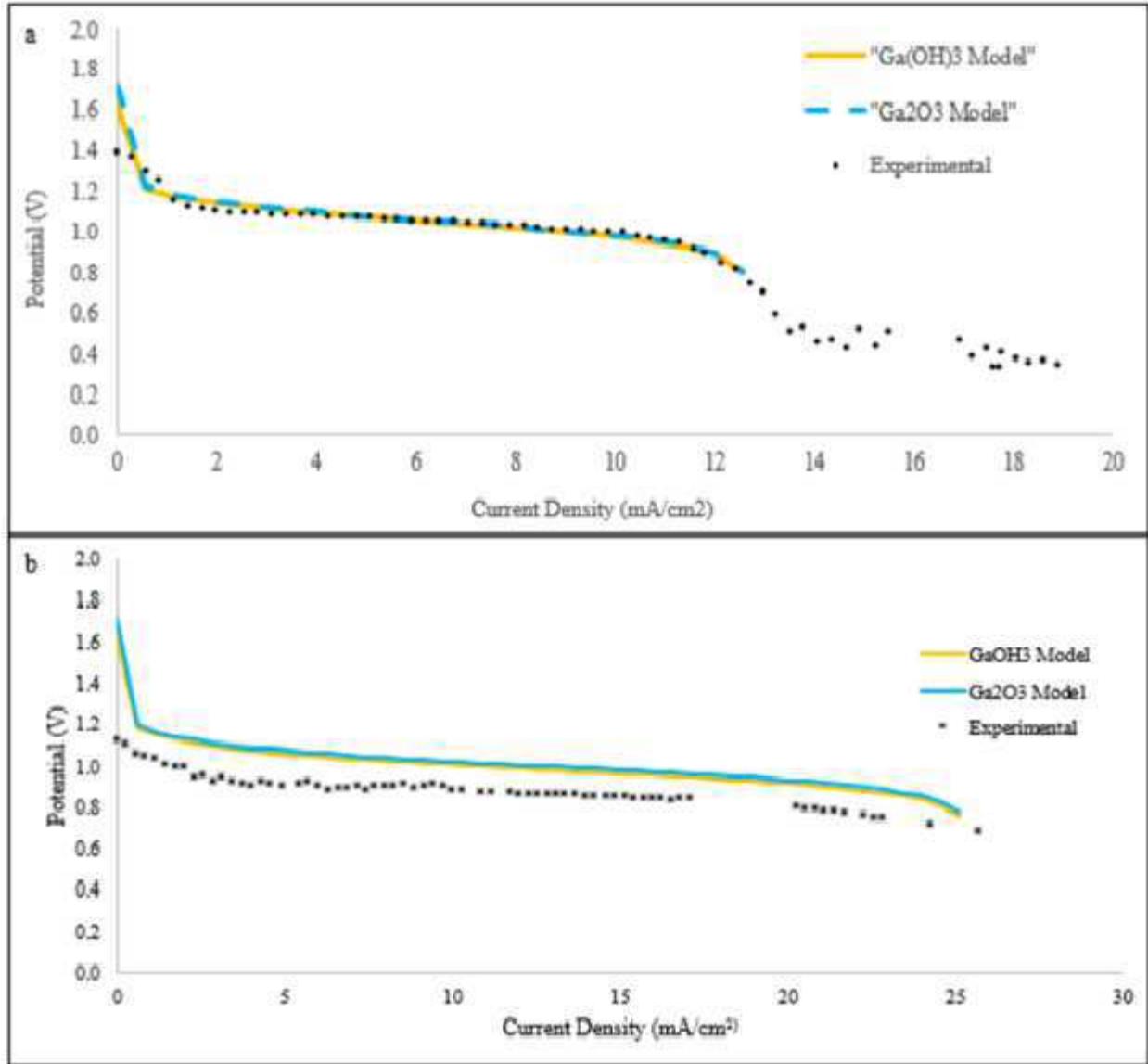
Figure 4-4: Polarization models for the Ga-air system assuming either a Ga_2O_3 or $Ga(OH)_3$ product with (a) zirconia cloth or (b) anion exchange membrane

It is important to note, that despite the assumption of 0 interfacial contact resistance (R_I), the model is nearly identical to the experimental data with a zirconia cloth layer. This also supports similar shapes of the model and the experimental data for the anion exchange membrane, despite an offset. This offset is most likely because the AEM conductivity is actually larger than originally estimated.

4.2 Open Circuit Voltage (OCV) Theory and Experiments

To establish a better understanding of the Ga-air system, the open circuit voltage (OCV) of the system should be established. Theoretically, the OCV can be calculated simply with knowledge of the standard Gibbs free energy change of a given reaction. The exact relation between the Gibbs free energy (ΔG^0) and the OCV (V^0) is described in equation 4.2.

$$V_{rxn}^0 = -\frac{\Delta G^0}{nF} \qquad (4.3)$$

Where n is the number of electrons involved in the reaction and F is the Faraday's constant. Because there are two alternate possible final products for the Ga-air system (Ga_2O_3 and $Ga(OH)_3$), the OCV for both reactions was calculated in Tables 4.3 and 4.4.

Table 4-3: OCV and Gibbs Free Energy for Proposed Anodic and Cathodic Reactions for Ga₂O₃ Generation

Electrode	Reaction	Potential	ΔG^0 (kJ/mol)
Anode	$Ga + 4OH^- \rightleftharpoons Ga(OH)_4^- + 3e^-$		
	$Ga(OH)_4^- \rightleftharpoons Ga(OH)_3 + OH^-$		
	$Ga(OH)_3 \rightleftharpoons Ga_2O_3 + 3H_2O$		
Overall Anode	$Ga + 3OH^- \rightleftharpoons \frac{1}{2}Ga_2O_3 + \frac{3}{2}H_2O + 3e^-$	$V_A^0 = -1.323$	-383
Cathode	$O_2 + 2H_2O + 4e^- \rightleftharpoons 4OH^-$	$V_C^0 = +0.401$	-155
Overall	$Ga + \frac{3}{4}O_2 \rightleftharpoons \frac{1}{2}Ga_2O_3$	$V^0 = V_C^0 - V_A^0$ $V^0 = 1.724\ V$	-499

Table 4-4: OCV and Gibbs Free Energy for Proposed Anodic and Cathodic Reactions for Ga(OH)₃ Generation

Electrode	Reaction	Potential (V)	ΔG^0 (kJ/mol)
Anode	$Ga + 4OH^- \rightleftharpoons Ga(OH)_4^- + 3e^-$		
	$Ga(OH)_4^- \rightleftharpoons Ga(OH)_3 + OH^-$		
Overall Anode	$Ga + 3OH^- \rightleftharpoons Ga(OH)_3 + 3e^-$	$V_A^0 = -1.242$	-360
Cathode	$O_2 + 2H_2O + 4e^- \rightleftharpoons 4OH^-$	$V_C^0 = +0.401$	-155
Overall	$Ga + \frac{3}{4}O_2 + \frac{3}{2}H_2O \rightleftharpoons Ga(OH)_3$	$V^0 = V_C^0 - V_A^0$ $V^0 = 1.643$ V	-476

Due to the differences in Gibbs free energies between Ga_2O_3 and $Ga(OH)_3$, the OCV for Ga_2O_3 is approximately 0.08 V higher than for $Ga(OH)_3$. While this could be used as a clear indication for the exact mechanism for the overall reaction and final product, anodic and cathodic losses make it difficult to determine the OCV and the exact nature of the reaction.

Considering both of these two reactions in relation to the Zn-air standard, the OCV is near the same level. Thus, the OCV for Zn-air is found to lie between that of Ga_2O_3 and $Ga(OH)_3$. This result can be seen in Table 4.5.

Table 4-5: OCV and Gibbs Free Energy for Proposed Anodic and Cathodic Reactions for the Zn-air Reaction

Electrode	Reaction	Potential	ΔG^0 (kJ/mol)
Anode	$Zn + 4OH^- \rightleftharpoons Zn(OH)_4^{-2} + 2e^-$		
	$Zn(OH)_4^- \rightleftharpoons ZnO + H_2O + 2OH^-$		
Overall Anode	$Zn + 2OH^- \rightleftharpoons ZnO + H_2O + 2e^-$	$V_A^0 = -1.260$	-243
Cathode	$\frac{1}{2}O_2 + H_2O + 2e^- \rightleftharpoons 2OH^-$	$V_C^0 = +0.401$	-155
Overall	$\frac{1}{2}O_2 + Zn \rightleftharpoons ZnO$	$V^0 = V_C^0 - V_A^0$ $V^0 = 1.6661\ V$	-321

This calculation was a good indicator of the cell, and it was then decided to proceed with experimental testing for the Ga-air reaction. Before each discharge or polarization experiment in this study, the OCV of the system was measured. A running average of these pre-experiment OCV's was maintained, which was found to be approximately 1.16 V $\pm$ 0.03 V at ~55°C. Certain additional factors were found to influence the OCV, such as an increase in temperature to ~100°C, which resulted in a higher average OCV of 1.292 V $\pm$ 0.037. Because experimental OCV values were well below 1.643 V, it was not possible to experimentally conclude the validity of one Ga-air mechanism over the other.

Additional OCV tests were performed in order to test some qualities of the Ga-air reaction. For some selected tests, additional actions were performed to attempt to extend the life of the cell. The cell was shaken in an attempt to "break up" the formed Ga_2O_3 or $Ga(OH)_3$ covering the metal Ga surface, resulting in an OCV drop of 5.8% after being shaken after the first failure, and a 9.9% drop after the second failure. This corresponded to an OCV change of 1.196 V to 1.127 V to 1.015 V. An additional test re-wetted the zirconia oxide separator with

water, this resulted in a much smaller drop of 4.3%, from 1.172 V to 1.133 V. This suggested

that separator drying was a phenomenon worth investigating to determine cause of cell failure.

It should be noted that while both shaking and re-wetting the separator successfully re-

vitalized the cell's OCV, all discharge tests that followed failed within 5 minutes. While they do

provide small insights into potential cell failure, the immediate failure to continue discharging

may be linked with another factor that is limiting the chemistry. However, additional

investigations of the effect of separator drying on OCV performance was tested. The result of

this test is shown in Figure 4.5. The test was performed both with and without a Teflon coating

between the separator and cathode, which was removed for a part of the test.
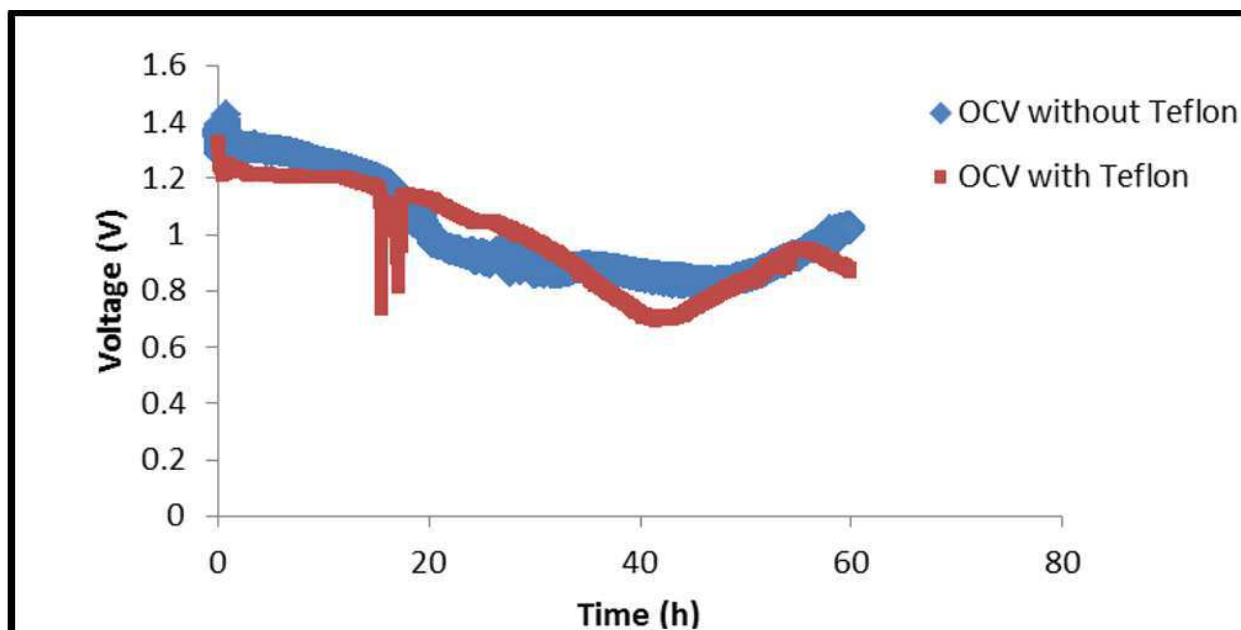
Figure 4-5: OCV performance over 60 hours using 3 glass fiber separators and a GDL both with and without Teflon

The initial OCV's for this test were significantly higher than the calculated running-

average, approximately 1.35 V. This is most likely the result of cell heating at ~60°C, the use of

3 glass fiber sheets as separators, and a manganese oxide GDL. The higher temperature is a

partial cause of the higher OCV. Additionally, it should be noted that near the 60-hour mark, the

OCV's have dropped to approximately 1.0 V, which is a strong indicator that cell drying has at least a small role in cell failure. Note, that two drop-offs at the 20-hour mark on the OCV with Teflon was the result of a disturbance to the cell when it was checked.

4.3 Polarization Performance

To determine the conditions under which a Ga-air system would discharge with the greatest amount of total power, Galvanostaircase Polarization (GSCP) tests were performed to establish the voltage of the cell at different current densities. By gradually drawing more current from the cell, a polarization curve can be generated, which presents helpful information for discharge testing. Figure 4.6 is a polarization curve generated with 33.6 wt% KOH wetted zirconia cloth separator at 50°C.
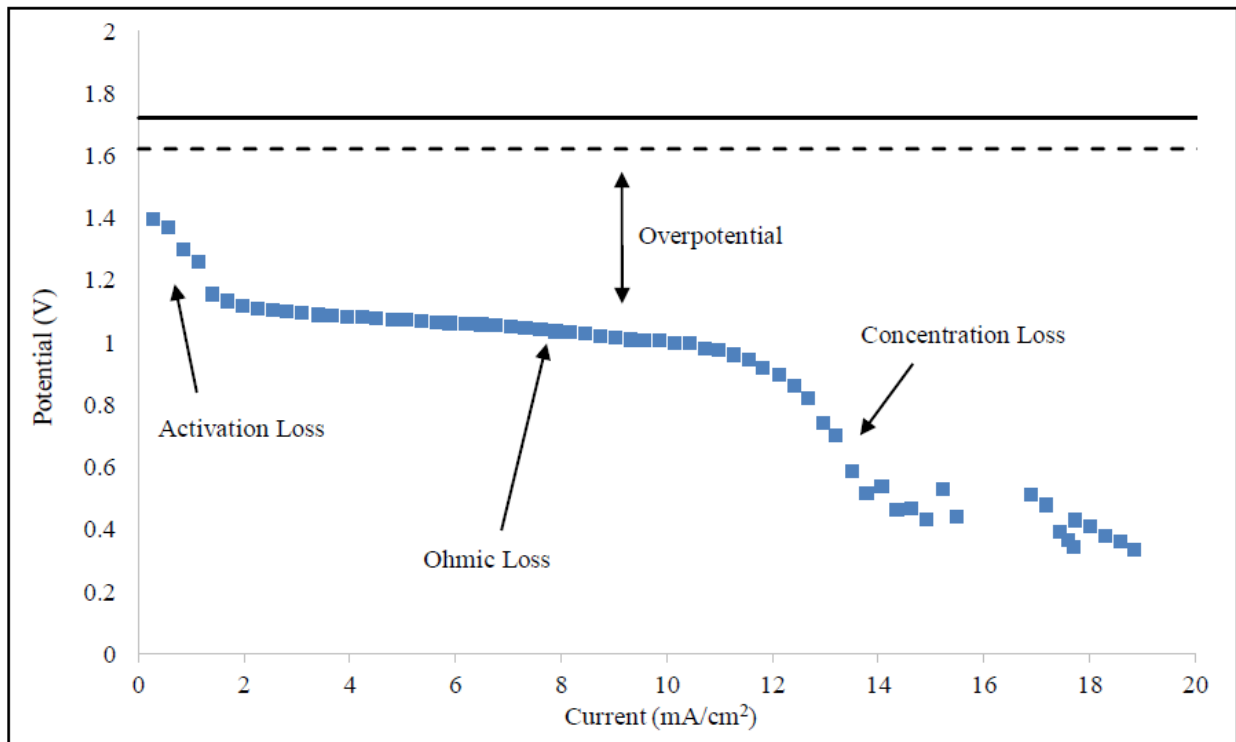
Figure 4-6: The polarization curve for the Ga-air system with a 33.6 wt% KOH wetted zirconia cloth separator at 50°C. The solid black line is the OCV for Ga_2O_3 generation (1.724 V) and the dashed black line is for $Ga(OH)_3$ generation (1.643 V).

Figure 4.6 is an excellent example of the standard shape of a polarization curve. The curve begins at its highest with 0 mA being drawn, this corresponding to the increased OCV. The difference between any given point on this curve and the theoretical OCV is considered the overpotential, and this value is the result of numerous voltage losses as described by Equation 4.1. Anodic, cathodic, and mass transfer losses are the primary reason experimental OCV is lower than theoretical OCV. As the current is increased, activation losses are observed up to 1.5 mA/cm^2. As the current is increased beyond this point, Ohmic losses begin to take effect, which are tied directly to the internal resistance of the cell. This is the linear region of the polarization curve. At around 12 mA/cm^2, a sharp drop is observed, which is the result of transport losses. The limiting current density is the highest current density that can be obtained, corresponding to zero circuit voltage and is the result of anion mass transport through the electrolyte.

Because the intention of this investigation was to observe the cell discharge behavior under various conditions, the polarization plots must also reflect these different conditions. The first variable that was tested was the effect of temperature on cell performance.
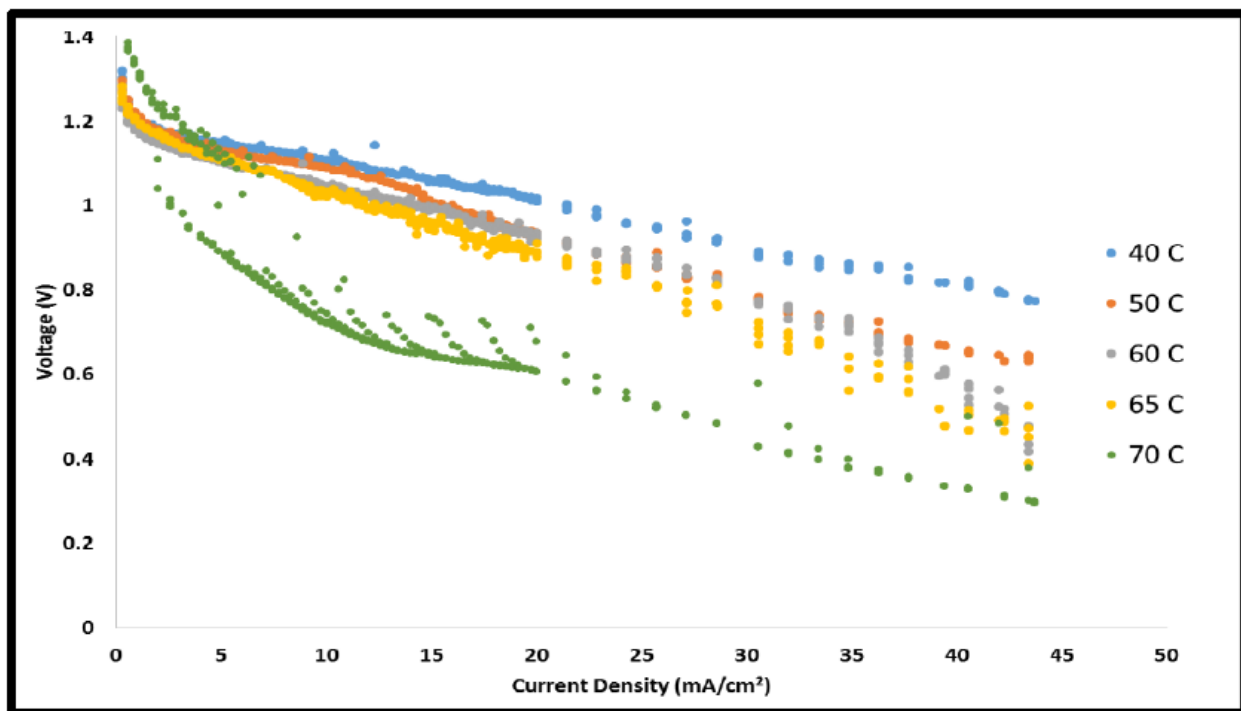
Figure 4-7: Polarization for the Ga-air system with 6 M KOH soaked zirconia cloth at various temperatures.

While it was expected that the activation overpotential reduces with temperature, this plot shows that temperature predominately affects the ohmic losses of the polarization curves in a negative fashion, causing the performance to drop with temperature. As temperature increases, the slope becomes more negative suggesting that an increase in the temperature increases the internal resistance. Also, at around 70°C, a significant change to the activation losses is also observed. This behavior is fairly similar to other results that were recorded at higher temperatures. The increase of ohmic resistance at higher temperatures is most likely the result of KOH carbonation or separator drying.

Additionally, different cell types were tested for polarization performance—most notably, 6M KOH wetted zirconia cloth and 6M KOH wetted AEM. The results of this test can be seen in Figure 4.8
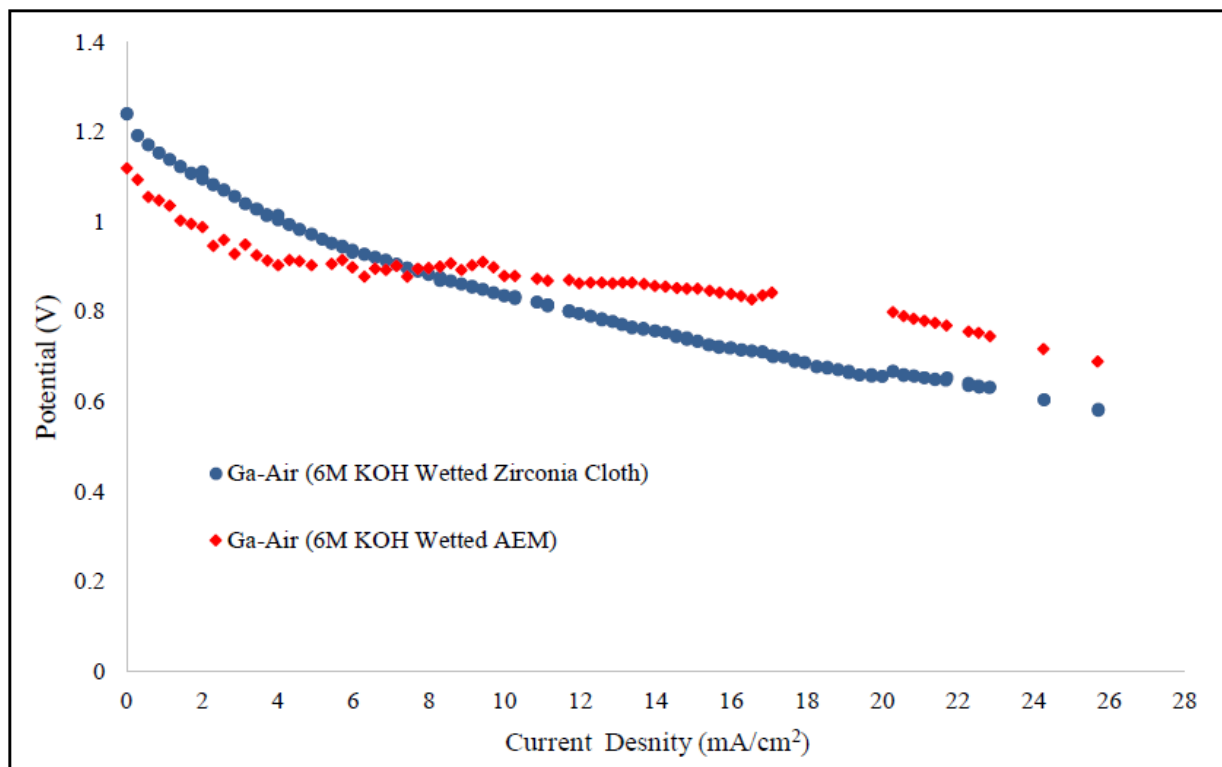
Figure 4-8: Polarization for the Ga-air system using a zirconia cloth separator and an AEM at 50°C.

While the shapes of these two polarization curves are quite similar, there are a few important distinctions between them. First, the anion exchange membrane (AEM) performed better at current densities above 8 mA/cm^2. This may be the result of the AEM's greater robustness to carbonation or separator drying. Second, the zirconia wetted cloth had an OCV that was about 0.1 V higher. This is a substantial difference that is maintained until 4 mA/cm^2. Despite these differences, both curves still experience significant concentration losses at around the same point, i.e., above 22 mA/cm^2.

For comparison, the commercial Zn-air battery (Duracell, product #675) was also tested and its polarization curve is shown relative to the Ga-air system polarizations in Figure 4.9.
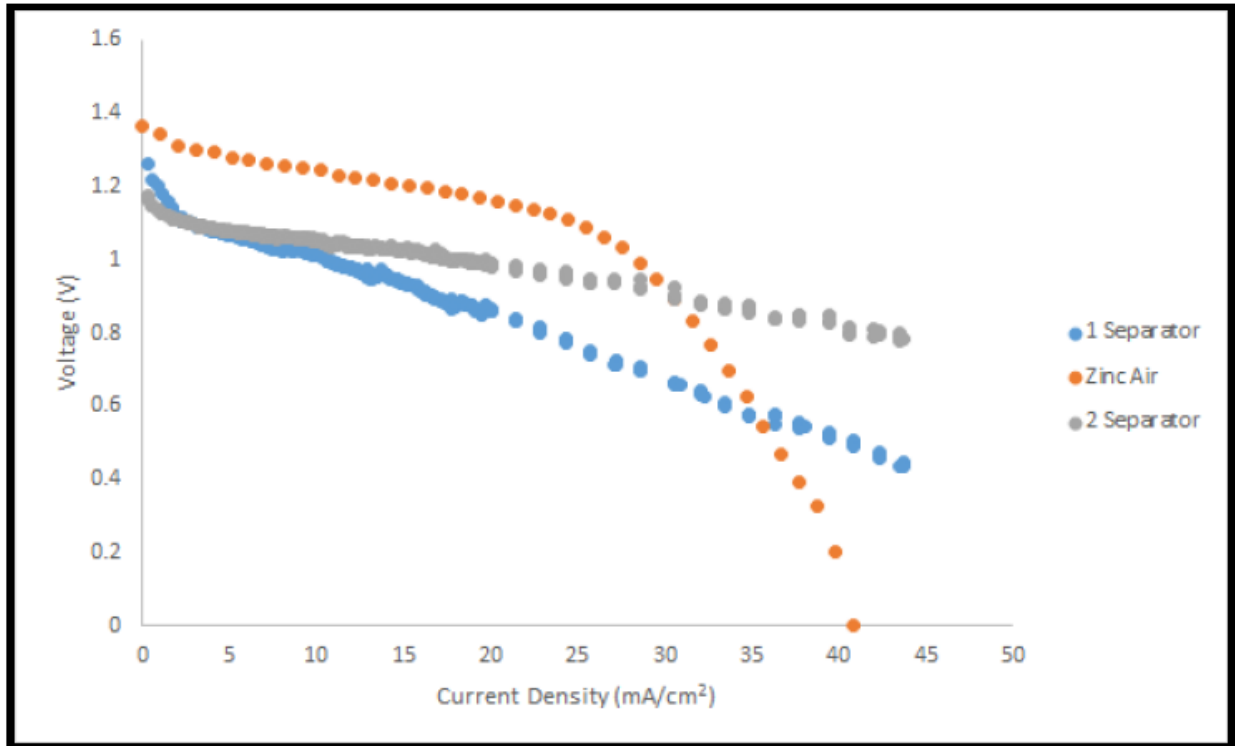
Figure 4-9: Comparative polarization performance of a Ga-air system with variable numbers of separators against the Zn-air system (Duracell 675).

The Zn-air polarization was obtained using a Duracell 675 zinc-air battery because its size and shape is comparable to the reaction surface used for the Ga-air cell (~0.35 cm^2 geometric area). From this data, it is clear that the Zn-air system significantly outperforms the Ga-air system until current densities above 30 mA/cm^2 (and above 35 mA/cm^2 for single separator systems). However, the Zn-air system is significantly more susceptible to transport losses, resulting in a sharp drop around 25 mA/cm^2. It is possible that this difference may be the result of the specific cell designs. While both systems have similar two dimensional active areas, the zinc-air battery is much more developed in terms of its design, taking advantage of a three dimensional reaction interface, as in the use of gelled Zn-KOH mixture used in the anode canister in Figure 2-9 (Page 22). This design offers significant advantages to reduce potential losses, but it comes at the price of an inability to provide higher current densities because of

increased transport resistance. Because the Ga-air cell was able to perform within range of the commercial Zn-air highly optimized system with only a two dimensional interface, it can be postulated that the Ga-air reaction system may actually have better reaction kinetics which could outperform the Zn-air system if a three dimensional reaction interface could be created for the Ga-air system.

The polarization curves of cell revitalization were also considered assuming that drying or carbonation is the cause of cell death. Results for separator resoaking are thus shown in Figure 4.10.
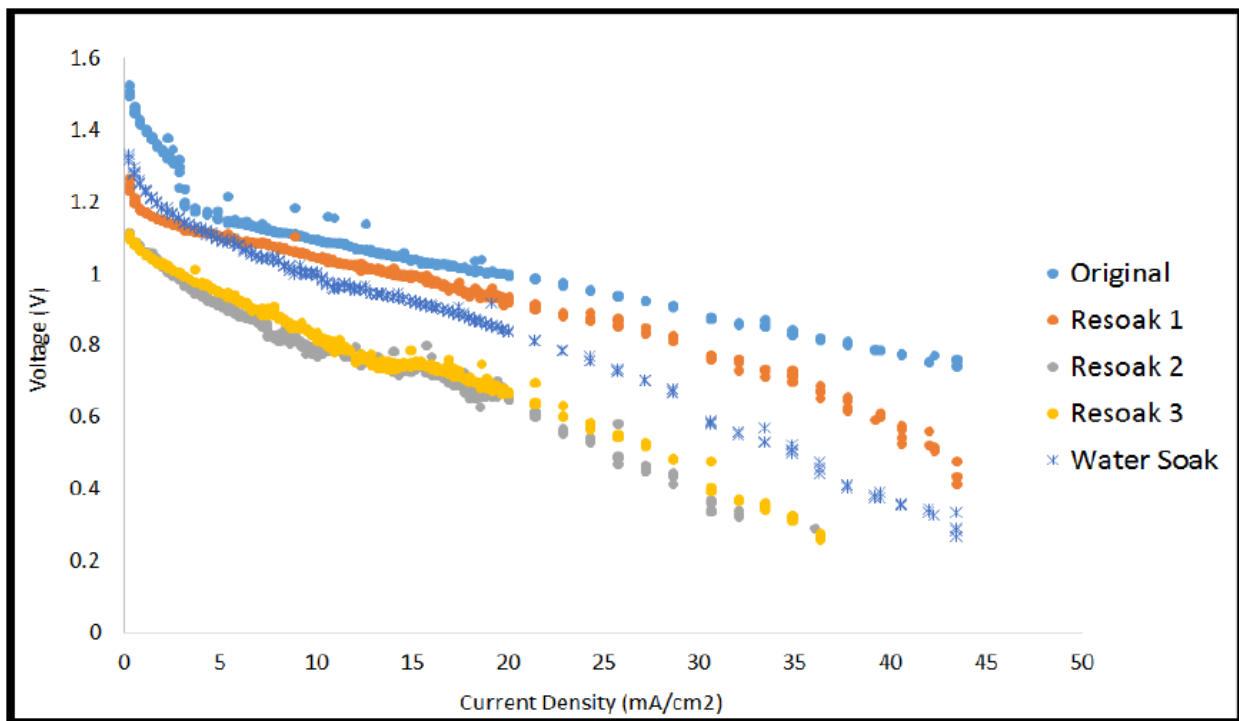
Figure 4-10: Polarization curves for a given trial and re-soaking it in 6 M KOH or water.

The behavior observed here shows that a single resoak in water versus a single resoak in 6 M KOH has different results. Compared to the original test, a water soak resulted in significantly higher overpotential losses, whereas the 6 M KOH resoak resulted in smaller

overpotential losses. This suggests that there is some extent of KOH loss throughout cell testing, which supports the KOH carbonation postulate with CO_2 in air:

$$2\ KOH + CO_2 \rightarrow K_2CO_3 + H_2O$$
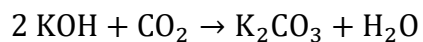
In order to further test this postulate, polarization tests were also performed with 8 M KOH, which can be found in Figure 4.11.
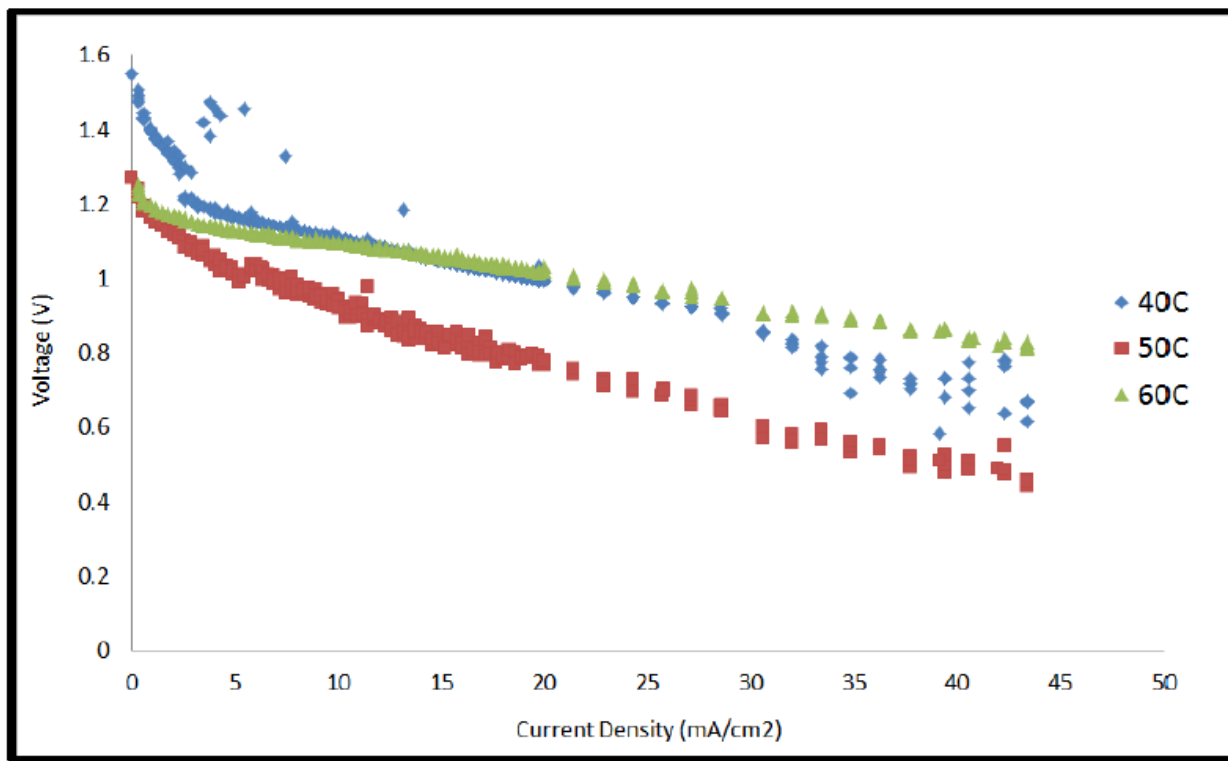
Figure 4-11: Polarization curves at various temperatures using two zirconia cloth separators wetted with 8 M KOH.

Unexpectedly, this result was actually had higher overpotential losses despite having a higher KOH concentration. This behavior was even observed when two separators were used to protect against electrolyte solution evaporation. A possible explanation for this behavior might be lower conductivity at higher concentration due to saturation. For this reason, 6 M KOH was considered preferable for subsequent tests.

4.4 Discharge Performance: Effect of Variables

4.4.1 Establishing a Baseline

Throughout the course of this investigation, numerous discharge curves were generated to investigate the effects of many factors on the overall discharge time and voltage. A general test baseline was first established to ensure that adequate experience in cell construction and testing was first obtained. This experience was fundamental for consistence of future discharge tests since even small changes in cell construction and procedure could result in a drastic result change. The general baseline for the majority of tests consisted of some variation on the primary factors of cell performance:

Table 4-6: Primary Parameters Influencing the Overall Discharge Performance of the Ga-Air System

Factor	Standard
Electrolyte	33.6 wt. % KOH
Separator	Zirconia Cloth 0.015" thick
Number of Separators	1
Catalyst Layer	Pt GDL
Current	0.5 mA
Current Density	1.41 mA/cm^2
Cell Orientation	Cathode facing down
Operating Temperature	40 - 50°C (unless otherwise specified)
Cathode Fuel	Air

The rationale for the electrolyte concentration used is that it provides the highest possible ionic conductivity relative to other electrolytes. 1 sheet of zirconia cloth was used as a separator since zirconia can successfully be wet by KOH solution and using 1 sheet minimizes the diffusion distance for the hydroxyl ions. A Pt GDL was used because platinum provides an active surface for oxygen reaction. Additionally, trial-and-error established that the cell orientation (for effective metal-electrolyte contact) and ambient temperature were very effective at these values. Remaining factors were simply chosen out of convenience or experimental limitations.

When these factors are combined into a single experiment, the best results are typically similar to Figure 4-12.
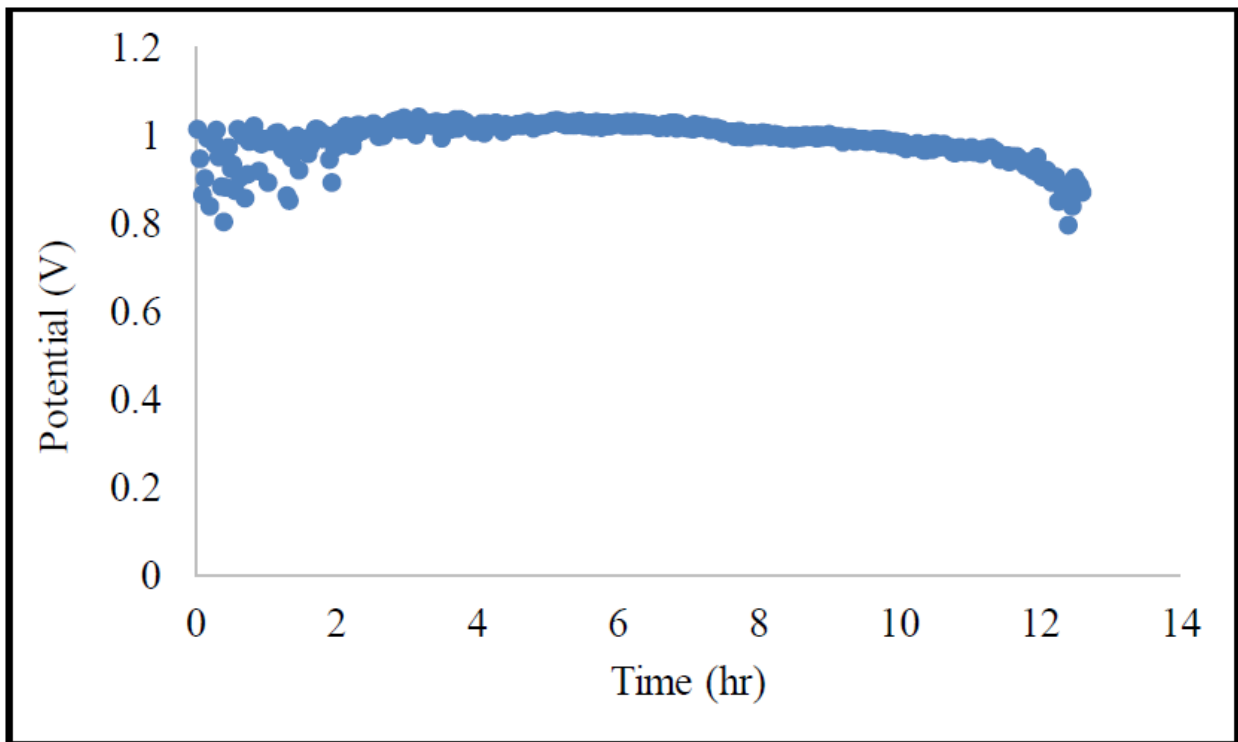
Figure 4-12: A generally good Ga-Air system discharge at 40°C.

This result illustrates that a generally good Ga-Air system discharge typically lies around 1V for over 12 hours. The OCV of this experiment was 1.3V, which quickly dropped upon discharge initiation. While there are discharge results that are significantly better than this, this level of performance was generally considered to be at a "successful" level for prototype-based tests. It should be noted, that due to the high variability in hand-made construction of the cell, the actual average for total discharge duration is approximately 5 hours, but the reason for these earlier cell failures is discussed in Section 4.5. For reference, a discharge plot for a commercial Zn-Air system button cell (Duracell 675) was also generated via the BAWIN500 program—the standard discharge testing program. This result is shown in Figure 4-13.
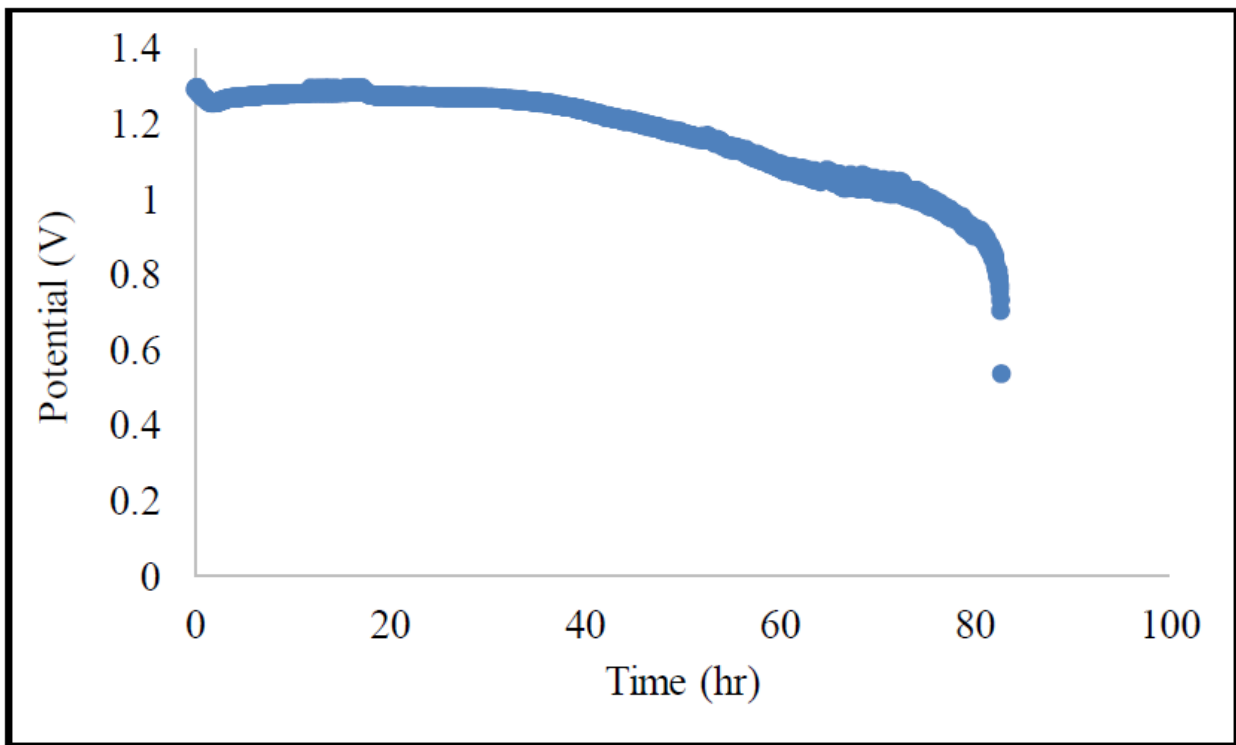
Figure 4-13: Zn-Air system discharge at 40°C.

Naturally, this commercially established battery had significantly better results, starting with a similar OCV of 1.3V, but lasting for just over 80 hours of discharge. Moreover, the average voltage for this test was in the range of 1.2V with a current draw of 7 mA (compared to

the 0.5 mA for the Ga-Air system). This suggests that the cell would have lasted significantly

longer at a comparable current draw to the Ga-Air system. While this difference is significant, it

implies that the Ga-Air system with improved design and construction could potentially improve

to this level as well. To continue with this baseline, some discharge curves should also be plotted

against capacity. For the Ga-Air system, this performance is shown in Figure 4-14.
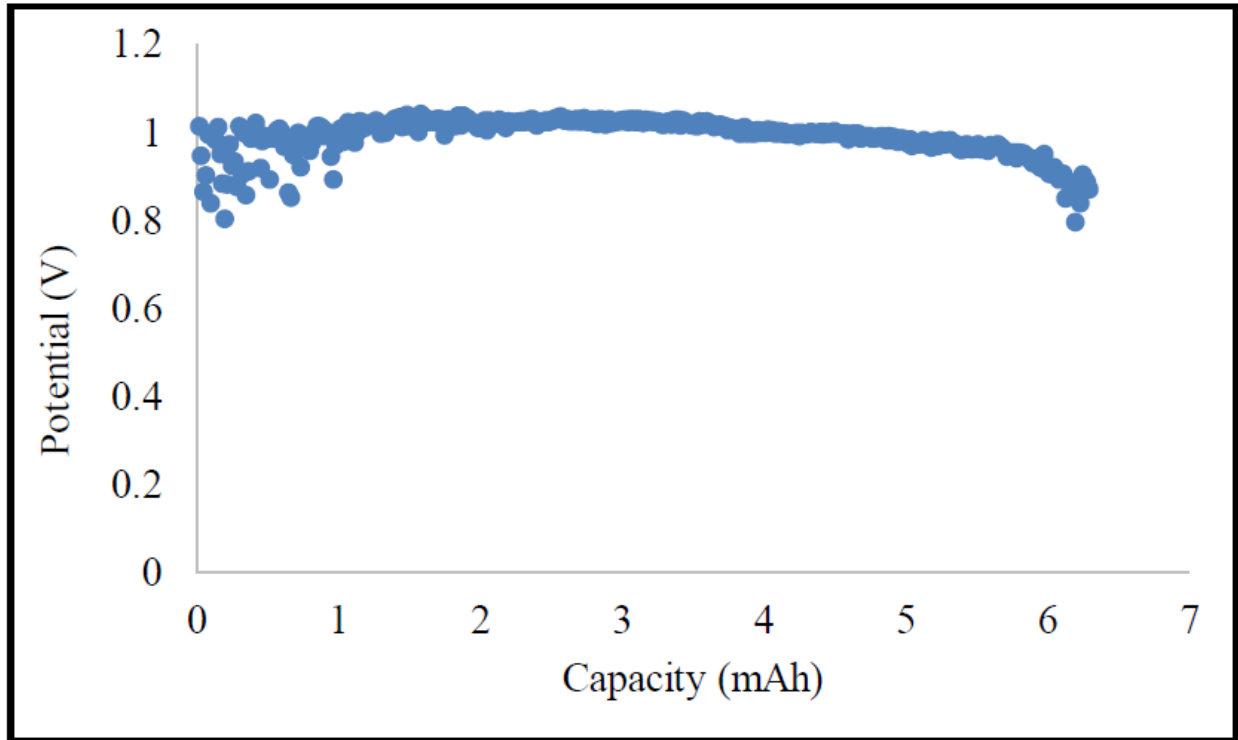
Figure 4-14: Ga-Air potential versus capacity at 40°C.

The theoretical capacity of this cell was predicted to be in the range of 1400 mAh, which

is significantly more than the observed 6 mAh. This is clear evidence that the Ga-Air cells of this

investigation have room to improve by a large margin. In comparison to the Zn-Air system, this

capacity is quite low. However, the Zn-Air system is a 3-dimensional metal-electrolyte network.

If the surface of the 2-dimensional Ga-Air system is solely considered (assuming an oxide

thickness of 0.5 nm), the observed capacity increases to 115 mAh. This result can be considered

against Figure 4-15. Clearly, factors yet unknown limit the capacity of the Ga-Air cell to much

less than its theoretical capacity.
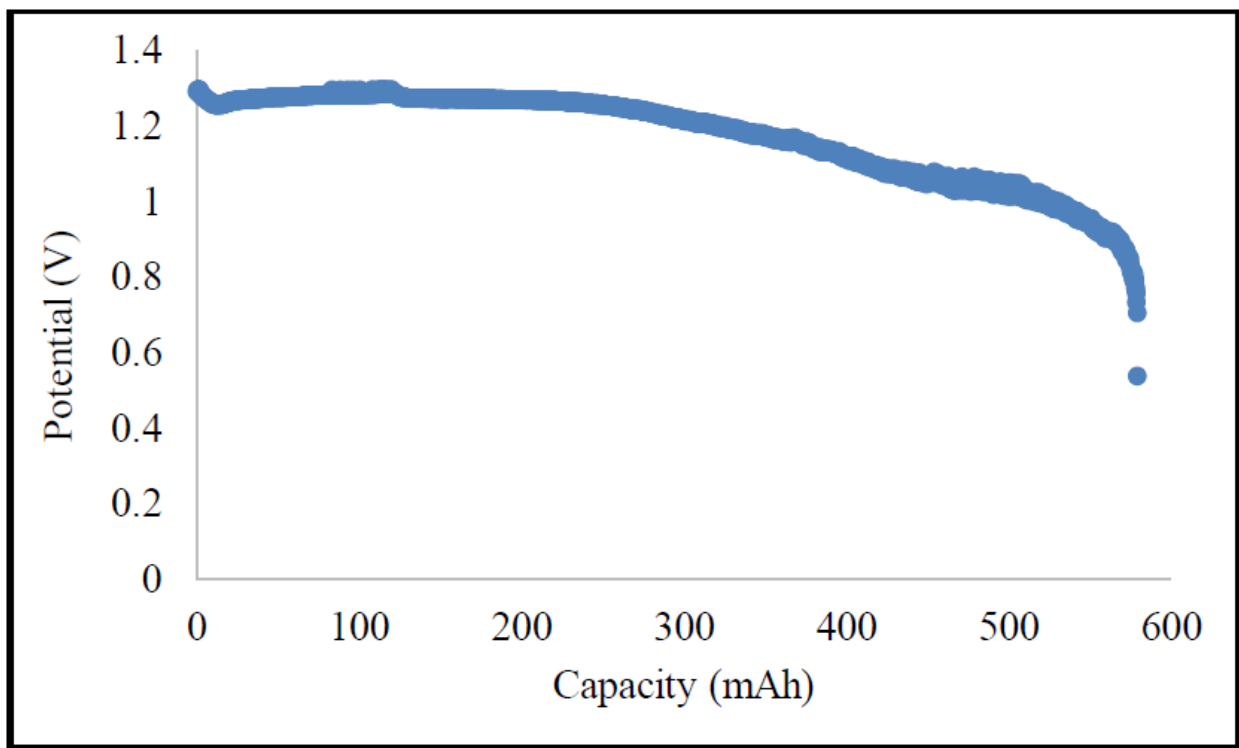
Figure 4-15: Zn-Air potential versus capacity at 40°C.

The discharge versus capacity of the Zn-Air system ends up reaching nearly 600 mAh in

terms of capacity. Even in comparison to the generous interpretation of the Ga-Air system

capacity, the Zn-Air system still remains well above the Ga-Air system. However, given the high

theoretical possibilities of the Ga-Air system, there is good reason to consider what factors could

be limiting the cell performance. First and foremost, the limited anode surface area, namely

being limited to a 2-dimensional interface, should play a large limiting role on the cell

performance. Creating a Gallium-electrolyte slurry in the anode may offer significant

improvements to future Ga-Air cells.

With a baseline effectively established and compared to the Zn-Air system, the Ga-air

system was more comprehensively investigated by varying the factors enumerated in Table 4-6.

While some of these factors essentially remained constant throughout testing, others had significant effect on discharge performance and rechargeability—which will be discussed in Section 4.6.

4.4.2 Discharge Performance: Effects of Separator

One of the most accessible factors of Ga-Air system testing is the effect of the separator. As outlined in Table 4-6, the typical system separator used was a single layer of zirconia cloth soaked in 6 M (33.6 wt %) KOH solution. Thus, the effect of the number of separator layers was considered. Changing the number of separators was motivated by the fact that prior research had demonstrated that increasing the electrolyte amount also increased the overall cell performance. This implies that the amount of electrolyte is important, and that this value could be increased by simply adding additional KOH soaked separators.

The first set of tests consisted of a zirconia cloth separator with a PTFE layer between the GDL and the separator. The purpose of the PTFE layer was to minimize separator drying, which was initially suspected to be a major cause of cell failure. This would help identify whether the cell failure was caused by a lack of water or a lack of KOH.
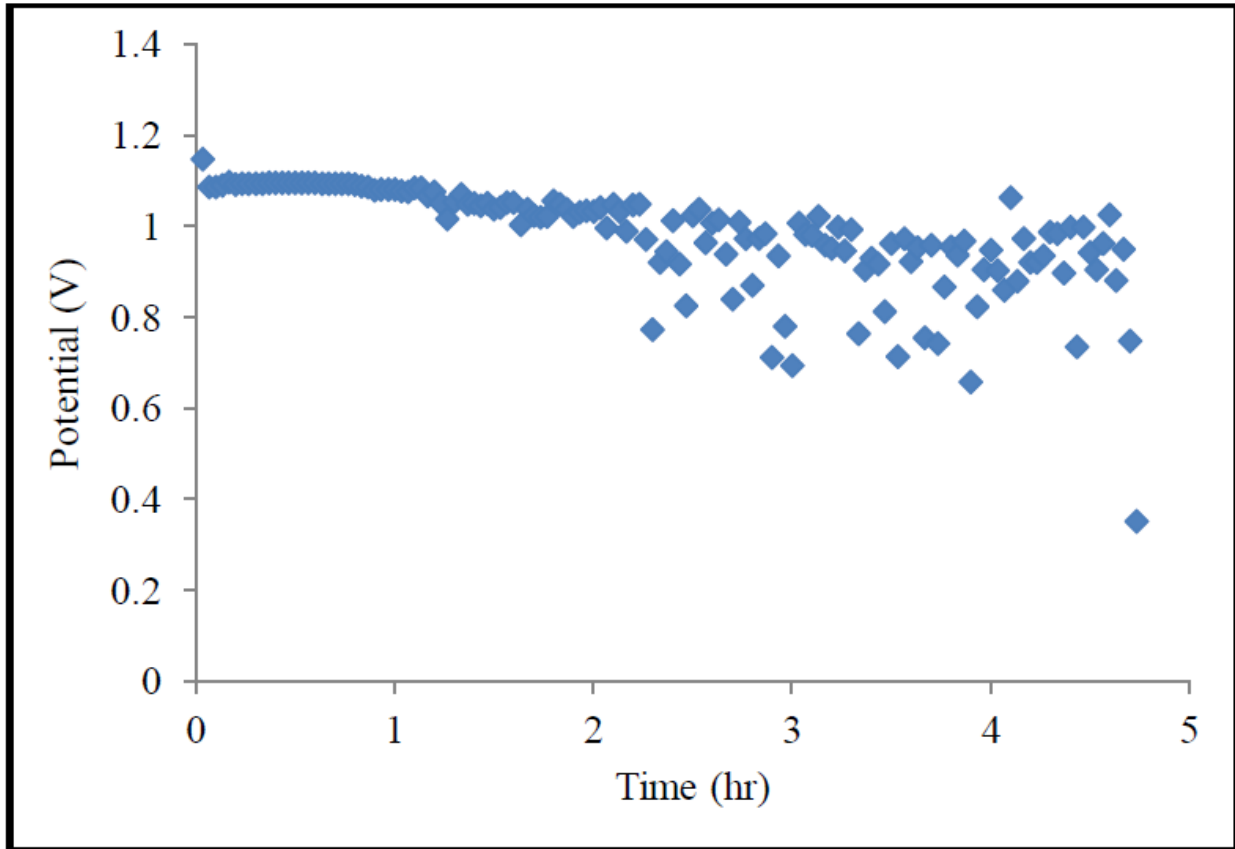
Figure 4-16: Standard Ga-Air system with a PTFE layer between GDL and Zirconia Layer at 68.9°C.

In Figure 4-16, the cell discharge appears to fall off around 4.7 hours when at 68.9°C, which is noteably below the average discharge time. However, this difference from the average discharge time (5 hours) is quite small, and the higher temperature of the test should also be considered. Generally, higher temperatures have a more adverse effect on drying and on discharge results, which is further explained in Section 4.4.3. Therefore, it would seem that the PTFE layer had little effect on the overall cell discharge performance, but also allowed for the system to operate at higher than average temperatures.

While the addition of the PTFE layer was considered to help reduce separator drying, carbonation of KOH in separators was also a potential cause of cell death. For this reason, other separators were considered that were more robust to carbonation. The first material that was

investigated was the Anion Exchange Membrane (AEM) since it continues to behave as a reasonably effective electrolyte even after becoming partially carbonated. Carbonation of AEM separators is considered to proceed as follows:

$$R^+ + OH^- + CO_2 \leftrightarrow R^+ + HCO_3^- \tag{4.4}$$

$$R^+ + OH^- + R^+ + HCO_3^- \rightarrow R_2CO_3 + H_2O \tag{4.5}$$
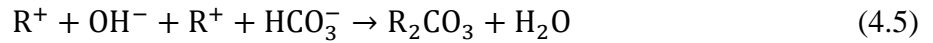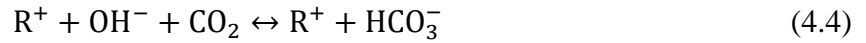
Considering the products of the reaction, it is clear that all of them except R_2CO_3 are still conductive. This implies that the natural carbonation process of the AEM should allow the cell to continue to function, even if less effectively, as HCO_3^- conductivity is less than that of OH^-. However, the AEM is still susceptible to drying out, which may also be a significant stumbling block. The overall performance of the Ga-Air system with the 6 M KOH soaked AEM (AMI-7001S) is shown in Figure 4-17.
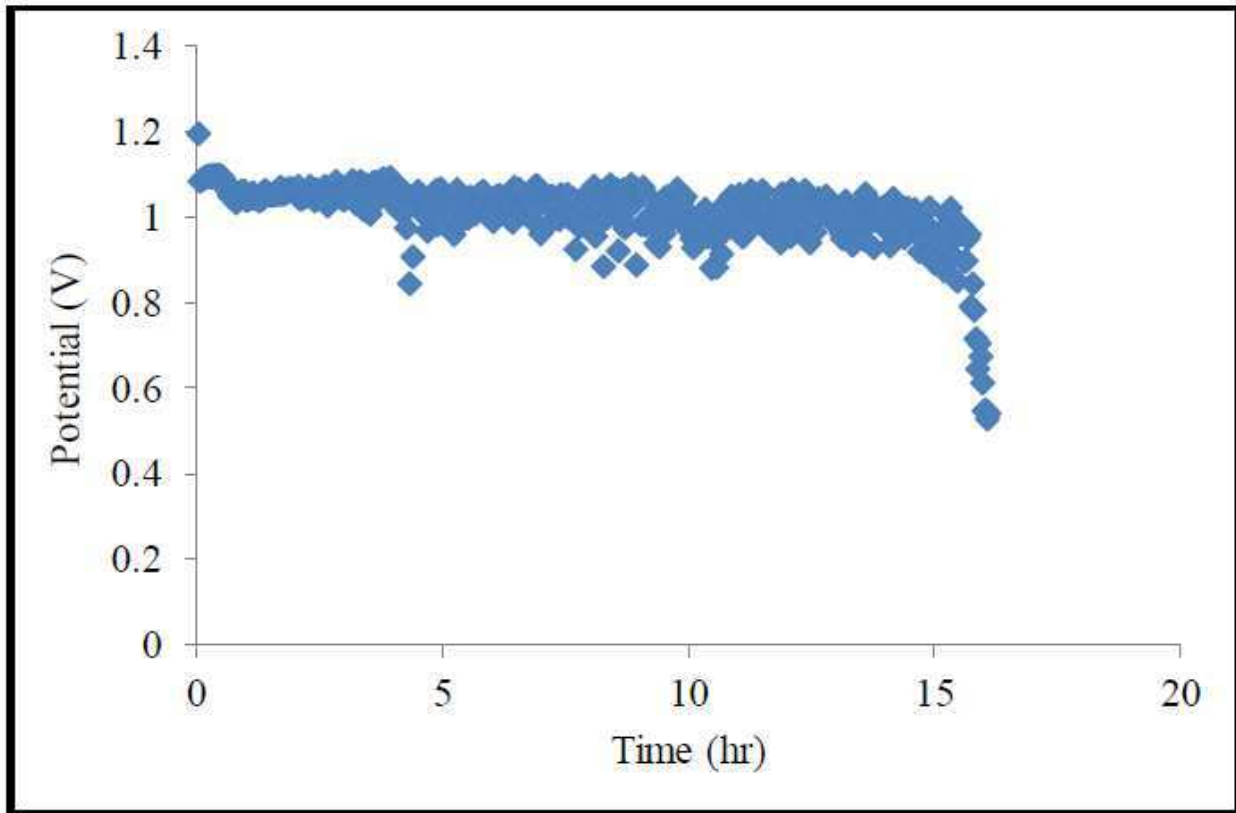
Figure 4-17: Discharge of Ga-Air system with an AEM separator (AMI-7001S) at 50°C.

Figure 4-17 shows an impressive total discharge time of approximately 16 hours at around 1 V. This result is significantly above average at the same average temperature of 50°C. However, among even the best discharge results, this separator also falls short, possibly due to cell drying. Nevertheless, this separator can potentially remain functional even after drying, which also makes it a useful candidate for rechargeability investigations.

In an effort to further extend the total discharge duration, the amount of KOH in the separator was increased. One simple method to increase this value while maintaining the optimal KOH concentration is to add additional soaked separators. Thus, while the overall concentration of the electrolyte remains unchanged, the total amount of solution is increased, thereby increasing the KOH amount. First, zirconia cloth separators were tested in varying numbers.
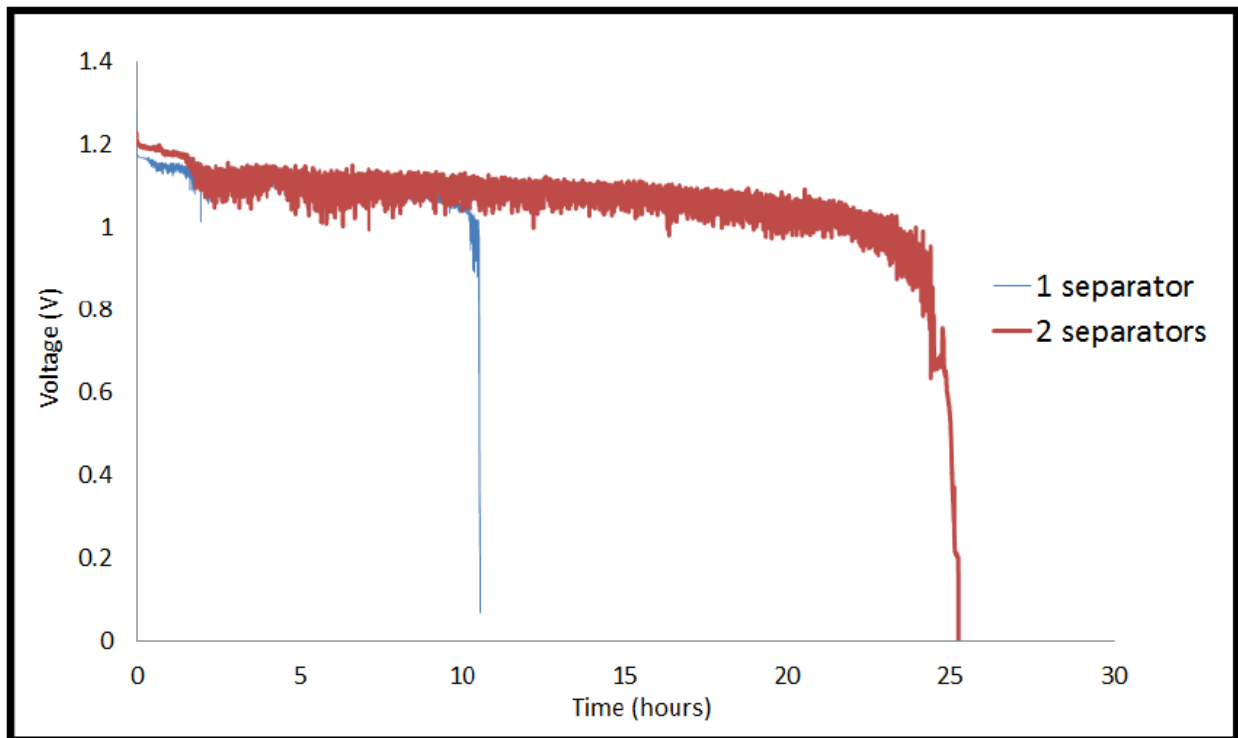
Figure 4-18: Discharge of Ga-Air system with a 1 or 2 KOH soaked zirconia cloth separators at 50°C.

The comparison in Figure 4-18 shows an incredibly clear result, adding just one additional soaked separator can dramatically increase overall discharge duration. In Figure 4-18, this additional separator resulted in a 127% increase in discharge duration. Even when compared to the best of single separator discharge durations (16 hours), two separators is still a 56% increase. Possible reasons for this increase may be due to KOH presence and total solution volume. Since there is approximately twice the volume of solution, it would suggest that it would also take longer to dry and/or entirely carbonate. Adjusting the number of separators was also investigated with glass fiber separators. The following tests were performed with glass fiber separators, with a manganese oxide catalyst layer and a nickel mesh, which were made-to-specification by a proprietary supplier.
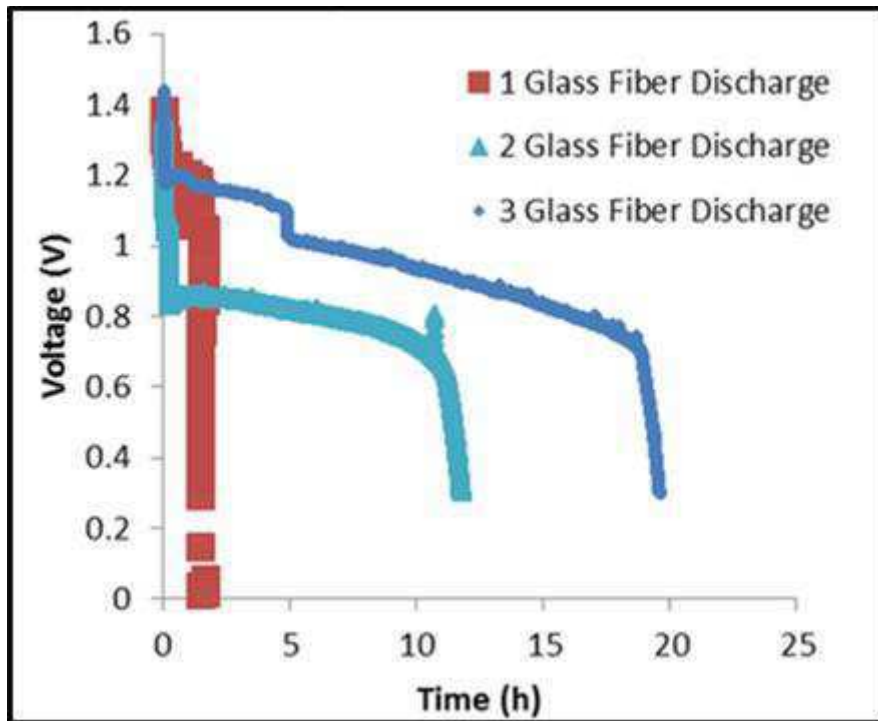
Figure 4-19: Discharge of Ga-Air system with a 1, 2, or 3 KOH soaked glass fiber separators of thickness 0.01" and at 50°C.

In relation to the zirconia cloth separator, Figure 4-19 shows that glass fibers demonstrate a slightly lower performance per separator, reaching only 20 hours of discharge with 3 glass fiber

73

separators. This difference may in part be due to the difference in catalyst layers since platinum

is generally considered to be a better surface than nickel for oxygen adsorption. Moreover, the

glass fiber sheets (thickness: 0.01") were slightly thinner than zirconia cloth separators

(thickness: 0.015"), which, despite having a concentration of 6 M KOH, would result in a lower

electrolyte content. Despite these shortcomings in overall discharge duration, the typical OCV

for the Ga-Air systems with manganese oxide catalyst and glass fiber separators was 1.4 V on

average, higher than the platinum GDL and zirconia cloth separator OCV of 1.3 V.

The glass fiber separators with manganese oxide catalyst performs like zirconia cloth

separators with platinum GDL. These manganese oxide catalyst layers were tested both with and

without a Teflon layer attached. Additional tests were performed with SEPARION (Litarion

S240P30) separators, which are composed of "ceramics and a porous polyethylene terephthalate

(PET) non-woven […] homogeneous single-layer network" (Morris, 2015).
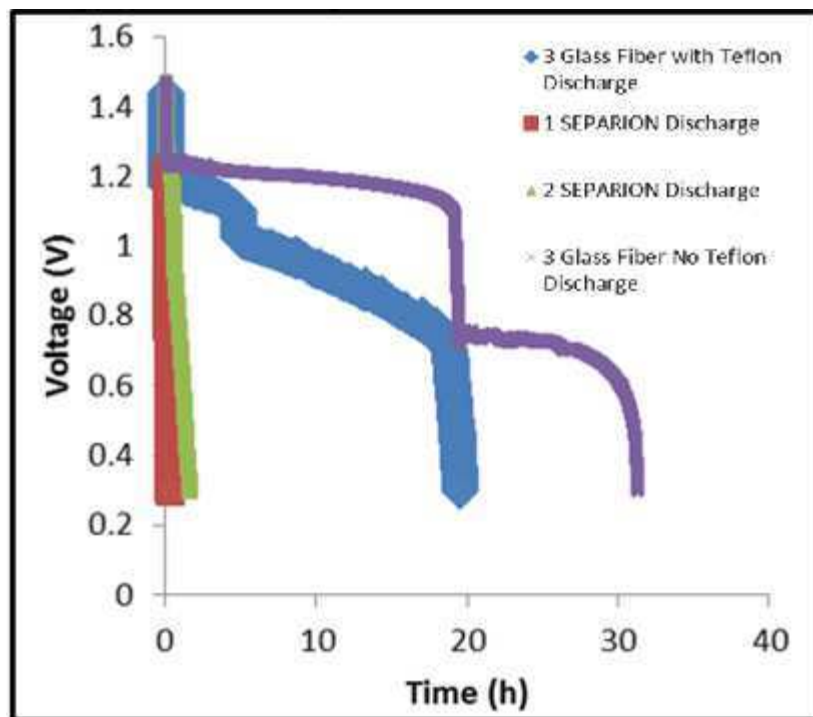
Figure 4-20: Discharge of Ga-Air system with a 3 KOH soaked glass fiber separators (with and without Teflon) or 1 or 2 KOH soaked SEPARION (Litarion S240P30) separators at 50°C.

In Figure 4-20, glass fiber separators with manganese oxide catalyst was found to achieve 20 hours of discharge with Teflon and 30 hours without. This result begins to rival the performance of multiple zirconia cloth sheets, and may have been more successful due to the Teflon removal, which appeared to have limited oxygen diffusion in the Ga-Air system. The SEPARION (Litarion S240P30) separator, however, did not have successful results, even when multiple sheets were used in series. No test managed to exceed an hour of discharge performance and all dropped in voltage very quickly. Upon inspection of the cell following testing, it became clear that the SEPARION material was soluble in KOH electrolyte solution and there were no separators within an hour of discharge. This made it evident that ceramic/polymer composite electrolytes would not be effective for the Ga-Air system in alkaline electrolyte.

As an additional note, the discharge performance of the glass fiber separators with manganese oxide catalyst had an interesting shape. The curve appeared to be broken down into two plateaus, corresponding to 1.2 V and 0.8 V. This is most clear in Figure 4-20 for the glass fiber separators without Teflon. This behavior plays an important role in the investigation of rechargeability of the Ga-Air system, since it suggests a dual-mechanism system,

4.4.3 Discharge Performance: Cell Revitalization

When the standard zirconia cloth Ga-Air system ceased to discharge, some additional experiments were conducted to confirm whether this failure was due to surface contact issues, separator drying, or separator carbonation. These causes of failure were investigated using the three respective techniques: moderate cell agitation, separator re-wetting in water, and separator re-soaking in solution. Since, even the best results (30 hour discharges) fall well short of the theoretical discharge capacity (3000 hours), capacity losses should be investigated. First, surface contact resistance caused by oxide formation on metal surfaces was investigated:
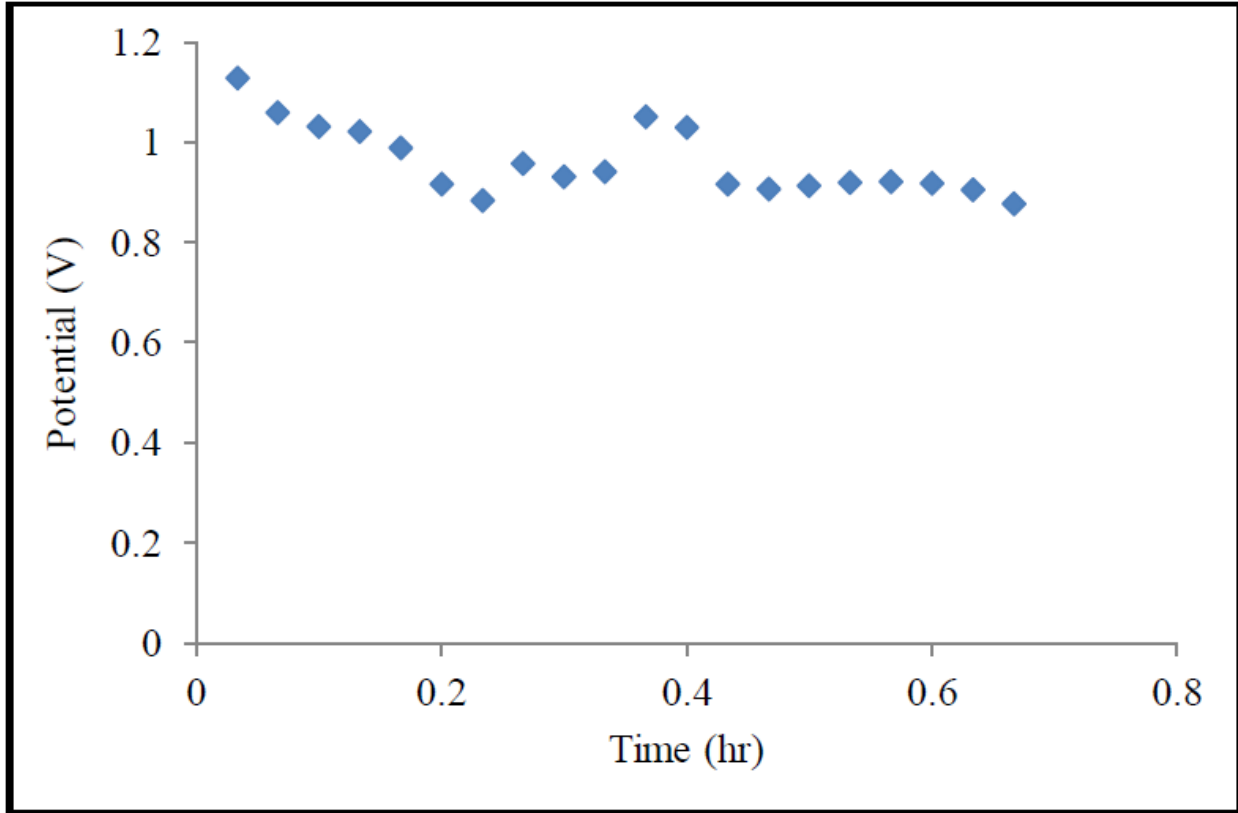
Figure 4-21: Discharge results following cell agitation of a zirconia cloth Ga-Air system for cell revitalization at 50°C

Figure 4-21 demonstrates that cell failure cannot primarily be attributed to oxide formation on the gallium surface. While the cell effectively discharged for 0.7 hours after agitation, it was not able to approach the standard single separator discharge result of 12 hours. This suggests that separator drying or carbonation may play a bigger role in cell failure than accumulation of oxide or hydroxide at the metal-electrolyte layer interface.
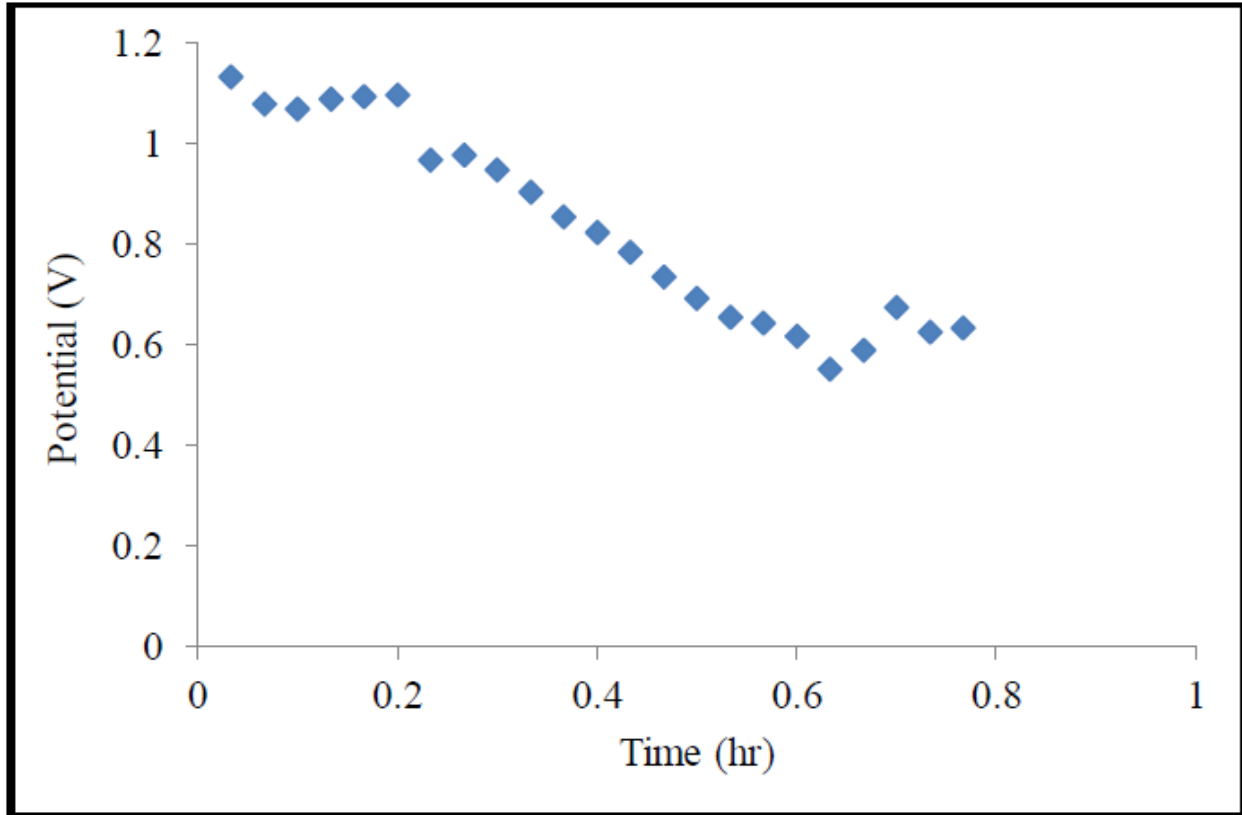
Figure 4-22: Cell separator re-wetting in water of a zirconia cloth Ga-Air system for cell revitalization at 50°C.

Figure 4-22 shows a similar result to cell agitation, with a lower overall potential over the total discharge duration, but a slightly longer discharge time of 0.8 hours. Further, re-wetting the separator in water also seemed to have very little impact on the overall cell performance for a second discharge. Moreover, because the potential was generally lower over this period, it may suggest that cell agitation may have had a greater effect on electrolyte diffusion than re-wetting the separator. If this is the case, ion diffusion limiting reaction products (Ga_2O_3 or $Ga(OH)_3$), may have a greater chance of forming on the gallium-zirconia cloth interface. Nevertheless, neither result suggests that either limitation is the primary cause of cell failure.
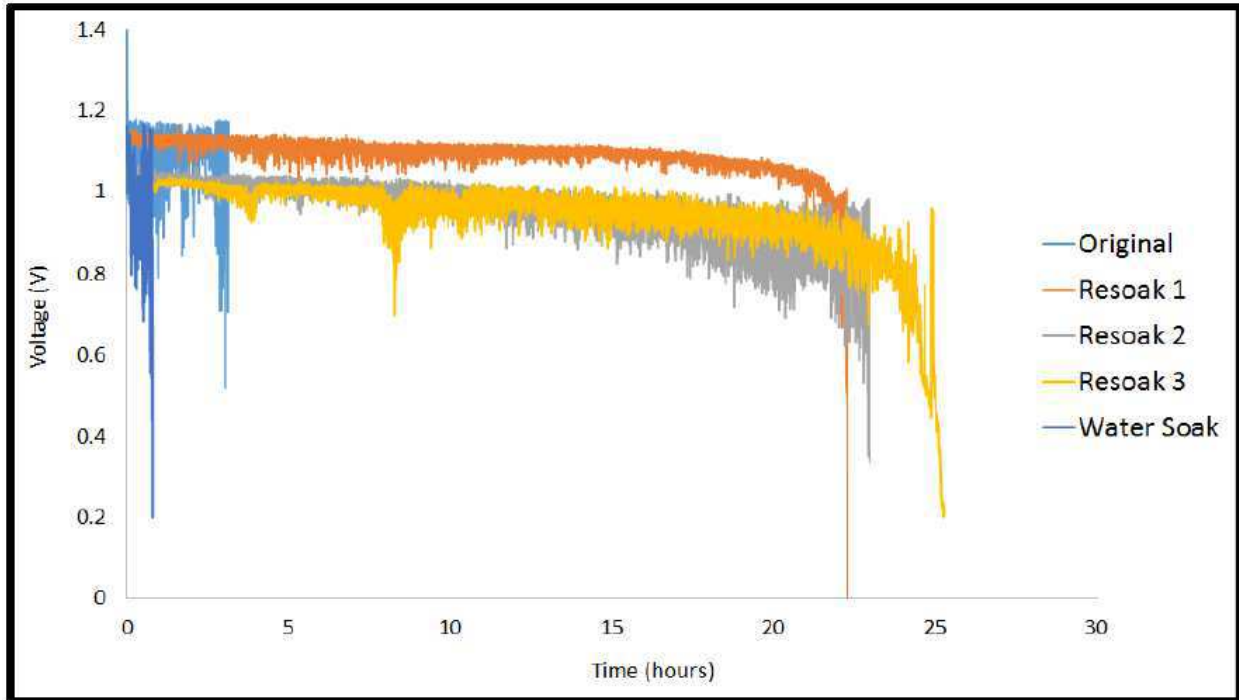
Figure 4-23: Cell separator re-wetting in water and re-soaking in 6 M KOH solution of a zirconia cloth Ga-Air system for cell revitalization at 50°C

In comparison to surface contact resistance failure and cell drying, Figure 4-23 shows that separator carbonation may be the most prominent cause of Ga-Air system failure. It can be seen that in comparison to the original test at 4 hours, cell re-soaks with a 6 M KOH solution not only revitalized the cell, but even increased its overall discharge length, growing progressively longer with each re-soaking, up to 25 hours. However, as soon as the cell was only re-wet in water, the total discharge length did not exceed 1 hour. This is strong evidence that separator re-soaking is replacing previously spent KOH electrolyte solution, which is postulated to become depleted because of carbonation. Moreover, considering that re-soaking the separator brought the discharge performance to original cell assembly levels suggests that carbonation is also a major contributor to the shortcomings of the Ga-Air system in its current form. Thus, if the KOH could be continuously replenished, it is possible that discharge of a much longer duration could be

achieved. This electrolyte flow is certainly indicated for a flow battery configuration based on a Ga-Air chemistry.

4.4.4 Discharge Performance: Effect of Temperature

Temperature is a key factor that should always be considered when the kinetics of a reaction are being evaluated. This is especially true for the Ga-Air system using 6 M KOH electrolyte because water limits the operating temperature range from approximately 0°C to 100°C, which can be partially extended in higher concentration solutions. Moreover, the gallium solidifies below 30°C, further restricting the operating temperature range to 30°C to 100°C if liquid gallium is to be maintained. These are the absolute limits of the system's operating temperatures in the present configuration.

Higher operating temperatures promote electrode kinetics as well as conductivity, but could also promote deactivation processes, e.g. carbonation. As a result, it is inferred that higher temperatures will result in a slightly higher voltage throughout the discharge duration, but will also cause the discharge curve to terminate more quickly. Other metal air batteries supports this postulate as a temperature increase resulted in a decrease in the total discharge duration (Zhou, 2014).

In a previous experiment of the Ga-Air System, a range of temperatures from 40°C to 70°C were tested for overall discharge performance. This system used a single zirconia cloth separator soaked in 6 M KOH and used a Pt-catalyzed GDL cathode. The discharge performance of this system is shown in Figure 4-24.
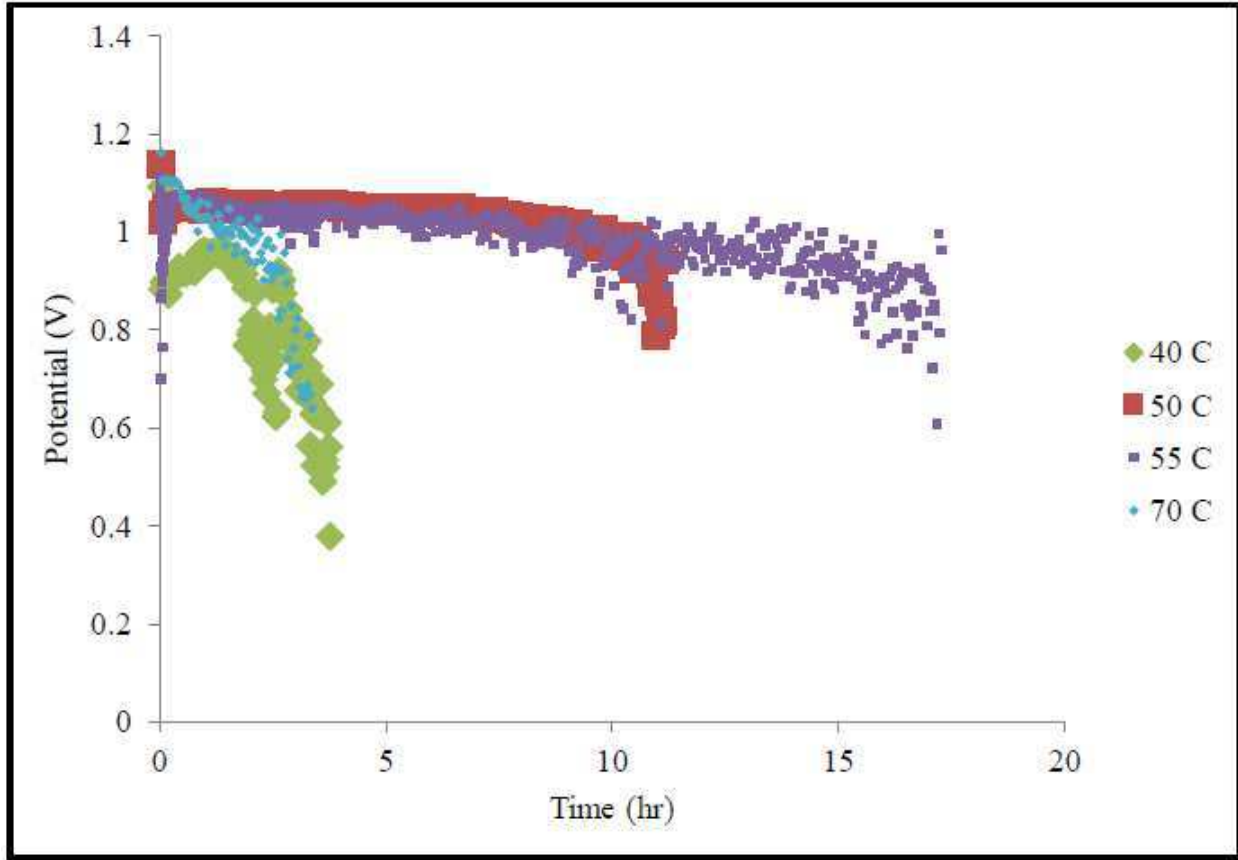
Figure 4-24: The effect of temperature on the Ga-Air System discharge with a 6 M KOH zirconia cloth and a Pt-catalyzed GDL cathode.

The results of this experiment actually demonstrated a behavior where cell performance increased with temperature but more extreme temperatures resulted in a poorer overall cell performance. At both 40°C and 70°C, the system could not discharge for longer than 4 hours. However, when a more moderate temperature was chosen, the discharge duration lasted up to 4 times longer, reaching up to 17 hours at 55°C. For higher temperatures, the postulates effectively explain the drop in performance as both the discharge duration decreased while the starting voltage slightly increased due to lower activation overpotential. This is most apparent when comparing 40°C and 70°C discharge voltages. Moreover, a higher temperature will also result in accelerating the proposed failure conditions: separator drying and KOH carbonation. As a result,

the drop off when increasing the temperature of the system may be more severe because of an acceleration of side-reactions that inhibit cell performance.

To understand the poor performance at 40°C, the most plausible explanation is that the temperature recorded on the outside of the cell did not accurately reflect the internal temperature of the cell for this experiment. Since wetted zirconia cloth is placed directly on the liquid gallium, there is a likelihood that the gallium remained solidified. As 40°C is fairly close to the melting point of gallium (29.8°C), which means the gallium may not have had enough time to thaw prior to testing. To account for this possibility, the variation in temperature tests were reproduced with similar conditions with the exception that two soaked zirconia cloth separators were used instead of one as in Figure 4-24. However, adequate heating time was provided for lower temperature tests. These results are shown in Figure 4-25.
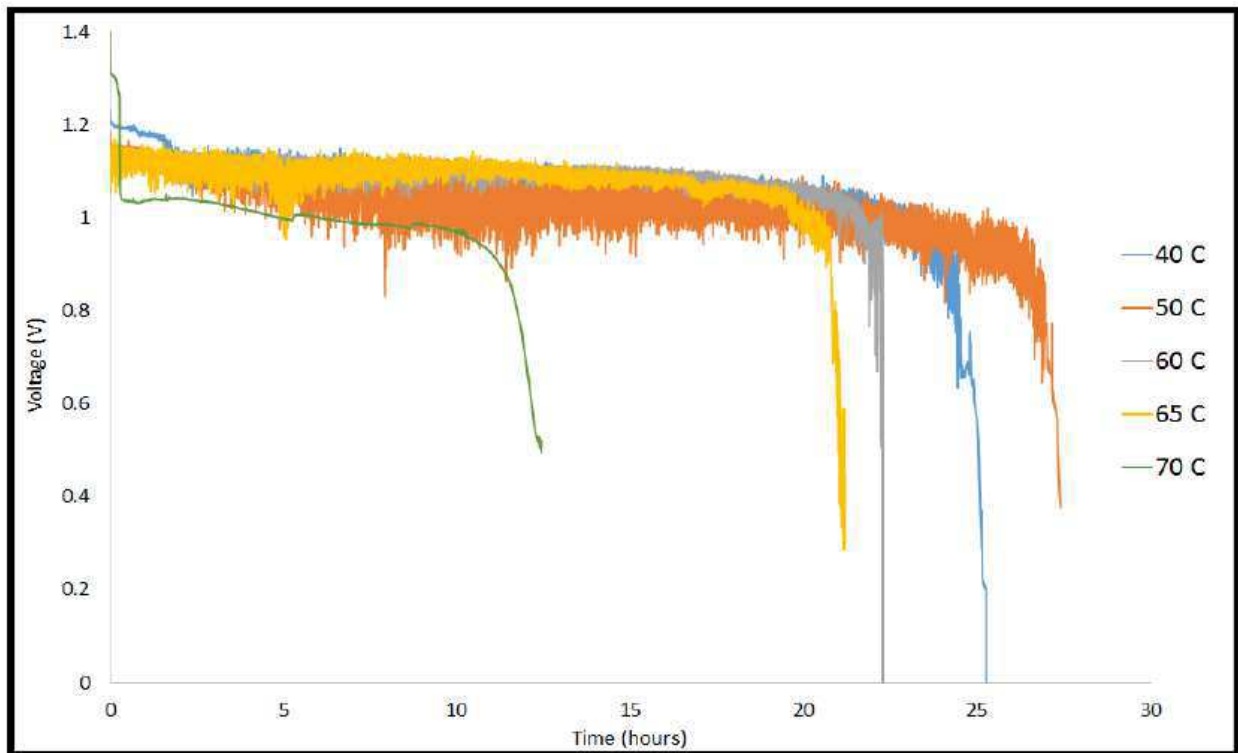
Figure 4-25: The effect of temperature on the Ga-Air System with two 6 M KOH zirconia cloth separators and a GDL cathode.

When the performance is revisited, it is clear that the optimal operating temperature for this system still lies somewhere around 50°C, reaching approximately 27 hours of total discharge. However, the performance at 40°C has significantly improved as wellcompared to that in Figure 4-24, performing only slightly worse at approximately 25 hours of discharge. Moreover, beyond 50°C the predicted behavior of increasing the temperature is shown. A significant decrease in performance at 70°C can be observed, reaching 13 hours, less than half the discharge time at 40°C. This strongly indicates a deactivation reaction that is promoted at higher temperatures

It was also mentioned earlier that the overall temperature performance range does increase slightly when the concentration of the electrolyte is increased. While the lower limit still remains at 30°C, the upper limit can still increase slightly. A test was performed to see if this increase in the temperature upper limit might also lessen the impacts of increasing the temperature above 50°C. This was most easily done by increasing the concentration of the solution to the saturation point, 8 M. Prior investigations had shown that increasing the solution concentration up to 6 M has a dramatically positive effect on cell performance, but little investigations have been conducted on concentrations above this value. To significantly increase the presence of KOH in the Ga-Air system, zirconia cloth separators were soaked in 8 M KOH solution, and two separators were used in the cell to further increase KOH presence. This result is shown in Figure 4-26.
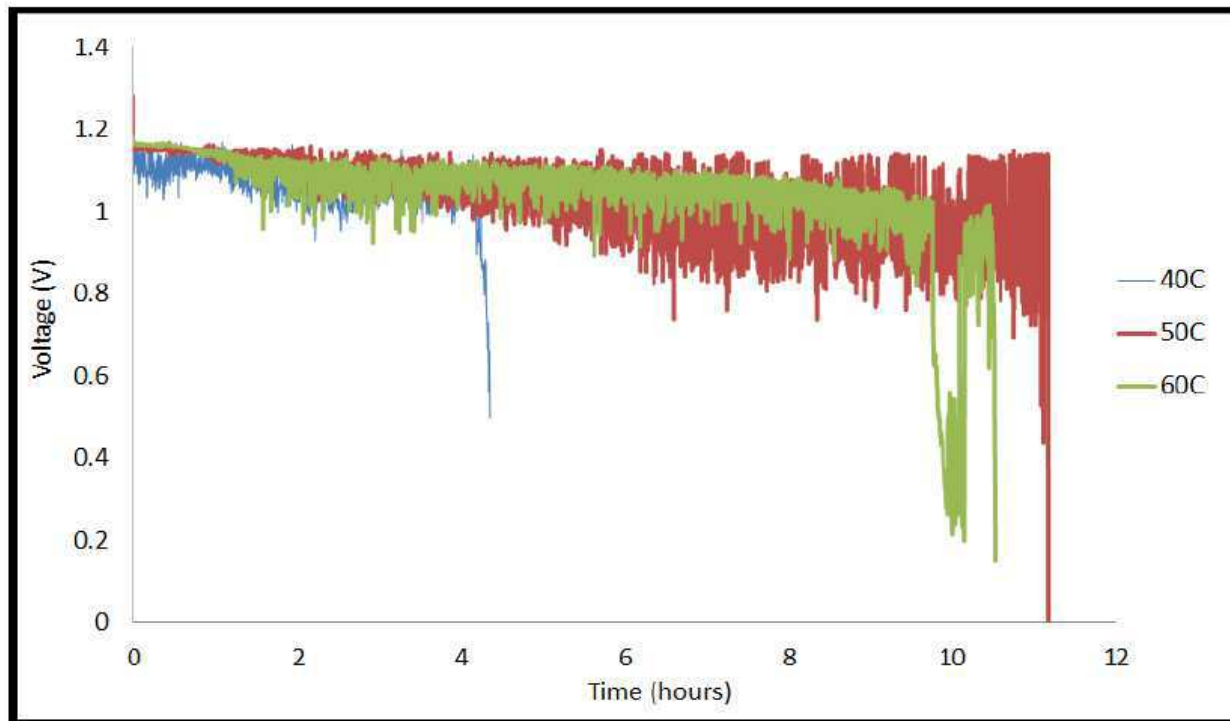
Figure 4-26: Discharge of Ga-Air system with two 8 M KOH zirconia cloth separators.

While 50°C did, in fact, slightly outperform 60°C at approximately 11 hours of discharge, the actual discharge performance of 60°C wasn't nearly as impacted, still reaching 10.5 hours. This suggests that higher temperature applications of the Ga-Air System could be accommodated for with changes to the system concentration.

Additional studies considered the performance of the Ga-Air system at temperatures higher than 70°C, which were difficult to reproduce using a heat lamp. In order to consistently reach these temperatures, a different heating method had to be used. It was found that the most consistent heating method outside of heat lamps was using vacuum ovens. For the sake of brevity, very few tests were performed using a vacuum oven since higher temperature tests generally yielded lower overall discharge times. The discharge time diminishes rapidly as temperature increases as well. From Figure 4-25, a change from 50°C to 60°C resulted in a 15%

drop in discharge time, and a change from 60°C to 70°C resulted in a 43% drop in discharge time.

For the majority of vacuum oven tests, failure was nearly immediate. Oftentimes, this was because the temperature controller of the oven cycled up to 103.7°C, which would cause rapid drying of the cell separator. Moreover, higher temperatures would accelerate carbonation for KOH, which also causes the cell to fail more quickly. The best performing result managed to stay at a temperature of 88°C throughout the entire tests; however, the overall length of this test was still quite short. The performance of the Ga-Air system with one 6 M KOH soaked zirconia cloth separator and Pt-catalyzed GDL is shown in Figure 4-27.
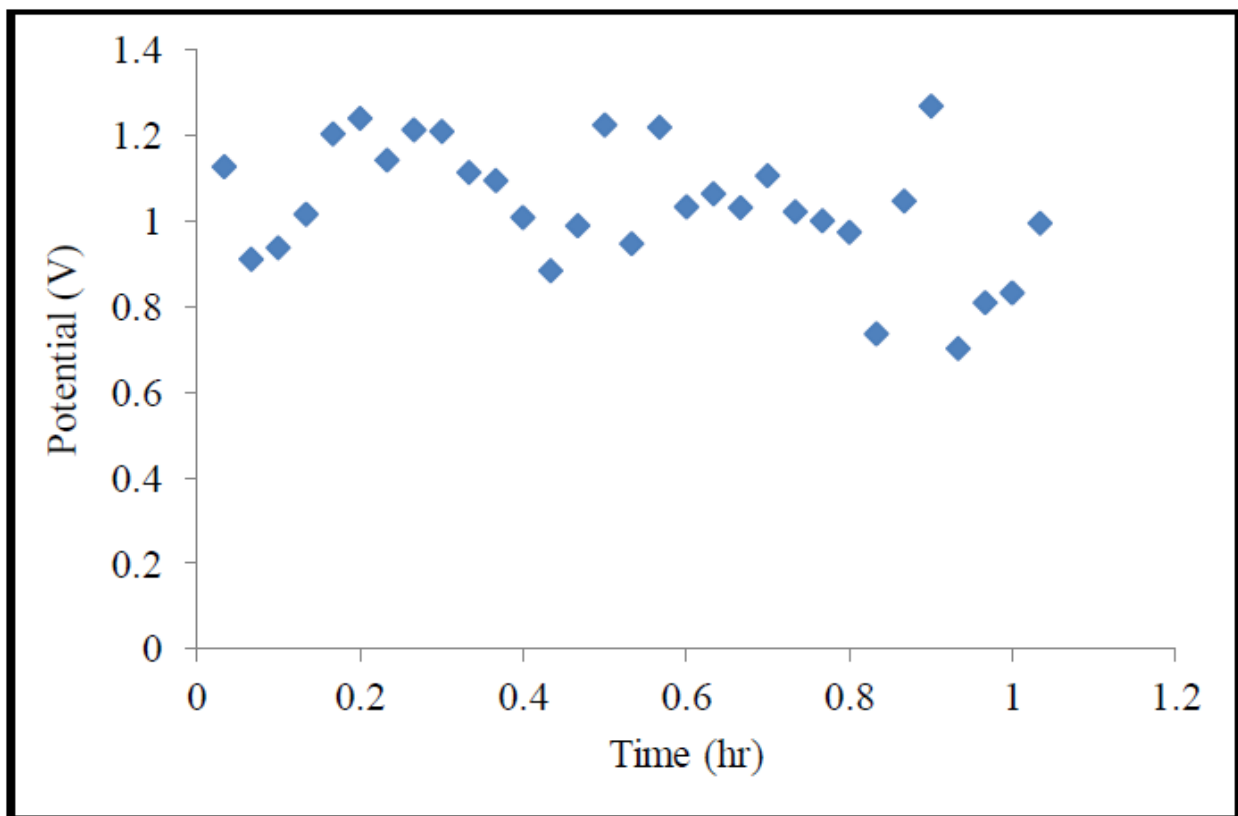
Figure 4-27: Discharge of Ga-Air system with one 6 M KOH zirconia cloth separators at an average of 88°C.

The total discharge time was barely over an hour, which is considerably lower than the other temperature results. In fact, the next lowest discharge time was in Figure 4-25 at 70°C for

13 hours. Moreover, this continues with the trend that increasing the temperature of the system to a point begins to have worsening effects on the overall discharge time because of drying and/or carbonation. However, a direct comparison, including the actual drop in discharge performance, to the results in Figure 4-25 and 4-26 could not be made because of the temperature inconsistencies in the vacuum oven.

This temperature inconsistency also played a role in the discharge voltage in Figure 4-27, which varied between 0.7 V to 1.3 V. Since the oven cycled temperatures, this variation in voltage may be related to this change, with higher voltages at higher temperatures and lower voltages at lower temperatures.

4.4.5 Discharge Performance: Pure O_2 as Cathode

All tests before this have been conducted in an ambient environment with humidity and oxygen content in the air left uncontrolled. To further investigate the causes of cell failure, a slightly more controlled environment was employed to remove one possible cause of cell failure: carbonation of KOH. This was achieved by using a pure O_2 feed at 40°C with a 6 M KOH soaked zirconia cloth separator. Since there was not any CO_2 in the cathode, carbonation would have to be limited entirely to the CO_2 in the cell before the O_2 feed was connected. On the other hand, a pure O_2 feed will increase the extent of cell drying since it has no water vapor content. These combined factors should result in a large change in performance if one of these causes of failure is prominent. The results of the pure O_2 feed test are shown in Figure 4-28.
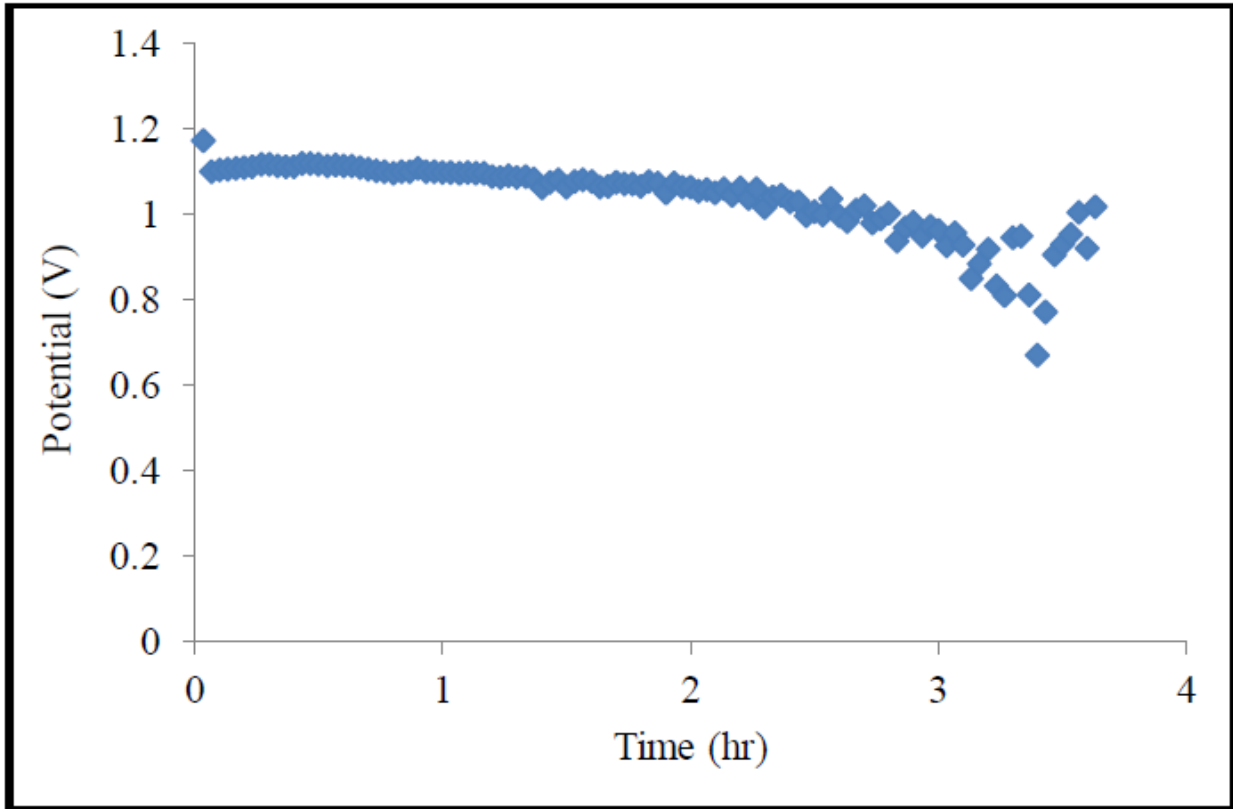
Figure 4-28: Discharge of Ga-Air system with one 6 M KOH zirconia cloth separators and pure O_2 feed at 40°C.

This test came to an overall discharge performance of just under 4 hours, which is comparable to the same result in ambient conditions in Figures 4-24 and 4-26. On the other hand, considering that Figure 4-25 demonstrated that the same temperature condition could achieve upwards of 25 hours, it is difficult to make an accurate comparison at this temperature.

In comparison to Figure 4-24, the total discharge time is quite similar for all results at 40°C. Since the results are similar, this can have a variety of interpretations. First, the cause of cell failure may not be the result of separator drying or carbonation, but instead a different factor. However, this alternate cause of failure would have to account for the differences in performance at different temperatures, KOH concentrations, and cathode materials. Second, the cause of cell carbonation may have a similar but opposite relation to separator drying. Since pure O_2 feed

would lessen the effects of carbonation and increase the effects of separator drying, it is possible that these effects may have cancelled one another.

In comparison to Figure 4-26, the discharge at 40°C is considerably worse for a pure O_2 feed when compared to ambient air. Since the removal of CO_2 from the cathode feed would decrease the effects of any carbonation, the primary losses for the O_2 feed would have to be attributed to separator drying. While this is the most conclusive postulate for the cause of cell failure with pure O_2. It still remains that the most prominent explanations for cell failure are both carbonation of KOH and separator drying.

4.5 Cause of Cell Failure

4.5.1 Cell Failure: Gallium Leakage

For this investigation, the Ga-Air system was assembled with materials that did not remain consistent between tests. Separators, catalysts, and cathode materials were all varied throughout the course of this investigation, but the few factors that were nearly consistent among all tests was the anode and cathode materials: liquid gallium and air, respectively. Since all components in this electrochemical system are fluid, leakage is an ever-present concern, affecting cell performance in a variety of different ways.

First, in-plane air leakage into the gallium anode can cause the gallium to react with oxygen directly. When oxygen and gallium react in this manner, the gallium is simply converted into Ga_2O_3 or $Ga(OH)_3$ without an electrical driving force. Unfortunately, this form of oxygen leakage is nearly unavoidable, and was partially avoided by placing a Teflon O-ring between the stainless-steel crucible and the separators. While this prevented the passage of some oxygen through the separator, it did not entirely stop in-plane oxygen leakage. In fact, the use of this Teflon O-ring appeared to have very little effect on overall discharge time. Moreover, the

87

addition of this space resulted in a systematic error in virtually all the tests of this investigation. However, since this systematic error affected all results, and was most likely minor in nature, which indicates that it can largely be discounted as the primary cause of cell failure.

The second form of leakage is significantly more problematic to results: in-plane gallium leakage to the cathode. While this result was significantly less consistent than oxygen leakage, its results were far more noticeable on the cell performance. An example of in-plane gallium leakage is shown in Figure 4-29.
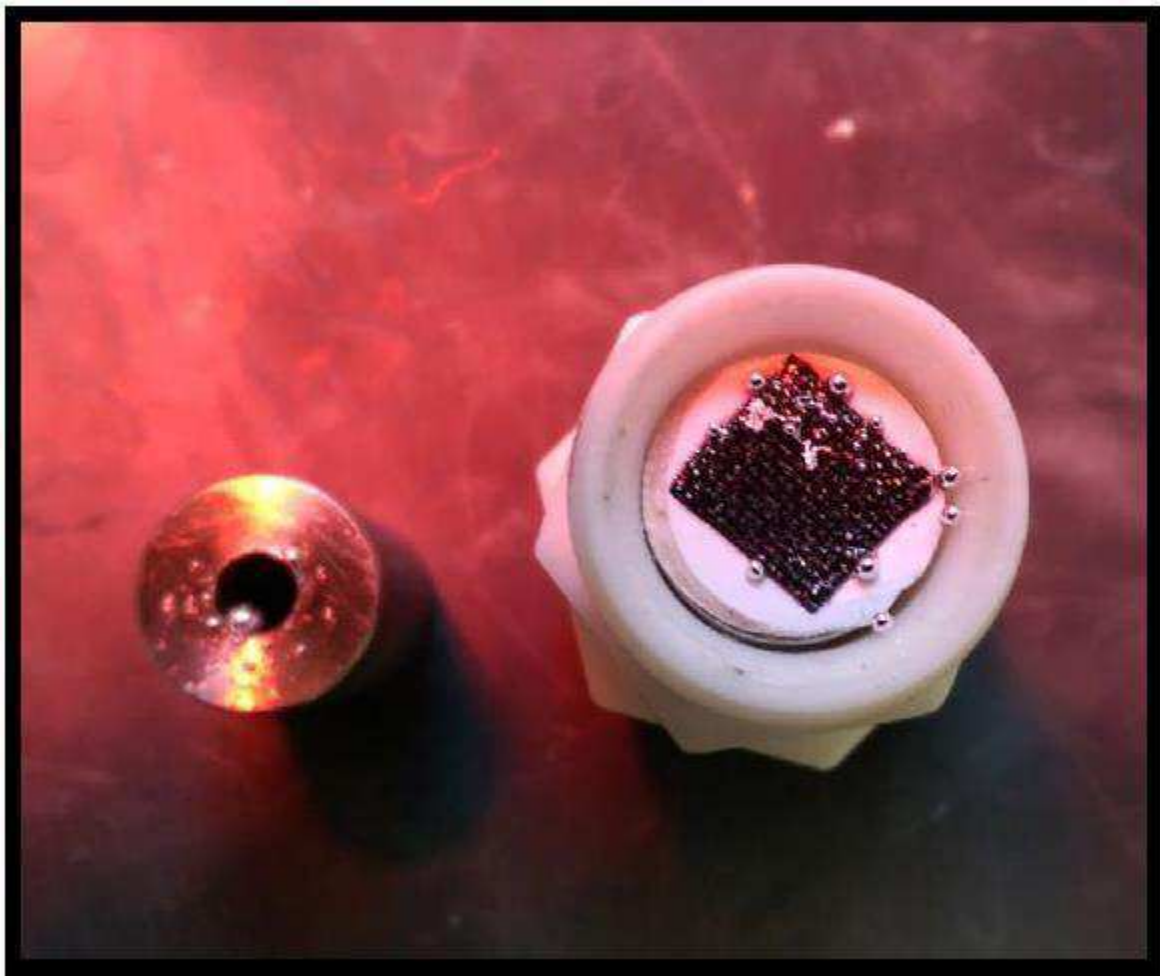
Figure 4-29: In-plane gallium leakage to the anode, contaminating the GDL and short circuiting the cell.

To ensure proper gallium contact with the separator, the Ga-Air system was inverted for tests, allowing gravity to pull the gallium into contact with the separator. While this method

often allowed good surface contact, it did not generate consistent results, possibly as a result of in-plane gallium leakage. This caused gallium to leak through the cathode, contacting the top of the separator and the catalyzed part of the GDL, ultimately short circuiting the cell. Figure 4-29 shows gallium on top of the GDL directly, which could have occurred if the gallium had leaked around the separator. Moreover, this form of leakage also resulted in the contamination of the GDL, affecting the Pt catalyst layer. This prevented the re-use of the cathode material, which was commonly employed since its re-use had virtually no effects on the results and was desirable to preserve an expensive component of the Ga-Air system. To avoid this undesirable effect, the same Teflon O-ring between the stainless-steel crucible and separator was installed to ensure a better seal, which ultimately prevented this form of leakage from short circuiting an otherwise good experiment.

The third and final possible form of leakage was through-plane gallium leakage, which was a rare and difficult to reproduce phenomenon. It most commonly occurred with a single glass fiber separator and resulted in the short circuit of the Ga-Air system and a complete contamination of the cathode material. While the events that lead to failure for through-plane gallium leakage are similar to those of in-plane gallium leakage, they are visually distinct. An example of through-plane gallium leakage is shown in Figure 4-30.

Figure 4-30: Through-plane gallium leakage to the anode, short circuiting the cell.

When considered against Figure 4-29, evidence of through-plane gallium leakage is much subtler than in-plane gallium leakage. In Figure 4-29, the leaked gallium is clearly more metallic, making it evident that it was unreacted gallium that reached the cathode of the cell. In contrast, Figure 4-30 shows smaller black flecks of gallium or its products with an in-tact seal between the separator and the Teflon O-ring. This form of leakage could also lead to the short circuiting of the cell, but it was uncommon throughout testing. Moreover, typically the effects of through-plane gallium leakage were much lower impact on the actual testing results, potentially contributing to results with more "noise" in the voltage reading. While it would be ideal to avoid this form of leakage entirely, it was ultimately dismissed as minimal in occurrence and impact.

4.5.2 Cell Failure: Potassium Hydroxide Carbonation

When the Ga-Air cell is properly assembled, it typically runs in the range of 4-30 hours, depending on the testing conditions. This duration is quite acceptable for the proposed smart grid system with Ga-air batteries since the maximum necessary time a battery would have to be

operated would be less than 24 hours before recharging. However, this range is also significantly shorter than calculated theoretical performance of 1384 hours for a complete discharge (Howard, et al., 2015). It is imagined that a better design along the lines of a commercial Zn-Air battery would allow increased capacity. Carbonation of KOH in the separator is one proposal to explain the maximum efficiency of 2.16% of the constructed Ga-Air system. Because ambient air is typically composed of 0.04% carbon dioxide (CO_2), carbonation is more likely to occur in an aqueous hydroxide. When these conditions are maintained at a slightly elevated temperature, carbonation becomes increasingly likely. For KOH specifically, carbonation would follow this reaction:

$$2\ KOH + CO_2 \rightarrow K_2CO_3 + H_2O \tag{4.6}$$
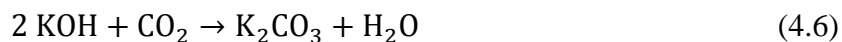
This reaction ultimately would cause the potency of the Ga-Air system to weaken as more KOH converted into K_2CO_3 and would ultimately cause the Ga-Air system to cease functioning. In order to investigate if this proposed cause of failure is significant enough to inhibit the reaction, KOH was directly monitored for carbonation. A eutectic of NaOH and KOH was used to create a liquid hydroxide that would still be susceptible to carbonation at 180°C. Figure 4-31 is a visual confirmation of carbonation of hydroxides in ambient air.

Figure 4-31: KOH/NaOH eutectic heated and monitored for carbonation.

The reflective liquid in the graphite crucible is the liquid eutectic of KOH and NaOH, which were mixed together as two separate powders. The entire crucible was cleaned with the powder only inside the crucible over the course of heating to 190°C. Despite this action, a white powder ring still formed on the edge of the graphite crucible, which remained solid despite heating. Naturally, this would not make sense if it were part of the KOH/NaOH eutectic, but a reasonable explanation is that it was K_2CO_3 or Na_2CO_3 formed through carbonation. These compounds have melting points of 891°C and 851°C, respectively, and would, consequently, remain solid at 190°C. For this reason, carbonation is most likely at least a partial cause to the premature failure of the Ga-Air system.

To look further into this cause of failure, a different cell design was proposed that was more resilient to carbonation. An anion exchange membrane (AEM) was tested since its organic properties allow it to have a similar solubility to its carbonated form. This phenomenon is described in Equations 4.4 and 4.5. When a single AEM separator was tested, the results were slightly longer when compared to a single zirconia cloth separator and a single glass fiber

separator (see Figures 4-17, 4-18, and 4-19). In fact, the AEM had approximately a 16 hour

discharge time, which was almost double the zircona cloth (10 hours) and quadruple the glass

fiber (5 hours). This is fairly evident that for tests of similar separator density, AEM's have some

of the greatest longevities.

4.5.3 Cell Failure: Separator Drying

While carbonation of KOH seems to be a leading cause of Ga-Air system failure, another

potential cause of failure was also considered: separator drying. Since the majority of Ga-Air

systems throughout this investigation require the use of aqueous electrolytes, the drying of the

separator would result in a lack of mobile ions to facilitate the Gallium-Oxygen reaction.

Separator drying can thereby be linked with carbonation with an overarching cause of failure:

KOH ion immobilization. Unfortunately, it was challenging to distinguish between the two

causes since they are often exacerbated by the same conditions, such as higher temperature and

duration of experimentation. A series of photographs were taken to monitor the process of the

drying of wetted zirconia oxide cloth in ambient air, which are shown in Figure 4-32. The time

frame of exposure to ambient conditions are comparable to some of the longer length discharge

results (24 hours).

Figure 4-32: Left: An unsoaked zirconia cloth separator.
Middle: A KOH wetted zirconia cloth separator.
Right: A dried zircona cloth separator, previously KOH wetted.

Figure 4-32 shows a zirconia cloth in three different conditions, which would be expected to exist at some point during experimentation. The dry non-soaked zirconia separator appears to have similar flexibility to the other separators, including the dried separator, which would presumably be more rigid if carbonation was common in ambient conditions. Moreover, this is quite different from the separators that were heated to higher temperatures, as shown in Figure 4-33, for example.

Figure 4-33: A zirconia separator covered with a GDL after a high temperature test

The zirconia separator was considerably less flexible after a higher temperature test, which might suggest that more than simply evaporation is occurring in this process. Ultimately, the difference in dried separators in ambient and heated conditions, suggest that both separator drying and carbonation play distinct but cooperative roles in causing the Ga-Air system to fail.

4.6 Rechargeability Performance

4.6.1 Rechargeability: Cell Cycling

The long-term goal of the Ga-Air system is to aid in a smart grid infrastructure that can effectively store electricity in a large collection of flow batteries. Most of this investigation has focused on the discharge capabilities of the Ga-Air system, but of course it is essential that the rechargeability of the system also be eventually considered. Similar to the discharge part of this investigation, a baseline of the current commercially available batteries was first established. Unlike system discharge however, rechargeability must be evaluated with battery cycling, which consists of discharging and recharging the battery multiple times to evaluate system longevity. Cycling was first performed with a commercially available nickel-metal hydride (NiMH) battery (AA Portable Power Corp 2552). The results are shown in Figure 4-34.
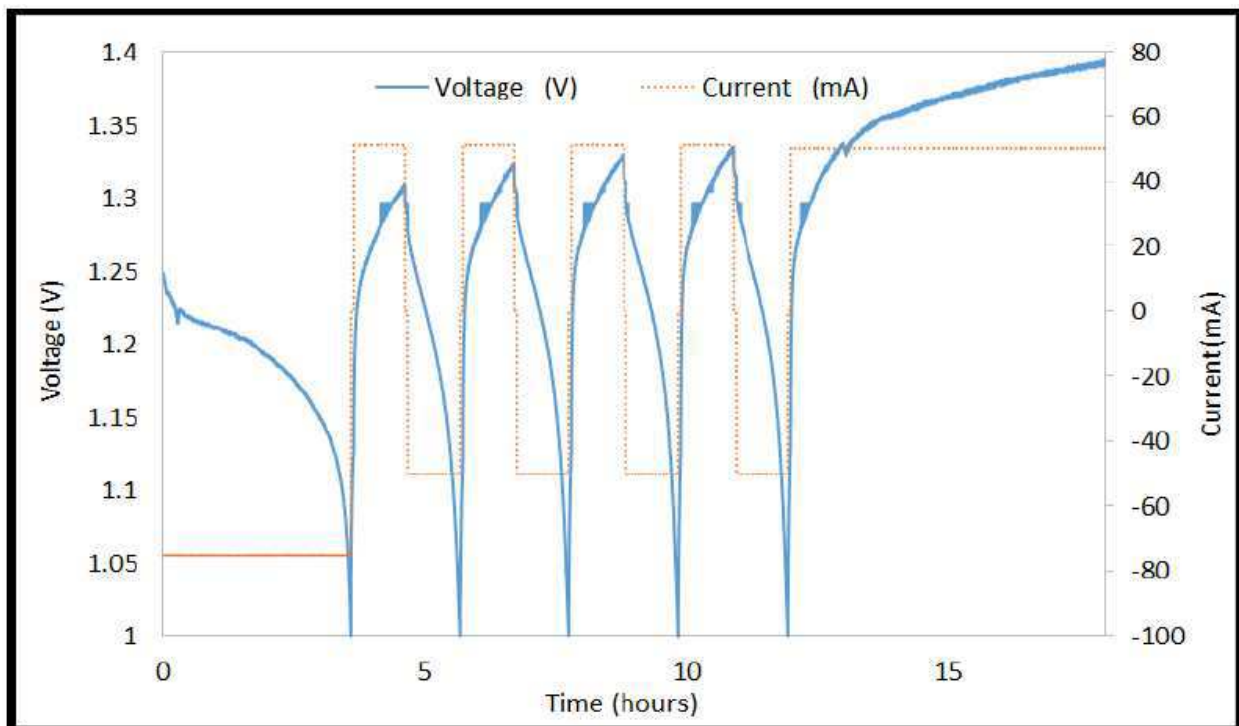
Figure 4-34: NiMH battery (AA Portable Power Corp 2552) cycling at a current of 50 mA at 50°C.

Figure 4-34 shows the NiMH battery is quite effective during the cycling process, completing 5 total charge/discharge cycles at a current of 50 mA. Naturally, this is to be expected of a commercially available rechargeable battery, since most of these systems are expected to have a long lifetime even when put under a high electrical load. Regardless, Figure 4-34 illustrates a performance which would also be desired of the Ga-Air system, similar to the Zn-Air system as a desirable performance of the Ga-Air system discharge. The first attempt of the Ga-Air system cycling was performed with wetted zirconia cloth and a Pt-catalyzed GDL. This result is show in Figure 4-35.
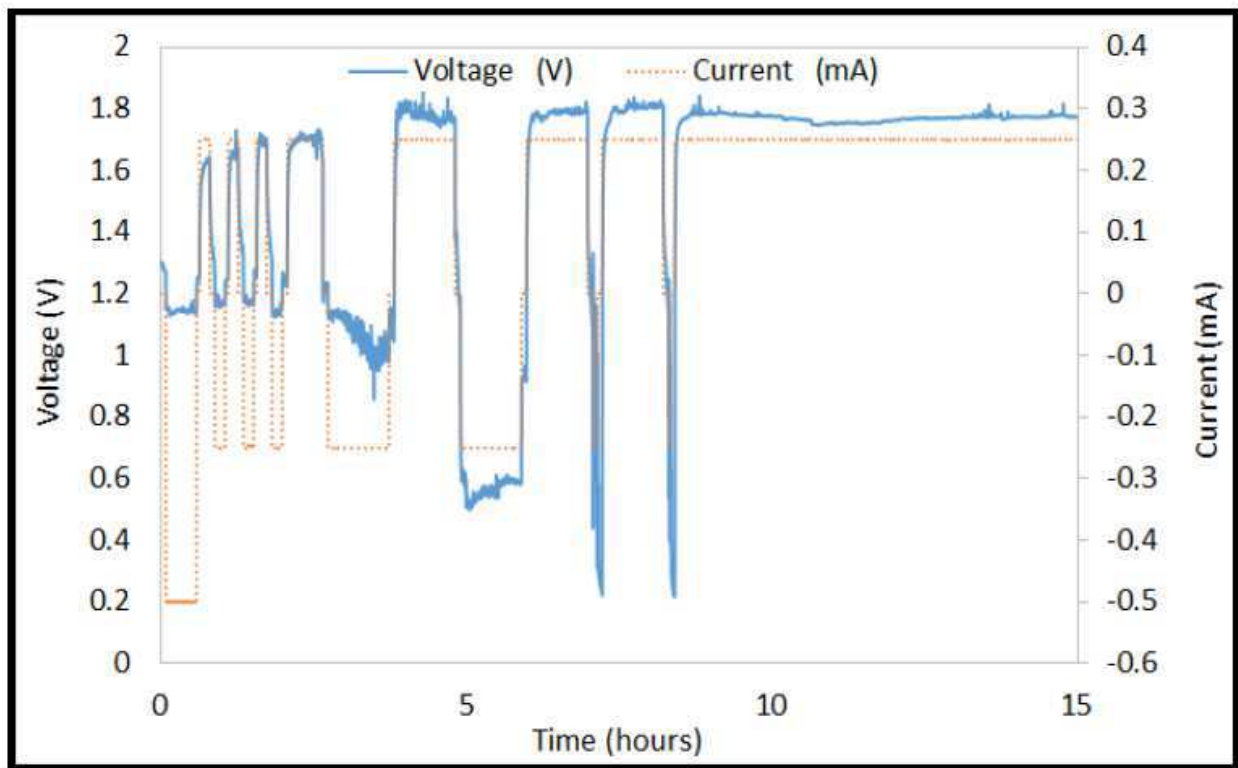
Figure 4-35: Ga-Air battery with Pt-catalyzed GDL cathode cycling at 0.25 mA at 50°C.

When the Ga-Air system was put under a load of 0.25 mA, which is considerably less than the load of 50 mA for the NiMH battery and only half the standard discharge current, it was put through a total of 6 cycles. Despite the squarer look to the curves, the Ga-Air system did complete about 4 cycles consistently. It was hypothesized that this poor performance was caused

96

by using platinum, which is an effective catalyst for water electrolysis above 1.2 V. Since

recharging the Ga-Air system required that the voltage increase up to 1.8 V, this may have

caused the water to electrolyze more quickly than the battery recharged, ultimately causing the

cycling to fail beyond the 4th cycle. In order to prevent the electrolysis of water, an alternate

cathode material was used. MnO_2 was chosen for this test, and a preliminary single cycle was

performed to evaluate the OCV of the battery after discharge and recharge. The results are shown

in Figure 4-36.
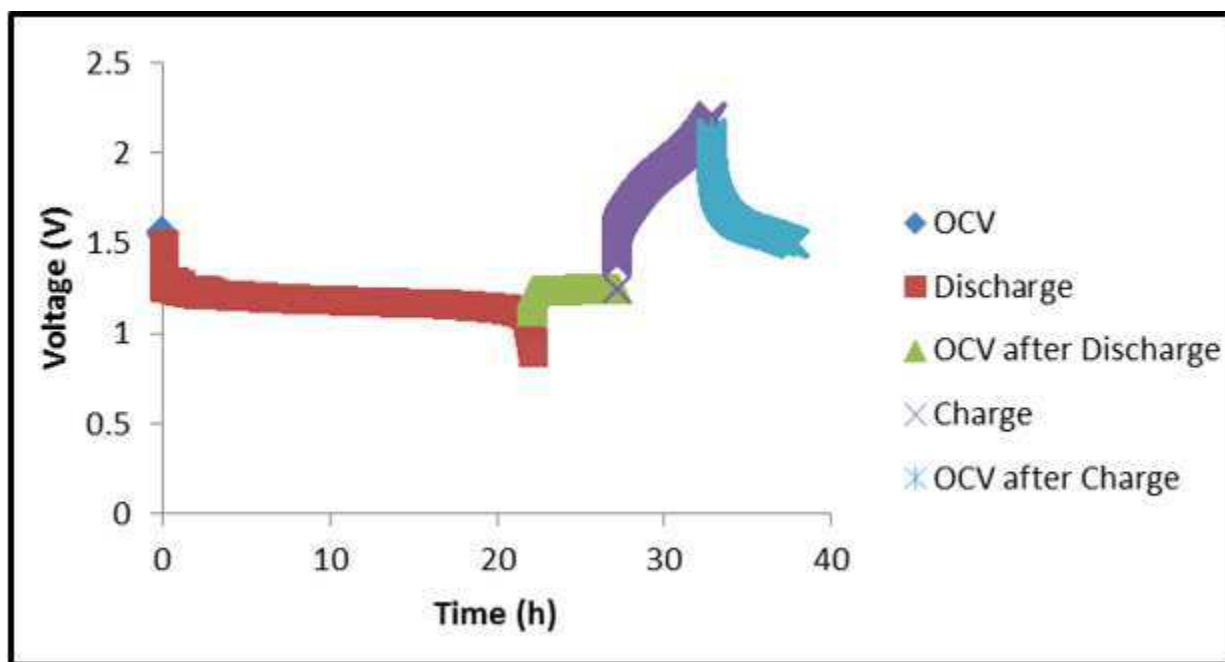
Figure 4-36: Ga-Air battery with MnO₂ cathode single cycle at 0.5 mA at 50°C.

This was a promising result, since the OCV was clearly lower after the Ga-Air system

discharged for 20 hours. But after the cell was recharged with 0.5 mA of current, the OCV

appeared to approach the starting OCV, which suggests potential for another successful

discharge. This system was then evaluated over 3 cycles at a lower current of 0.25 mA, shown in

Figure 4-37.
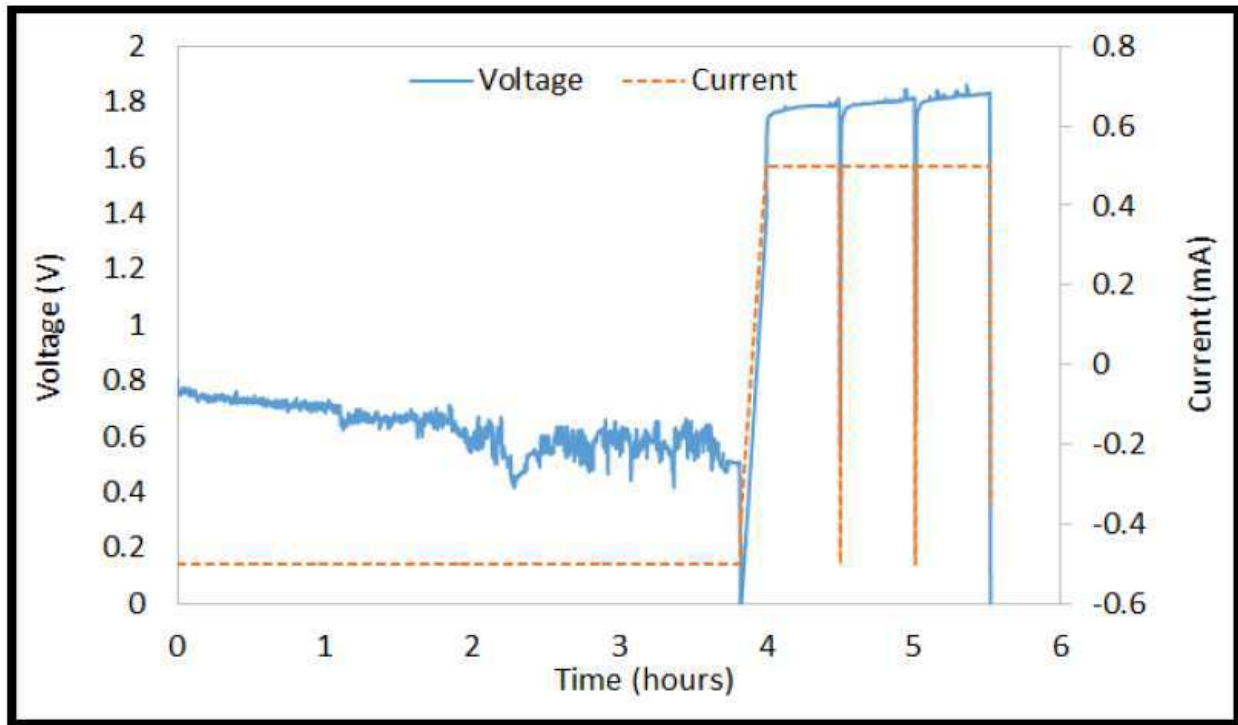
Figure 4-37: Ga-Air battery with MnO$_2$ cathode cycling at 0.25 mA at 50°C.

Only 3 cycles were attempted for this experiment because, despite the promise of the first cycle, the system appeared to hold nearly no charge once recharged. This result was significantly worse than the Pt-catalyzed GDL in Figure 4-35 even though it avoided catalyzing water electrolysis. However, this poor result may not actually be entirely indicative of the actual cycling performance of the Ga-Air system with a MnO$_2$ cathode. The reason for this is based on the discharge cutoff at 0.2 V, which is considerably lower than for the Pt-catalyzed GDL and even the first cycle of the MnO$_2$ cathode, 1V. Before this test, the lower voltage cutoff was set somewhat arbitrarily, but the poor recharge result of the 0.2 V cutoff established a more consistent cutoff of 1 V. This new cutoff was applied with an AEM separator, which presumably would also be more effective for a rechargeable system since it is more resilient to carbonation and separator drying, which also makes it effective to combat water electrolysis. The AEM

separator was used with a Pt-catalyzed cathode with a discharge and charge current of 0.5 mA. Figure 4-38 shows the overall cycling performance of this system.
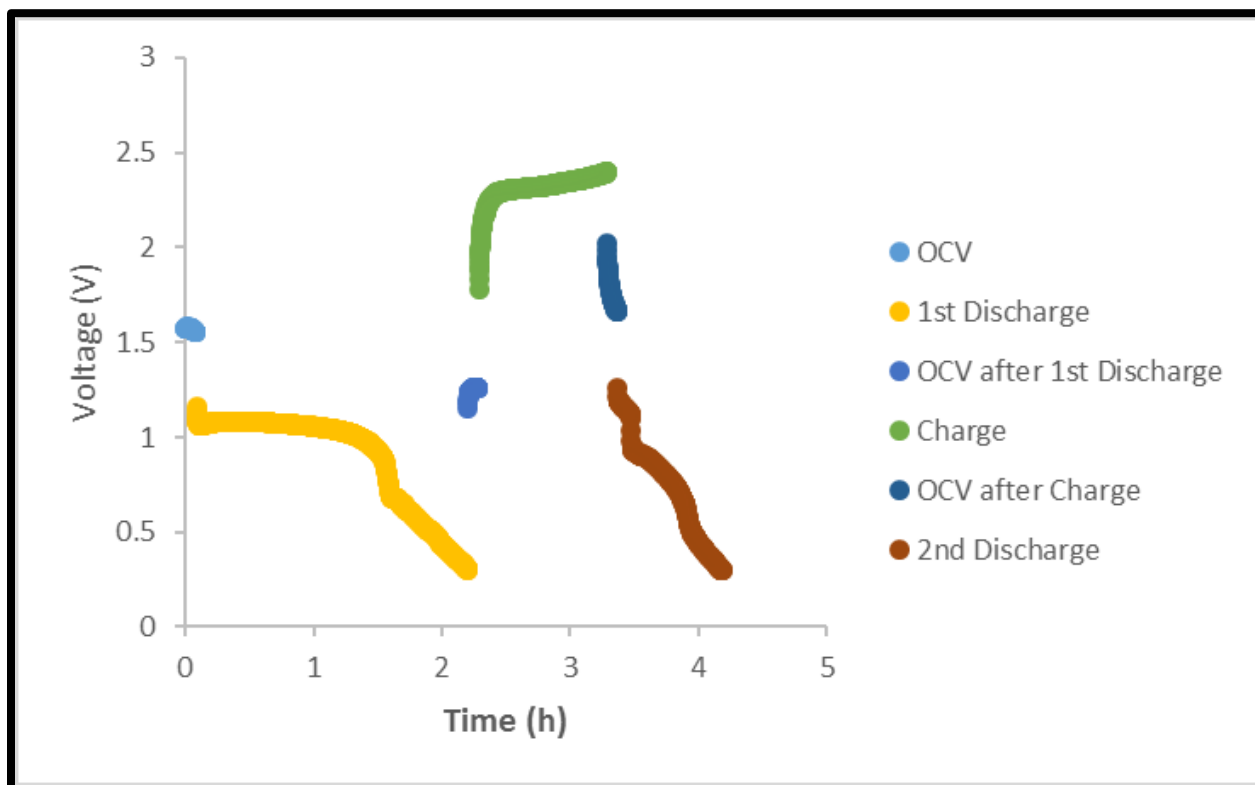
Figure 4-38: Ga-Air battery with AEM separator and a Pt-catalyzed GDL cathode single cycle at 0.5 mA at 50°C.

This single cycle of the system shows great promise since it was put under a slightly higher current load of 0.5 mA. Moreover, the second discharge of the cell lasted nearly an hour, which was only half of the original discharge. While this is not the ideal duration for the second discharge duration (which is obviously nearly the same as the first discharge), but it is one of longest achieved discharges throughout the course of cycling testing of the Ga-Air battery. Ultimately, this is another excellent reason to consider AEM separators for the Ga-Air system.

It should be noted that the lower voltage cutoff for the Ga-Air system was at a similar level to the NiMH battery—1 V. There were a few exceptions to this, like the 0.2 V cutoff for the MnO_2 cathode. However, 1 V became the established lower voltage cutoff because when a Ga-

Air battery was completely discharged with the MnO_2 cathode, recharging the cell became impossible. Instead of leaving this voltage cutoff as an arbitrary value that works, cyclic voltammetry was conducted to better understand the reason for this reaction irreversibility.

4.6.2 Rechargeability: Cyclic Voltammetry

During the cycling testing, most results were able to hold some level of charge during the discharge period following the charge. However, this did not hold true for the MnO_2 cathode test, which despite one cycle appearing promising, failed to hold any charge. The primary difference in the results between the single cycle (Figure 4-36) and the triple cycle (Figure 4-37) was the cutoff voltage for the discharge. The single cycle cutoff at 1V and appeared to hold a charge after the recharging, whereas the triple cycle cutoff and 0.2 V and failed to hold any charge for all three cycles. Cyclic voltammetry can provide some insights into the different behaviors at different cutoff voltages.

Testing for cyclic voltammetry is partly similar to polarization curve testing, but instead of varying the current over time, the voltage is adjusted linearly with time instead and the current is measured. Moreover, the voltage is often varied over multiple cycles during the duration of the test, which creates an outline of a curve that is sensitive to certain voltage cutoffs, changing the curve for future iterations. The voltage of the system was varied between 0.2 V and 1.6 V five times, extending beyond 1.6 V to 2.3 V for the final cycle. This was to confirm that the electrolysis of water also occurs during testing. This voltage cycling is illustrated in Figure 4-39.
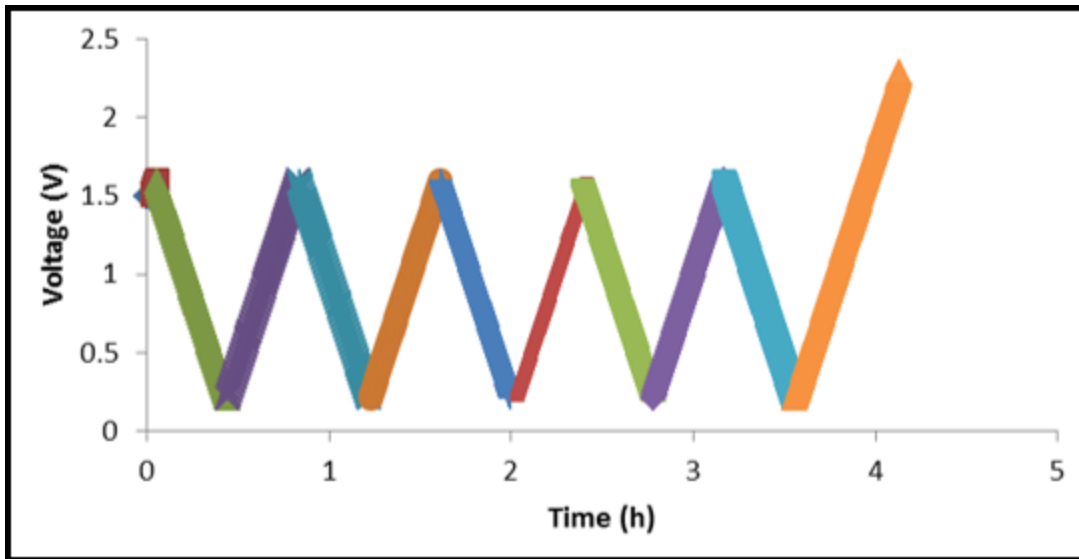
Figure 4-39: The cyclic voltammetry sequence for the Ga-Air system, cycling between 0.2 V and 1.6 V five times, and increasing to 2.3 V for the final cycle.

Using this cyclic voltammetry sequence, the test was performed on a Ga-Air system with three 6 M KOH soaked glass fiber separators and a MnO_2 cathode. This result is shown in Figure 4-40 in the form of the standard "sideways S" shape. This shape is the relation between the peak anodic and cathodic currents (Nicholson, et al., 1964).
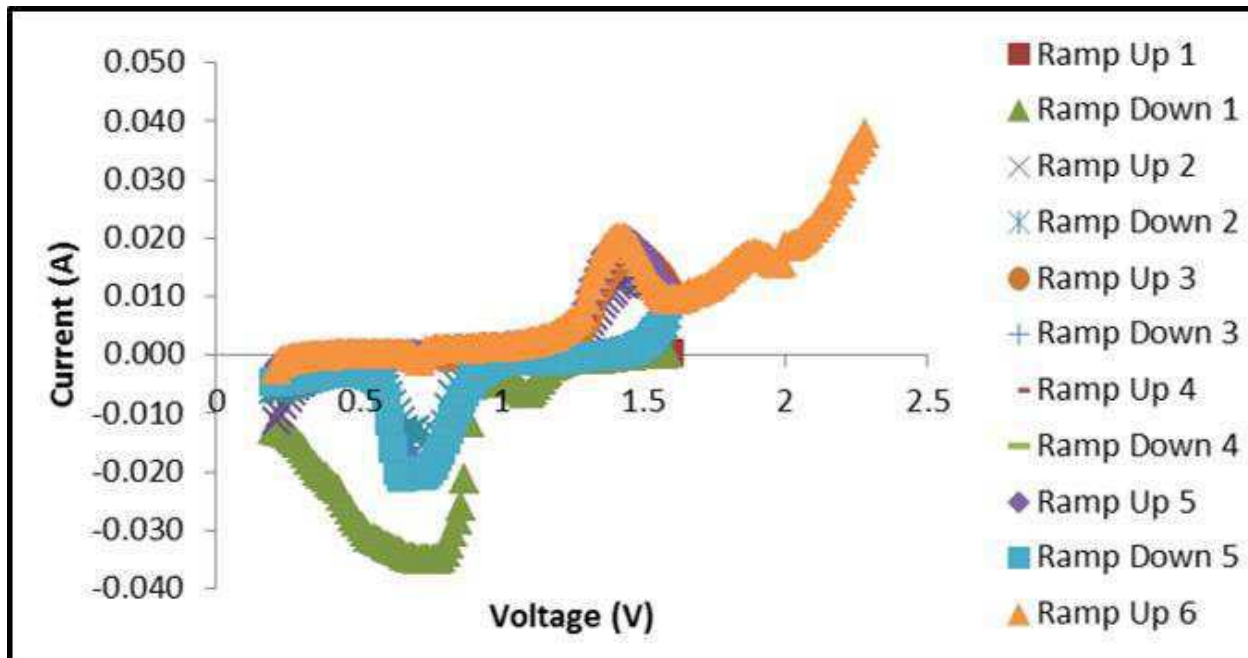
Figure 4-40: Cyclic Voltammetry of the Ga-Air cell with three 6 M KOH soaked glass fiber sheets and an MnO_2 cathode at 50°C.

While the test does have the general "sideways S" shape, there are actually a few other notable peaks in Figure 4-40. First, the first discharge curve has a larger peak around the 0.8 V mark. This is an indication that there was some form of loss during charging for the following discharges. Moreover, this 0.8 V level is confirmed by discharge results in Figures 4-19 and 4-20, which first dropped from a plateau at around 1.0 V, to stabilize again at another plateau at 0.8 V. This was only the case for tests that were constructed with glass fiber separators, however. Second, there is a cathodic limit that is well outlined at around 1.4 V, which suggests that this is the optimal general recharge voltage for the Ga-Air system. While these are general points about the general performance of the Ga-Air system, these peak limits do not explain the difference in shape of the first discharge.

There are two important points, which may explain the larger peak for the first discharge. First, there is a small, but distinct peak for the first discharge at approximately 1.0 V. This peak is not repeated for any other discharges, but should correspond to some form of reaction in the system. Furthermore, this value corresponds to the general discharge voltage for nearly all the discharge results. Additionally, it was the most effective cutoff voltage for cycling testing to ensure that the cells held some degree of charge. This may be some form of reaction that is only reversible at a voltage that greatly exceeds the electrolyzing voltage of water. Leading into the second point, there is a small peak right before the dramatic increase that occurs during the final charge. This peak exists at approximately 2.0 V, which is far above the effective water electrolyzing voltage of 1.48 V (Zoulias, E., et al.). However, this peak may exist as the reversing voltage for the peak anodic current at 1.0 V, which would explain the lack of this peak for future discharge cycles. Moreover, it may play a partial role in the recharging of the other

peak anodic current at 0.8 V, which would cause the first discharge peak to be larger than subsequent peaks.

Because of cyclic voltammetry, it was possible to evaluate the performance of the Ga-Air system over a wide range of voltages. This was able to find peaks that reasonably corresponded to the consistent voltages of the discharge results. Furthermore, it provided some insights into the the reason for a cutoff voltage of 1.0 V for cycling testing since the Ga-Air system actually has two peak anodic and cathodic currents. Additionally, the nature of the reaction has been partially revealed as well, showing that the process is not simply the formation of Ga_2O_3 or $Ga(OH)_3$, but also has an intermediate step with a much higher voltage required for reversibility.

5. Conclusions and Recommendations

5.1 Ga-Air System vs. Commercially Available Systems

As a part of this investigation, comparisons were made between the variations on the Ga-Air system and commercially available battery systems. While directly comparing the discharge results and cycling results of the Zn-Air system and the NiMH battery, respectively, seems reasonable, these graphs were always put under different test conditions than the Ga-Air system. While this does make it unreasonable to compare the results directly, equalizing the parameters to allow for a direct comparison would cause the Zn-Air system and NiMH batteries to perform for extremely long periods of time (>100 hours) or would cause the Ga-Air system to fail nearly instantly. Despite the lack of a direct comparison between commercially available systems and the Ga-Air system, tests were still performed on the Zn-Air system and the NiMH battery to establish a baseline of standard commercial performance.

Because the performance of the commercial Zn-Air system and the NiMH battery were significantly superior to the Ga-Air system, this made them a form of "long-term" goal in an effort to achieve a similar result with the Ga-Air system. Throughout the course of this investigation, the performance of the Ga-Air system was never able to directly compete with the commercially available batteries, but moderate improvements to the system over time allowed an increase in total discharge performance from an initial 4 hours up to 30 hours. It is postulated that this is because the liquid gallium-electrolyte interface was 2-dimensional, unlike the commercial Zn-Air battery, for instance, limiting the reaction to this interface, and leaving the bulk of the liquid gallium intact. In terms of discharge, when the Zn-Air system is corrected for differing operating currents, the most effective Ga-Air system performance was only just over

3% of the standard Zn-Air performance. However, over the course of this investigation, the Ga-Air system had an order of magnitude increase in discharge duration, from 4 hours to 30 hours.

Moreover, since theoretical considerations show that the Ga-Air system contains more potential than the Zn-Air system, there is still promise to continue to improve the Ga-Air system. Additionally, the abundance of gallium is quite competitive with other such as lithium metals in the Earth's crust, at 19 ppm. While gallium is currently expensive since it is primarily accessed as a byproduct of bauxite mining, its abundance in the Earth's crust could drive it to a more competitive pricing if a widespread use for gallium is established.

One possible improvement that can be made to the Ga-Air system to make it behave more like the Zn-Air system is to increase the reactive surface area of the gallium. The current Ga-Air system uses a two-dimensional reaction interface between the cathode and the anode, which is significantly more limited than the three-dimensional slurry used in a Zn-Air battery. By thoroughly emulsifying the gallium and electrolyte in the system, more active sites could be revealed, potentially improving the performance of the Ga-Air system. This method could also help mitigate cell drying as a possible cause of failure.

Cycling results were also evaluated under different conditions depending on the cell construction. For instance, the NiMH battery successfully completed at least 5 discharge/charge cycles at 50 mA of current during testing. However, the single 6 M KOH soaked zirconia cloth separator Ga-Air cell was only able to complete 3 discharge/charge cycles with a current of 0.25 mA. Naturally, these results just do not compare. Despite this, the Ga-Air system did demonstrate some promise with rechargeability, and while it did not match the commercially available results, cyclic voltammetry was able to provide further insights in to possible improvements of the Ga-Air system. One possible improvement is to limit the lower voltage

cutoff to 1V instead of 0.3 V. This allows for the first and more easily reversible gallium-air reaction to be reversed without electrolyzing the water in the system. Additionally, any possible changes that would improve the discharge performance of the Ga-Air system should conceivably also improve the charging performance of the same system. For that reason, it is recommended that non-aqueous Ga-Air systems be investigated since they largely avoid both electrolyte carbonation and separator drying.

The culmination of these findings was a currently-optimized design of the Ga-Air system in a Swagelok cell. While zirconia cloth and glass fiber sheet separators had overall the longest discharge performance, the AEM membrane is recommended for the optimal design. AEM is the optimal choice because its discharge performance was well within a 24 hour performance scope, it is more resilient to carbonation than KOH, and it is the most responsive to recharging. A Pt-catalyzed GDL should be used with the AEM initially and the cell should be maintained at 50°C.

5.2 Causes of Failure

Virtually all tests performed in this investigation took the form of exhaustive battery testing, pushing a given system to the point at which it ceases to perform any further. Naturally, the limiting factor of an exhaustive battery test should primarily be the result of the theoretical capacity of the system, with anodic and cathodic losses being minimized as much as possible. Unfortunately, this was rarely the case with the exhaustive discharge tests of the Ga-Air system. Oftentimes, the tests were simply stopped by some form of leakage causing the cell to short circuit. If a test was constructed robustly enough to avoid leakage, it still ended significantly earlier than expected because of presumably KOH carbonation or separator drying. It is also possible that the reaction interface between the anode and the cathode only caused the topmost part of the gallium surface to react, leaving the vast majority of the remaining gallium unreacted.

A purpose of this investigation was also to establish the most prominent causes of cell failure that the current construction of the Ga-Air system has. Some methods were instituted to help mitigate these issues; however, many of these causes of failure were ultimately left unanswered. As it stands, the two most challenging causes of failure that currently face the Ga-Air system is KOH carbonation and separator drying; these causes of failure are currently both considered to play an active role in cell failure. Additionally, while construction of the cell was improved over the course of this investigation, it is always desirable to assemble a more robust cell that is generally less susceptible to short circuiting. Finally, a mostly unanswered limiting factor the Ga-Air system is the use of a two-dimensional reaction interface. Even if this reaction interface is not a cause of cell failure, advancing to a three-dimensional reaction interface would undoubtedly greatly increase the efficiency of the cell. This hypothesis can also be tested by continuously replenishing the electrolyte as in a flow cell.

The key recommendation to try to avoid Ga-Air system failure in future investigations should be to address carbonation. As mentioned above, this can be accomplished with a continuous supply of the electrolyte. In a different vein, it might be better to consider using an AEM or separator containing ionic liquids, which are less susceptible to carbonation, although the AEM can still dry. This AEM separator has also demonstrated promise for rechargeability as well, which makes it a promising candidate for future study. To potentially improve the Ga-Air system even further, it would be advisable to also avoid separator drying in future designs. While the AEM is somewhat resistant to this cause of failure, creating a design that is entirely unaffected by separator drying would be preferable. One possible design would consist of a flow battery design that continually refreshes any electrolyte and encourages anode flow for more surface contact. A potential design is shown in Figure 5-1.
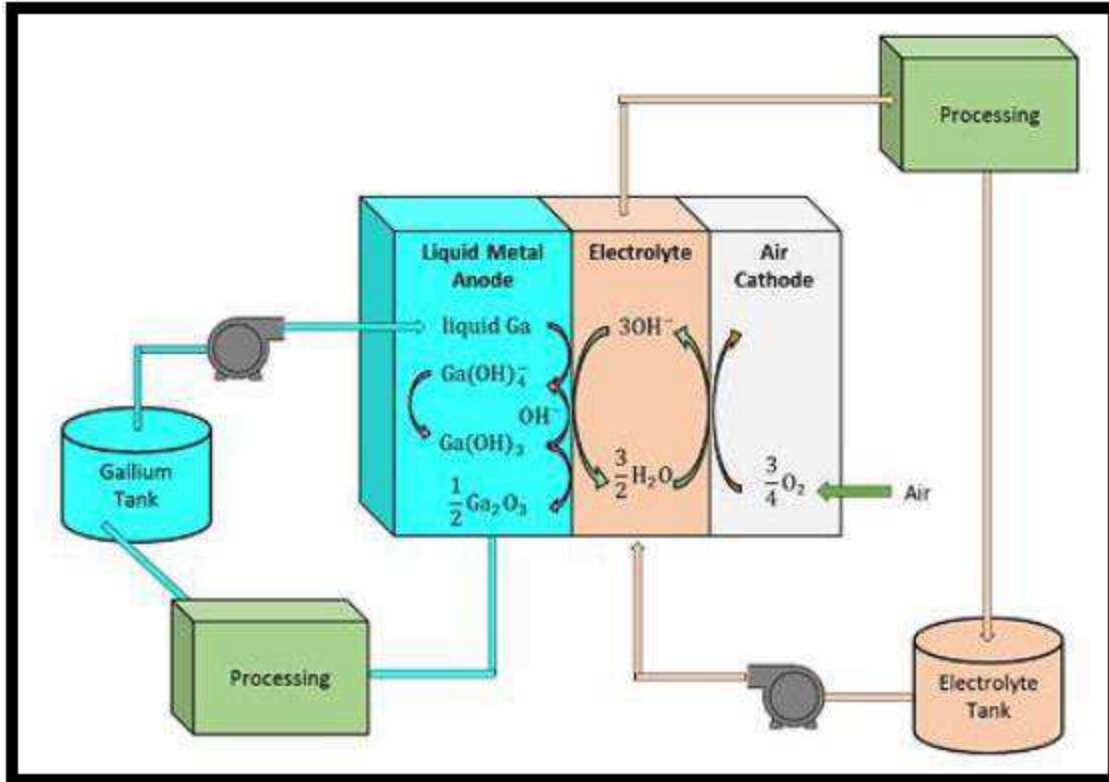
Figure 5-1: A Proposed Ga-Air Flow Battery Design (Howard, et al. 2015).

A flow battery design would not only be effective for preventing separator drying, but it would be more easily sealable, increasing its resistance to carbonation. Moreover, a more sealed design would naturally be more robust and would short circuit significantly less often than a hand constructed cell. Finally, creating a flow battery design of the Ga-Air system would put the gallium anode in a continuous state of flow, which would help mitigate the limitations of a two-dimensional reaction interface, Moreover, the interface can be designed with reaction channels, similar to a hydrogen fuel cell, which could help push the reaction interface to a more three-dimensional design. As it stands, a flow battery design of the Ga-Air system is a design that shows great promise to address the majority of causes of cell failure that the hand constructed cells currently face.

While the construction of a flow battery would be the optimal case to circumvent the potential causes of failure for the Ga-Air system, smaller scope investigations to pinpoint the cause of failure are also recommended. A post-mortem material analysis is strongly recommended since detection of KCO_3 in a failed cell would be strong evidence of carbonation as a cause of failure. Additionally, it is recommended that more closed-system tests, such as the pure O_2 test, be performed since the elimination of CO_2 from the cathode would allow it to overcome the effects of carbonation. More tests can also be performed with materials other than O_2 as the electrode material (e.g., Cl_2) in a closed system, which would further, allow investigation of the effects of separator drying on cell failure.

5.3 System Rechargeability

The ultimate focus of this investigation is to push the limits of a new type of battery: the liquid metal-air battery. This battery design was chosen over the currently existing batteries because of its theoretical greater longevity, high energy density, and resilience to numerous discharge/charge cycles because of the all-fluid components. The Ga-Air system was investigated not only because of these factors, but also because of the low melting point of gallium. Since this cell could be tested near room temperature, it was a highly feasible concept allowing determination of the feasibility of this concept. While the final result of the system's rechargeability fell short, adding some improvements to the design of the battery might allow development of a long-term rechargeable battery, potentially for use in a microgrid.

Numerous cycling tests were performed on various iterations of the Ga-Air system. While not every test was effective in achieving high cyclability, insights were gained from every test. Moreover, cyclic voltammetry was a helpful tool to determine the optimal cathodic voltages for the system recharge. This was particularly interesting because it was found that there were

two nodes corresponding to the optimal recharge voltage, which gave solid evidence for the discharge cutoff of 1.0 V. Even though most of the rechargeability tests were not replicated, they provided a good baseline to improve on in future investigations. Additionally, the tests were effective to demonstrate that the Ga-Air system can potentially be rechargeable.

For future recharge tests, it is strongly recommended to continue to investigate the recharge capacity of the AEM Ga-Air system. Since this separator is automatically more resistant to carbonation and separator drying, it seems to be the most immediately accessible design in which recharging can be investigated. Further, it might allow higher rechargeable voltages due to lower amounts of water, improving the scenario for ionic liquids. Naturally, it would stand to reason that the flow battery design suggested in Section 5.2 would also be a worthwhile system to evaluate the rechargeability for; however, this is a higher effort undertaking. As a result, it is recommended that the AEM separator and ionic liquids should first be investigated for repeatable cycling performance, while general improvements are made to the overall discharge performance of the Ga-Air system. If the system continues to perform effectively with the AEM separator or ionic liquids, it is then recommended that a flow battery be pursued since a Ga-Air flow battery would significantly improve most of the hand constructed system's limitations.

However, if a flow battery cannot be investigated other methods for cell recharging are recommended. Since a key limitation of cell charging is the concurrent water electrolysis as the voltage is increased, efforts should be made to avoid the use of water electrolytes. First, molten KOH, NaOH, or a eutectic of the two can be used as an electrolyte instead of aqueous hydroxide. This will increase the operating temperature of the cell to above 170°C, but this is still a relatively low operating temperature when compared to other technologies such as solid-oxide fuel cells. Another method is the use of ionic liquids, which are organic salts that are liquids at a

room temperature. Similar to molten salts, ionic liquids can eliminate the need for water in the Ga-Air system with the added advantage of allowing operation at room temperature or at a moderately higher temperature. Even if a flow battery is not immediately feasible, these liquid salts could easily provide new insights to the Ga-Air system.

Work Cited

Ambri. (2016). Storing Electricity for Our Future [Brochure]. Boston, MA:

Dean, J. A. and N. A. Lange (1999). Lange's Handbook of Chemistry, McGraw-Hill.

Deiss, E., Holzer, F., & Haas, O. (2002). Modeling of an electrically rechargeable alkaline Zn air
battery. Electrochimica acta, 47(25), 3995-4010.

Dunn, B., Kamath, H., & Tarascon, J. (2011). Electrical Energy Storage for the Grid: A Battery
of Choices. Science, 334(6058), 928-935. doi:10.1126/science.1212741

Friedman, T. (2008). "Hot, Flat, and Crowded". Farrar, Straus and Giroux, New York.

Gagnon, Steve. "It's Elemental — The Periodic Table of Elements" (2007). Jefferson
Lab. <https://web.archive.org/web/20070429032414/http://education.jlab.org/itselement
al/index.html>

Gilliam, R. J., Graydon, J. W., Kirk, D. W., & Thorpe, S. J. (2007). A review of specific
conductivities of potassium hydroxide solutions for various concentrations and
temperatures. International Journal of Hydrogen Energy, 32(3), 359-364.

Howard, T. T., Merrill, L. C., Johnston, S. P., & Datta, R. (2015). A new liquid metal-air battery.
Worcester, MA: Worcester Polytechnic Institute.

Horiba, T. (2014). Lithium-Ion Battery Systems. Proceedings of the IEEE,102(6), 939-950.

Arora, P., & Zhang, Z. (2004). Battery separators. Chemical reviews, 104(10), 4419 4462.

Huggins, R. A. SpringerLink ebooks - Engineering. (2010).Energy storage. New York: Springer.
doi:10.1007/978-1-4419-1024-0

Hu, V., Vu, H., & Zagorski, J. (2016). Liquid Metal-Air Battery for Energy Storage. Worcester,
MA: Worcester Polytechnic Institute.

IAE. (2014). World Energy Outlook 2014, Executive Summary. International Energy Agency,

OECD/IEA, Paris. Retrieved from:

<http://www.iea.org/Textbase/npsum/WEO2014SUM.pdf>

Ibrahim, H., Ilinca, A., & Perron, J. (2008). Energy storage systems—Characteristics and

comparisons.Renewable and Sustainable Energy Reviews, 12(5), 1221-1250.

doi:10.1016/j.rser.2007.01.023

Kiehne, H. A. (2003). Battery technology handbook (Vol. 60). CRC Press.

Kipnis, N. (2003) "Changing a theory: the case of Volta's contact electricity", Nuova Voltiana,

Vol. 5. Università degli studi di Pavia, 2003 pp. 144–14

Kim, H., Boysen, D. A., Newhouse, J. M., Spatocco, B. L., Chung, B., Burke, P. J., ... & Egan,

D. R., Ponce de León, C., Wood, R. J. K., Jones, R. L., Stokes, K. R., & Walsh, F.

C.(2013). Developments in electrode materials and electrolytes for aluminium–air

batteries.Journal of Power Sources, 236, 293-310.

Kramer, Deborah A. "Mineral Commodity Summary 2006: Gallium" (2006). United States

Geological Survey.

LaMonica, M. (2013). A tiny startup called ambri wants to transform our energy system with

massive liquid-metal batteries. CAMBRIDGE: TECHNOL REV.

Lee, J. S., Tai Kim, S., Cao, R., Choi, N. S., Liu, M., Lee, K. T., & Cho, J. (2011). Metal–air

batteries with high energy density: Li–air versus Zn–air.Advanced Energy Materials,

1(1), 34-50.

Martin, J. L., Zamora, I., Martin, J. I., Aperribay, V., & Eguia, P. (2011, April). Energy Storage

Technologies for Electric Applications. Retrieved April 14, 2016, from

<http://www.sc.ehu.es/sbweb/energias-

renovables/temas/almacenamiento/almacenamiento.html >

Morris, Chargles (2015). Separion P20 – a new flexible ceramic separator. Charged Electric

Vehicles Magazine. Web. <https://chargedevs.com/newswire/separion-p20-a-new-

flexible-ceramic-separator/>

Nicholson, R. S.; Irving. Shain (1964-04-01). "Theory of Stationary Electrode Polarography.

Single Scan and Cyclic Methods Applied to Reversible, Irreversible, and Kinetic

Systems.". Analytical Chemistry. 36 (4): 706–723.

Ober, Joyce A. "Lithium" (1998). United States Geological Survey. pp. 77–78.

Ohiostandard at English Wikipedia - Transferred from en.wikipedia to Commons by Burpelson

AFB using CommonsHelper., CC BY-SA 3.0,

<https://commons.wikimedia.org/w/index.php?curid=11236033>

Otaegui, L., Rodriguez-Martinez, L. M., Wang, L., Laresgoiti, A., Tsukamoto, H., Han, M. H., ...

& Rojo, T. (2014). Performance and stability of a liquid anode high-temperature metal air

battery. Journal of Power Sources, 247, 749-755.

Schweitzer, G. K., & Pesterfield, L. L. (2009). The Aqueous Chemistry of the Elements. Oxford

University Press.

Schwenzer, B., Zhang, J., Kim, S., Li, L., Liu, J., & Yang, Z. (2011). Membrane development for

vanadium redox flow batteries.Chemsuschem, 4(10), 1388-1406.

doi:10.1002/cssc.201100068

Skyllas-Kazacos, M., Chakrabarti, M. H., Hajimolana, S. A., Mjalli, F. S., & Saleem, M. (2011).

Progress in flow battery research and development. Journal of the Electrochemical

Society, 158(8), R55-R79.

Song, C., & Zhang, J. (2008). Electrocatalytic oxygen reduction reaction. In PEM fuel cell electrocatalysts and catalyst layers (pp. 89-134). Springer London.

USGS Minerals Commodity Surveys: "Gallium" (2013 ed)

Vega, J. A., Chartier, C., & Mustain, W. E. (2010). Effect of hydroxide and carbonate alkaline = media on anion exchange membranes. Journal of Power Sources, 195(21), 7176-7180.

Wang, H., & Turner, J. A. (2010). Reviewing metallic PEMFC bipolar plates. Fuel Cells, 10(4), 510-519. doi:10.1002/fuce.200900187

Weber, A. Z., Mench, M. M., Meyers, J. P., Ross, P. N., Gostick, J. T., & Liu, Q. (2011). Redox flow batteries: A review. Journal of Applied Electrochemistry, 41(10), 1137-1164. doi:10.1007/s10800-011-0348-2

White, L. J. (2005). An approximate analytical model for the discharge performance of a primary zinc/air cell (M.S. dissertation, WORCESTER POLYTECHNIC INSTITUTE).

Zhou, Ruolin. (2014). The Development of Zinc Air Battery's Efficiency and Rechargeability in Molten Alkaline Electrolyte. (Masters Research Report). Worcester Polytechnic Institute, Worcester, MA.

Zoulias, E., Varkaraki, E., Lymberopoulos, N., Christodoulou, C. N., & Karagiorgis, G. N. A Review on Water Electrolysis. Centre for Renewable Energy Sources (CRES).

APPENDIX

Appendix A: Anode Procedure and General Cell Assembly

The anode was prepared with liquid gallium active material and a stainless steel current collector (in the form of a crucible) according to the following procedure:

1. Liquid Gallium Preparation:
    1.1. Measured weight of the bottom half of the cell with the crucible (pictured).
    1.2. Added approximately 1.2 g of Gallium metal to the steel crucible to fill it.
    1.3. Applied heat from heating lamp to Gallium such that it becomes liquid.
    1.4. Measured weight of crucible with liquid Gallium to determine amount of Gallium used.
    1.5. Adjusted amount of Gallium until measured weight was 1.25g.
2. Cell Assembly:
    2.1. Fit stainless steel tube, Node B, into the bottom hexagonal PTFE Swagelok nut.
    2.2. Placed compression spring into Node B.
    2.3. Hand tightened middle hexagonal PTFE Swagelok union to bottom nut containing Node B.
    2.4. Place crucible in bottom half, measure out gallium.
    2.5. Assemble the layers on top of the cell:
        2.5.1. Gasket
            2.5.1.1. Teflon with an inner diameter of 6.6mm and an outer diameter of 11.8mm.
        2.5.2. Separator/electrolyte
        2.5.3. Gas Diffusion Layer
    2.6. Place the second node on top and screw on, hand tightening, the PTFE Swagelok nut.

Appendix B: Electrolyte Procedure

B.1 Zirconia Paper

The electrolyte layer was assembled with Zirconia separator material (ZYK-15 from Zircar, Zirconia Inc.) wetted with aqueous 33.6 wt.% KOH by the following procedure:

1. KOH Solution Preparation:

    1.1. Measured 3.36g of KOH (Sigma Aldrich, solid pellets ≥85%)

    1.2. Measured 10 mL of distilled water.

    1.3. Transferred KOH and water to 50 mL beaker.

    1.4. Mixed until KOH was dissolved completely.

2. Zirconia Separator Preparation:

    2.1. Cut zirconia paper using punch with a diameter of 11.8mm.

    2.2. Transferred zirconia separator to 6M KOH solution with forceps.

    2.3. Allowed separator to soak for 15-20 minutes.

3. Cell Assembly

    3.1. Applied gasket then separator to the exposed surface of the liquid Gallium anode
    material with forceps.

    3.2. Then add on GDL and complete the cell assembly as previously described.

B.2 Anion Exchange Membrane

For some tests, an anion exchange membrane (manufactured by Membrane International) was
used to block cation permeation from the anode to the cathode; thus, preventing carbonation. The
procedure used was:

1. KOH Preparation

    1.1. A 33.6 wt.% solution of KOH was prepared similarly to the solution used for the
    zirconia paper.

2. AEM Preparation

    2.1. Cut AEM using punch with a diameter of 11.8mm.

    2.2. Transferred AEM to the KOH solution using forceps.

    2.3. Allowed for the AEM to soak for at least 24 hours.

3. Cell Assembly

    3.1. Applied gasket, separator, and GDL in that order, to the exposed surface of the liquid
    Gallium anode material with forceps.

Appendix C: Cathode Procedure

The air cathode consisted of a carbon GDL pre-coated with platinum catalyst (LT140EW Low Temperature manufactured by E-TEK) prepared by the following procedure:

1. Air Cathode Preparation:
   1.1. Cut catalyzed GDL using a punch with a diameter of 11.8mm.
2. Cell Assembly:
   2.1. Placed catalyzed GDL at the center surface of the electrolyte separator material.
   2.2. Fit stainless steel tube, Node A, into top hexagonal PTFE Swagelok nut.
   2.3. Hand tightened the top nut containing Node A into the middle hexagonal PTFE Swagelok Union.

Appendix D: Swagelok Assembly Procedure
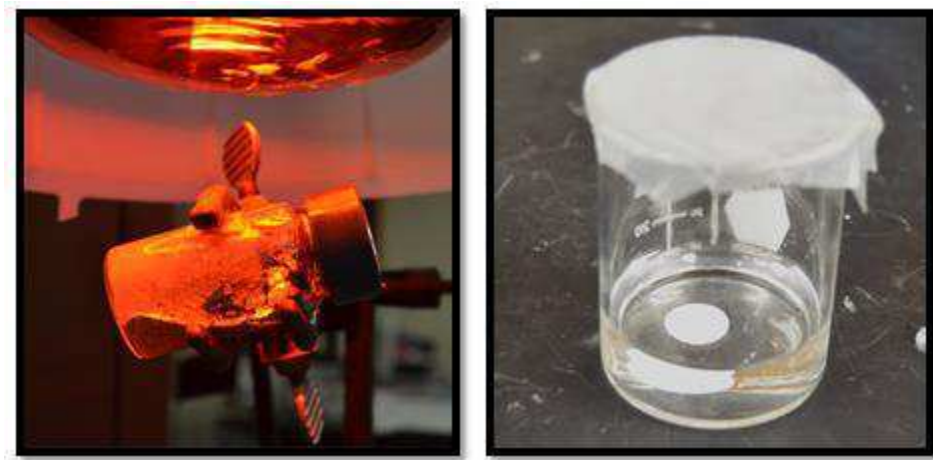
Figure 1: Heating gallium in glass vial under a heating lamp (left). Soaking zirconia cloth separator in 30 wt.% KOH (right).

Figure 2: Ferrule orientation on anode current collector (left) in Swagelok PTFE fitting (right).
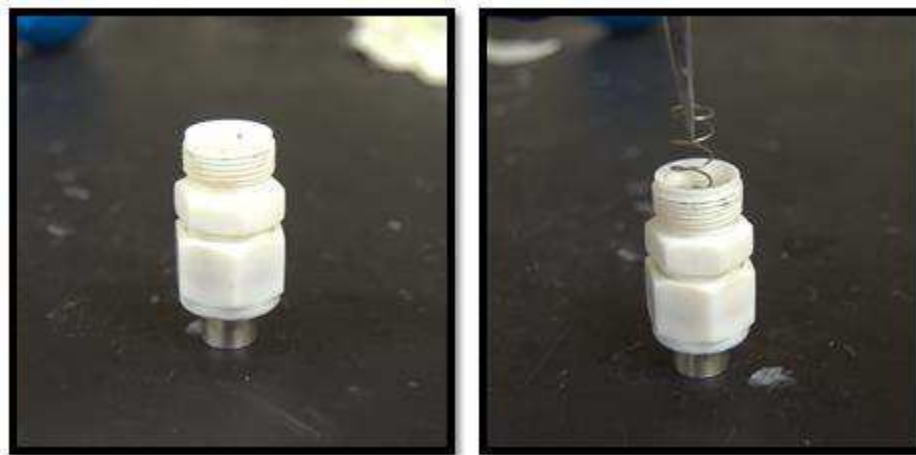
Figure 3: Swagelok PTFE union connected to fitting holding anode current collector (left). Addition of compression spring (right).

Figure 4: Addition of stainless steel crucible to top of compression spring (left). Addition of liquid gallium to the crucible using a syringe (right).

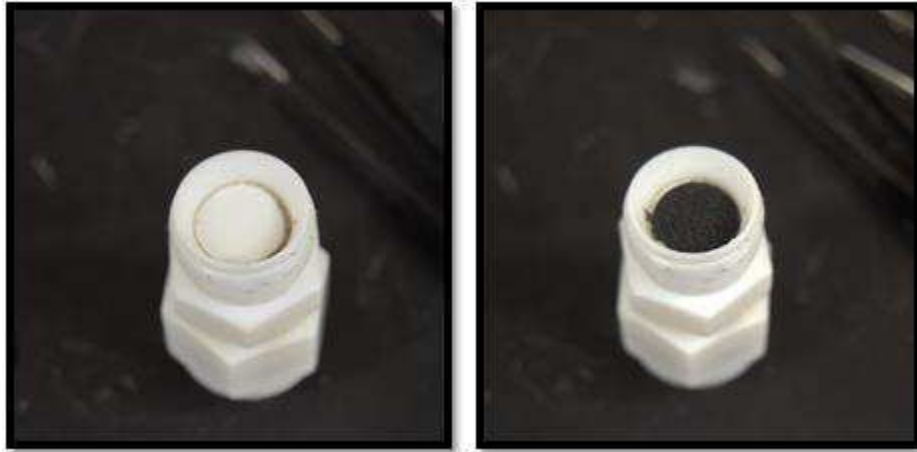*Figure 5: View of liquid gallium in crucible (left). Teflon gasket above anode crucible (right).*

Figure 6: Zirconia cloth separator wetted with 30 wt.% KOH above the gasket (left). Catalyzed gas diffusion layer above separator, with platinum coated catalyst facing the electroylte (right).

Figure 7: Ferrule orientation on air cathode current collector (left) with Swagelok fitting added (right).
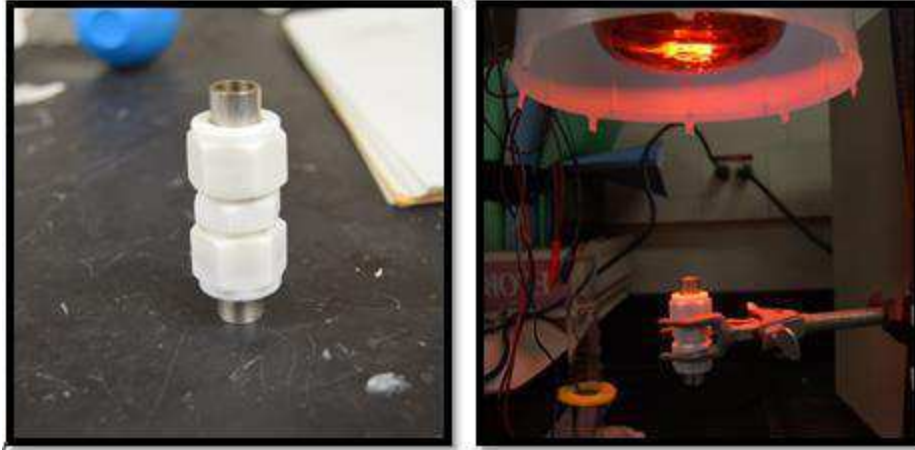
Figure 8: Completed cell configuration (left. Cell held by a ring stand clamp under a heating lamp oriented so that liquid metal anode is above the air cathode (right).
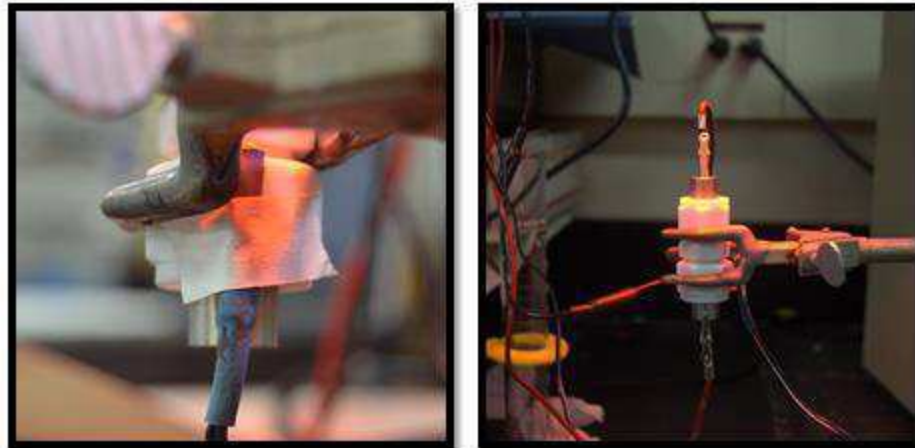
Figure 9: Taped temperature probe from battery analyzer taped to the Swagelok fitting on the air cathode side of the cell (left). Analyzer cathode and anode electrical leads attached to current collector (right).

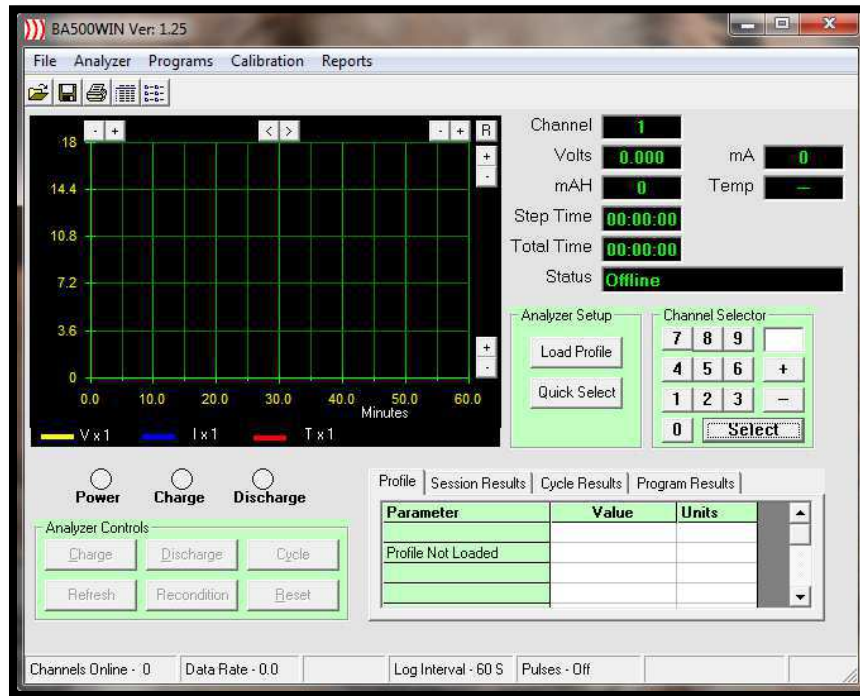# Appendix E: Battery Analyzer Program (BA500WIN) User Guide

Figure 10: Start page of the BA500WIN program. Features a real time graph that charts voltage, current and temperature.
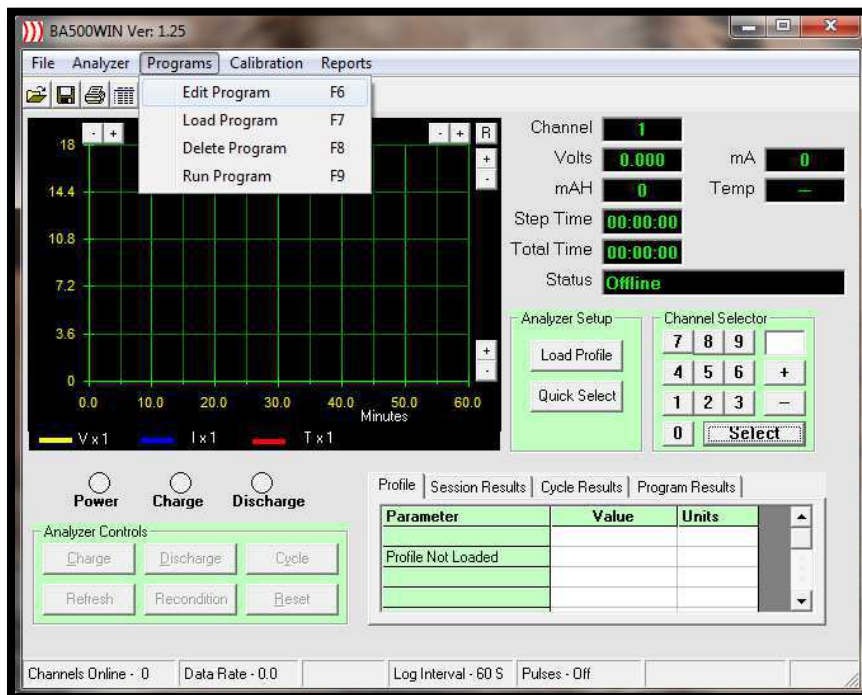
Figure 11: Programs drop down menu opened. Tests can be made with the program editor.

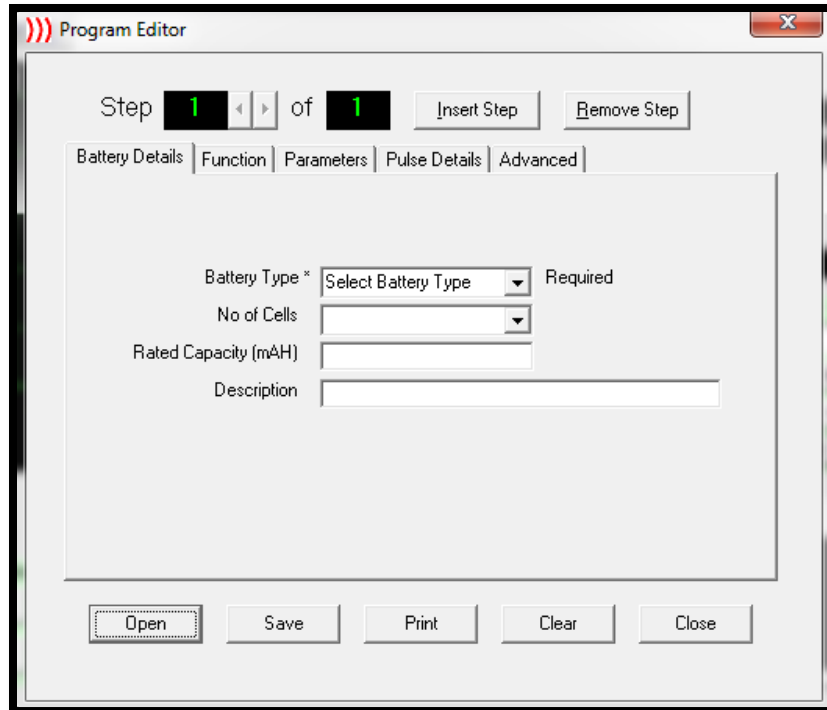*Once saved, these programs can be run by first loading them, then clicking run program.*

Figure 12: By choosing edit program from the programs dropdown menu, the program editor window opens.

Under the battery details tab there are several options such as battery type, number of cells, rated capacity and description. The only required field is battery type. For discharging purposes a primary non-rechargeable battery type was chosen. For instances to test charging, any of the other battery types may be chosen.
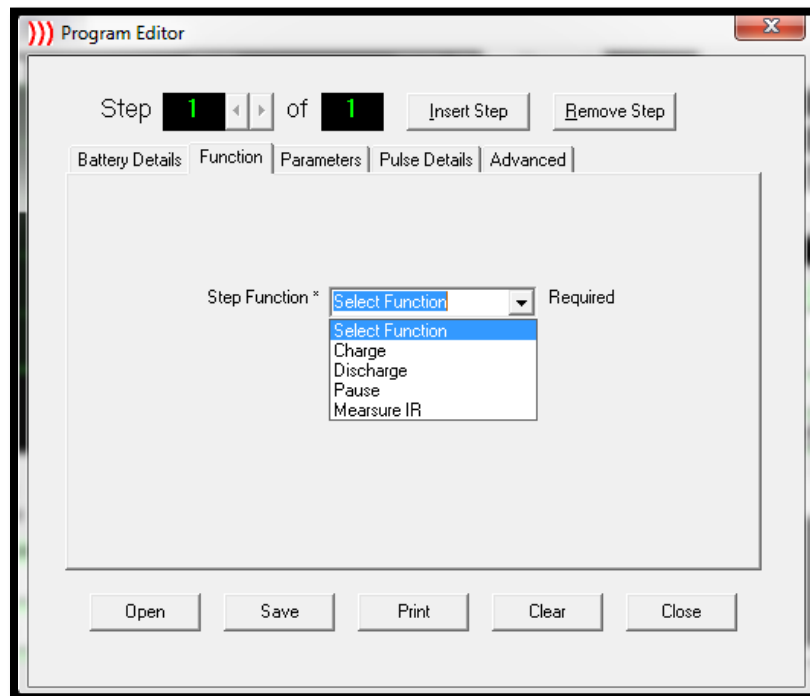
Figure 13: The second tab of the program editor requires a step function. To gather an open circuit voltage measurement, the pause function can be chosen.
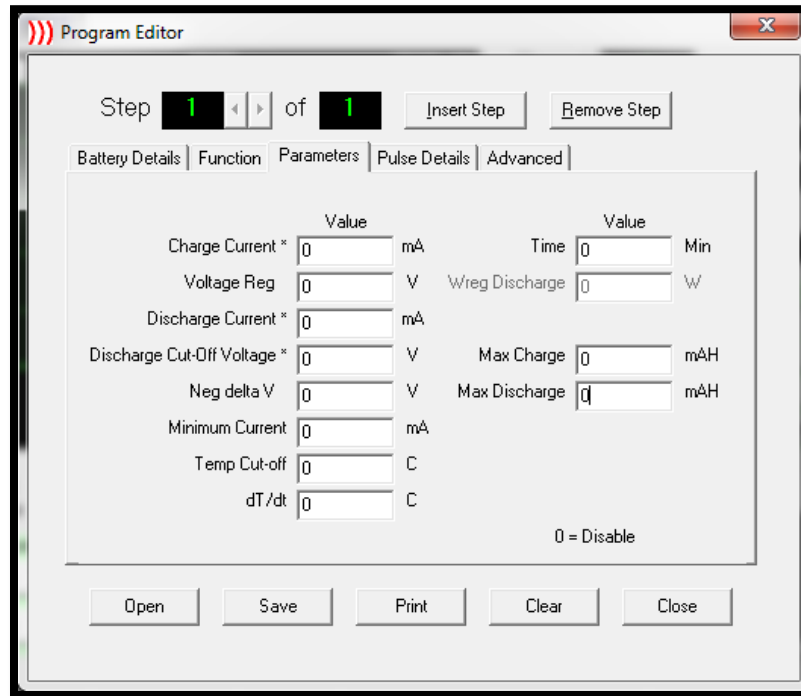

Figure 14: The third tab of the program editor lets the user define the parameters of the test.

Depending on the step function chosen before, certain parameters are required. For example, discharge tests can be conducted with a discharge current of 0.5mA to a cut-off voltage of 0.01 V while other parameters can be ignored. The other two program editor tabs, 'pulse details' and 'advanced,' can also be ignored for typical discharge tests. Additional steps with various functions and parameters can be added by the insert step button, typically an open circuit voltage measurement for a period of time followed by discharge was performed. Once completed, the file is saved in a .pg4 format and loaded from the programs menu dropdown. Once the program is run, a prompt window to save the file in a .csv format is generated for further analysis in Microsoft Excel.
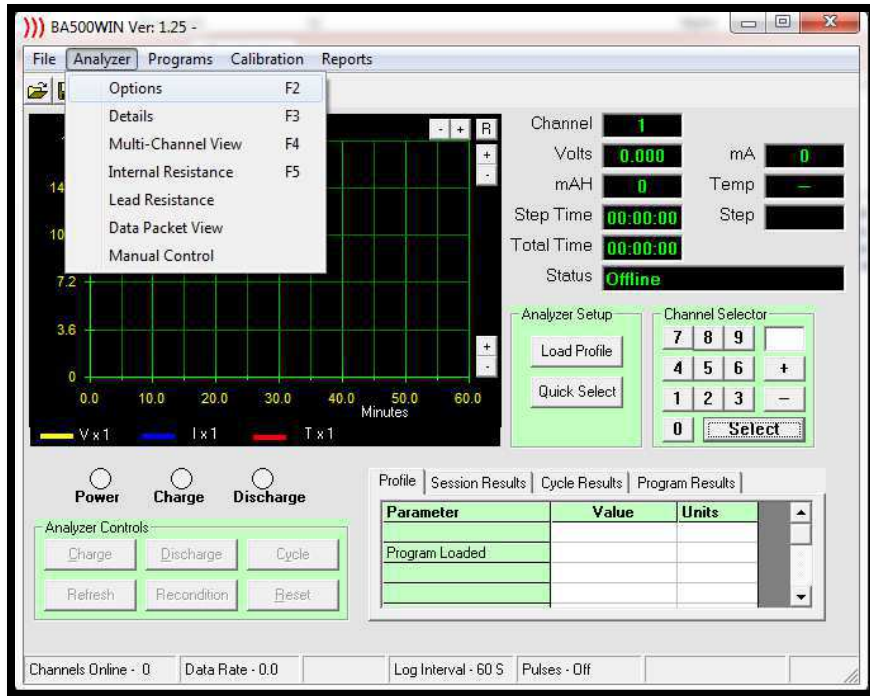
Figure 15: Often it is necessary to change the analyzer options which can be found from the drop down menu shown above or by keyboard shortcut F2.
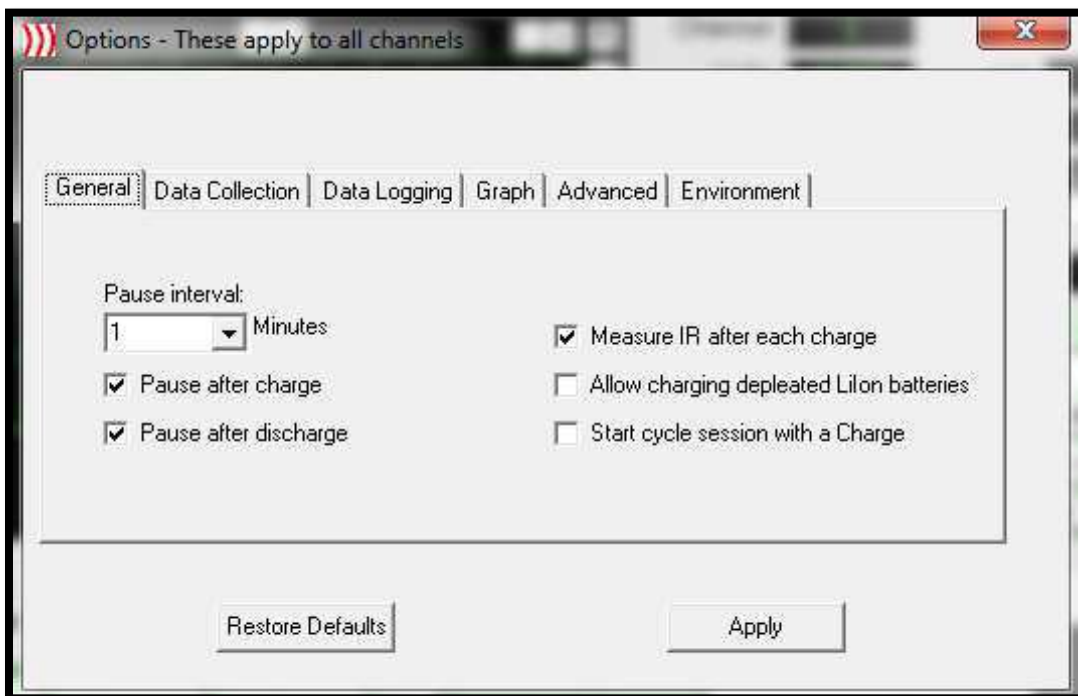

Figure 16: The analyzer options window opens when prompted to show various tabs ranging from 'general' to 'environment.' These options can be set to the user preference. For polarization curves, it is often necessary to change the data logging tab to a shorter time interval.